HYDROGEN SULFIDE CAPTURE USING AMINE-MODIFIED MESOPOROUS OXIDES

A Dissertation
Presented to
The Academic Faculty

by

Claudia N. Okonkwo

In Partial Fulfillment
of the Requirements for the Degree
Doctor of Philosophy in the
School of Chemical & Biomolecular Engineering

Georgia Institute of Technology
May 2020

HYDROGEN SULFIDE CAPTURE USING AMINE-MODIFIED MESOPOROUS OXIDES

Approved by:

Dr. Christopher W. Jones, Advisor
School of Chemical & Biomolecular Engineering
Georgia Institute of Technology

Dr. Carson Meredith
School of Chemical & Biomolecular Engineering
Georgia Institute of Technology

Dr. Krista S. Walton
School of Chemical & Biomolecular Engineering
Georgia Institute of Technology

Dr. Meisha L. Shofner
Materials Science and Engineering
Georgia Institute of Technology

Dr. Ryan P. Lively
School of Chemical & Biomolecular Engineering
Georgia Institute of Technology

Date Approved: [March 17, 2020]

ACKNOWLEDGEMENTS

I would first like to give all the praise to God, for with him, all things are possible. Furthermore, with sincere gratitude and thanks I would like to acknowledge the following individuals, whom as a result of their support and encouragement I have been able to accomplish this tremendous feat:

- My advisor and mentor, Chris W. Jones, for believing in me and supporting me through my journey at Georgia Tech both in my desire to be active on campus as a part of different organizations, in addition to providing sincere and constructive feedback to aid in my professional growth as a researcher.
- My committee members: Krista Walton, Ryan Lively, Carson Meredith and Meisha Shofner, for their in depth questions and feedback, which helped me develop my work.
- The Jones group family recent and past, for all the training in lab, answering all my questions and helping me develop into a well-rounded researcher.
- My husband, Vince Chukwukelu, and all my family and friends, for their consistent emotional support, love and prayers throughout this journey.

TABLE OF CONTENTS

ACKNOWLEDGEMENTS **iii**

LIST OF TABLES **vii**

LIST OF FIGURES **viii**

SUMMARY **xiv**

CHAPTER 1. AN INTRODUCTION TO H_2S CAPTURE USING AMINE-FUNCTIONALIZED SUPPORTS **1**
1.1 Introduction **1**
1.2 Amine-Modified Adsorbents for H_2S Capture **3**
1.2.1 Classes of Amine-Modified Adsorbents 4
1.2.2 CO_2 vs. H_2S Nature of Adsorbed Species 7
1.2.3 Effect of Humidity 10
1.3 Goals and Objectives **12**
1.4 References **13**

CHAPTER 2. ROLE OF AMINE STRUCTURE ON HYDROGEN SULFIDE CAPTURE FROM DILUTE GAS STREAMS USING SOLID ADSORBENTS **19**
2.1 Background **19**
2.2 Experimental Section **21**
2.2.1 Materials 21
2.2.2 Material Synthesis 22
2.2.3 Grafting of aminosilanes on SBA-15 22
2.2.4 Material Characterization 23
2.2.5 Adsorption Measurements 24
2.3 Results and Discussion **25**
2.3.1 Textural Properties of Materials 25
2.3.2 Baseline H_2S Adsorption Performance 27
2.3.3 Impact of Amine Type on Cyclic Stability 27
2.3.4 Effect of Adsorption Temperature 30
2.3.5 Effect of H_2S Concentration 31
2.3.6 Estimated Heats of Adsorption 32
2.4 Conclusion **38**
2.5 References **38**

CHAPTER 3. SELECTIVE REMOVAL OF HYDROGEN SULFIDE FROM SIMULATED BIOGAS STREAMS USING STERICALLY HINDERED AMINE ADSORBENTS **42**
3.1 Background **42**
3.2 Methods **46**
3.2.1 Materials 46
3.2.2 Material Synthesis 46

3.2.3 Grafting of Aminosilanes on SBA-15 48
3.2.4 Material Characterization 48
3.2.5 Dynamic Adsorption Measurements 49
3.2.6 CO_2 Adsorption Isotherm Measurements 50
3.2.7 H_2S Adsorption Isotherm Measurements 50
3.2.8 In Situ Fourier-Transform IR (FTIR) Spectroscopy 50
3.2.9 Computational Methods** 51
3.3 Results and Discussion 52
3.3.1 Material Characterization 52
3.3.2 FTIR Spectra of Adsorbed H_2S on SHA Sorbents 53
3.3.3 Understanding the Effects of Steric Hindrance on H_2S Selectivity 54
3.3.4 Multicomponent Adsorption Measurements 56
3.3.5 Desorption Kinetics 59
3.3.6 CO_2 and H_2S Adsorption Isotherms 61
3.3.7 Discussion of H_2S-amine adsorption mechanism and CO_2 selectivity 63
3.3.8 Discussion on the Impact of heat of adsorption on CO_2 vs. H_2S selectivity 65
3.3.9 Cyclic Stability of Sterically Hindered Amines 70
3.4 Conclusions 71
3.5 References 72

CHAPTER 4. EFFECT OF HUMIDITY ON THE SORPTION OF H_2S FROM MULTI-COMPONENT ACID GAS STREAMS ON SILICA-SUPPORTED STERICALLY HINDERED AND UNHINDERED AMINES 76
4.1 Background 76
4.2 Methods 80
4.2.1 Materials 80
4.2.2 Material Synthesis 80
4.2.3 Grafting of Aminosilanes on SBA-15 81
4.2.4 Material Characterization 81
4.2.5 Water Sorption Isotherms 82
4.2.6 Dynamic Sorption Measurements 82
4.2.7 In Situ Fourier-Transform IR (FTIR) Spectroscopy 83
4.2.8 NMR Spectroscopy 83
4.2.9 Computational Modeling Method** 84
4.3 Results & Discussion 85
4.3.1 Material Characterization 85
4.3.2 Fixed Bed Sorption Measurements 86
4.3.3 Computational Analysis of H_2S Sorption Mechanism 91
4.3.4 FTIR Spectra of Sorbed H_2S in Humid and Dry Conditions 96
4.3.5 Sorbent Degradation 100
4.3.6 Sorbent Regeneration in Humid Conditions 103
4.4 Conclusion 105
4.5 References 106

CHAPTER 5. A REVIEW OF CO_2 & H_2S ADSORPTION ON SILICA SUPPORTED SORBENTS STUDIED IN THIS DISSERTATION 112
5.1 Introduction 112

5.2 Discussion 113
5.2.1 Unhindered Amines for CO_2 and H_2S Adsorption 113
5.2.2 Hindered Amines for CO_2 and H_2S Adsorption 114
5.3 Conclusion 116
5.4 References 117

CHAPTER 6. SUMMARY & FUTURE DIRECTIONS 119
6.1 Summary 119
6.2 Future Directions 121
6.2.1 Evaluation of Dendrimers for H_2S Capture 121
6.2.2 Expanding the Selection Criteria for H_2S Capture Adsorbents 121
6.2.3 Molecular Level Insight into Inter vs. Intra Molecular H_2S Adsorption on Silica-Supported Amine Adsorbents 123
6.2.4 Impact of Regeneration Temperature on H_2S Capture 123
6.2.5 NMR Investigation of Chemisorbed Species 124

APPENDIX A. SUPPLEMENT TO CHAPTER 2 126
A.1 Ex-Situ Characterization of adsorbent after H_2S capture 126

APPENDIX B. SUPPLEMENT TO CHAPTER 3 128
B.1 Material Characterization 128
B.2 Dynamic Adsorption Measurements 129
B.3 Multicomponent Adsorption Data 129
B.4 Single Component Adsorption Data 131
B.5 Selectivity Comparisons to Literature Data 131
B.6 Ideal Adsorption Solution Theory 133
B.7 Computational Data 134
B.8 Coordinates of Optimized Structures 135
B.9 References 141

APPENDIX C. SUPPLEMENT TO CHAPTER 4 142
C.1 Dynamic Adsorption Measurements 142
C.2 Material Characterization 143
C.3 Fixed Bed Measurements 144
C.4 Sorption Measurements 145
C.5 Computational Analysis 146
C.6 In-situ FTIR Spectroscopy 147
C.7 NMR Spectroscopy 150
C.8 N_2 Physisorption Post H_2S Adsorption 152
C.9 Cyclic Stability 153

LIST OF TABLES

Table 2.1	Aminosilanes Used to Functionalize Silica Adsorbents	23
Table 2.2	Structural Properties of Amine-Modified Silica Adsorbents	26
Table 2.3	Isosteric heat of amine containing molecules for H_2S capture	34
Table 3.1	Structural Properties of Materials	52
Table 3.2	Assignments of FTIR absorption bands [22]	54
Table 3.3	Isosteric heat of Adsorption for Sterically Hindered Amine Adsorbents	64
Table 4.1	Structural Properties of Sorbent Materials	86
Table 4.2	Dry and Humid H_2S Capacities using 1% H_2S in N_2 at 30 °C	91
Table 4.3	Comparison of the computed and experimental vibrational frequencies of the chemisorbed HS^-–NH_2^+ and physisorbed S-H⋯N hydrogen bonded species on the amine sites of TBAPS	98
Table A. 1	^{13}C Peak Assignments	126
Table B. 1	H_2S selectivity in solid adsorbents (approximate selectivity values)	132
Table B. 2	Summary of CO_2 and H_2S Toth adsorption isotherm model parameters for IAST selectivity predictions for all adsorbents.	133
Table B. 3	Computational assessment of the TMB basicity and proton affinity of different hindered amines	135
Table C. 1	^{29}Si DP MAS NMR data for bare and functionalized SBA-15 before and after humid H_2S experiments. Values in square brackets indicate the relative integrated peak intensities as area percentages.	150

LIST OF FIGURES

Figure 1.1	Biogas Processing	3
Figure 1.2	Classes of Amine-Modified Adsorbents	7
Figure 1.3	Zwitterion mechanism for CO_2 capture, valid for primary and secondary amines	8
Figure 1.4	Reaction mechanism for CO_2 capture for tertiary amines in the presence of water. Manifold is also available for primary and secondary amines in the presence of water.	9
Figure 1.5	Proposed H_2S-amine reaction mechanism, suggested to be valid for primary, secondary and tertiary amines on solid adsorbents	10
Figure 2.1	Chemical names and structures of aminosilanes used in this study	23
Figure 2.2	Nitrogen adsorption/desorption isotherms at 77 K for bare and functionalized SBA-15 materials	26
Figure 2.3	Low angle X-ray diffraction patterns for bare and functionalized SBA-15 materials.	27
Figure 2.4	H_2S (a) adsorption capacities and (b) amine efficiencies of amine-modified adsorbents over four adsorption-desorption cycles using 1% H_2S in N_2 and 30 °C	28
Figure 2.5	Cyclic performance of (a) SBA-15_MAPS and (b) SBA-15_DMAPS at 10% H_2S in N_2 and 30 °C	29
Figure 2.6	(a) H_2S adsorption capacity (b) amine efficiency of secondary and tertiary amine adsorbents at different temperatures using 10% H_2S in N_2	31
Figure 2.7	(a) H_2S adsorption capacity (b) amine efficiency of secondary and tertiary amines at different H_2S concentrations and 30 °C *error bars from standard deviation of three runs*	32
Figure 2.8	(a) H_2S adsorption isotherms (b) amine efficiency of secondary and tertiary amines at different temperatures	33

Figure 2.9	Isosteric heat of adsorption for H_2S on secondary and tertiary amine-modified mesoporous oxides	35
Figure 2.10	Adsorption capacities for SBA-15_APS, SBA-15_MAPS and SBA-15_DMAPS over 10 cycles of adsorption and desorption at 10% H_2S in N_2 and 30 °C.	36
Figure 2.11	Normalized weight of (a) SBA-15_APS (b) SBA-15_MAPS (c) SBA-15_DMAPS after 10 cycles of adsorption and desorption at 10% H_2S in N_2 and 30 °C *normalized weight to 120 °C*	37
Figure 3.1	Chemical names and structures of aminosilanes used in this study	48
Figure 3.2	FTIR spectra for 10% H_2S in N_2 adsorption on (a) bare silica, SBA-15 (b) SBA-15_TBAPS (c) SBA-15_CHAPS (d) SBA-15_AMBS with activated sample as background.	54
Figure 3.3	CBS-QB3 calculated TMB basicity and proton basicity at 298.15K and 1 atm of different hindered amines. Previous work with this model indicated a maximum deviation from experimental values of 2.1 kJ mol-1 for the TMB basicity and 4.4 kJ mol-1 for the proton basicity.	56
Figure 3.4	H_2S adsorption capacity with and without CO_2. The error bars were estimated with two independent experiments. (b) 1% H_2S/ 10% CO_2/89% CH_4 breakthrough curves on hindered amines with H_2S (filled circle) CO_2 (open circle).	58
Figure 3.5	Desorption profile for hindered amines in 1% H_2S/ 30% CO_2/ 69% CH_4 for (a) SBA-15_TBAPS, (b) SBA-15_CHAPS and (c) SBA-15_AMBS.	60
Figure 3.6	H_2S selectivity obtained from IAST predictions and experimental data using a multicomponent mixture at the following operating conditions (a) 1% H_2S/ 10% CO_2/ 89% CH_4 and (b) 1% H_2S/ 30% CO_2/ 69% CH_4 at 30 °C and 1 atm.	63
Figure 3.7	Calculated isosteric heats of adsorption of H_2S vs. surface coverage for all adsorbents at 30°C.	64
Figure 3.8	Computationally Optimized Structures at the B3LYP/6-31G** level of theory for H_2S-Amine Adsorbent Interaction in (a) SBA15-TBAPS (b) SBA-15_CHAPS (c) SBA-15_AMBS. (Grey = carbon, white = hydrogen, blue = nitrogen, yellow = sulfur)	65

Figure 3.9 (a) Isosteric heats of CO_2 adsorption under dry conditions for all sorbents at 30 °C. Reprinted with permission from ref 10. Copyright (2018) American Chemical Society. (b) Measured isosteric heats of CO_2 adsorption and calculated heats of H_2S adsorption from Toth isotherm fits at different temperatures for SBA-15_TBAPS. 70

Figure 3.10 Adsorption capacities for SBA-15_TBAPS, SBA-15_CHAPS, and SBA-15_AMBS over 10 cycles of adsorption and desorption at 10% H_2S in N_2 at 30 °C 71

Figure 4.1 Chemical names and structures of aminosilanes used in this study. 81

Figure 4.2 (a) H_2S sorption capacities and (b) amine efficiencies for hindered and unhindered amine sorbents with and without CO_2 under dry conditions at 30 °C. The error bars were estimated with three consecutive experiments 89

Figure 4.3 H_2S sorption capacities under dry and humid conditions (49% RH) at 30 °C. The reported error in the humid and dry runs is the standard deviation calculated from three independent runs. 90

Figure 4.4 Comparison of normalized H_2S uptake profiles for SBA-15_TBAPS and SBA-15_DMAPS under humid (filled symbols) and dry (open symbols) conditions using 1% H_2S in N_2 at 30 °C. 90

Figure 4.5 Computationally optimized structures for sorption complexes of H_2S and H_2O on one amine site of TBAPS through (a–c) H_2S-amine interactions and (d–f) H_2O-amine interactions. Sorption energies of the molecules (in kJ/mol) and main atomic distances (in Å) are shown. 92

Figure 4.6 Computationally optimized structures for sorption complexes of H_2S and H_2O on two amine sites of TBAPS through (a–c) H_2S-amine interactions and (d–f) H_2O-amine interactions. Sorption energies of the molecules (in kJ/mol) and main atomic distances (in Å) are shown. 92

Figure 4.7 Computationally optimized structures for sorption complexes of CO_2 on one amine site of TBAPS (a–b) in the absence of H_2O and (c-f) in the presence of one H_2O molecule via physisorbed and chemisorbed interactions. Sorption energies of the molecules (in kJ/mol) and main atomic distances (in Å) are shown. 95

Figure 4.8	The S-H···N and HS^{-}-NH_2^{+} intensity region for (a) SBA-15_TBAPS after dry H_2S sorption and (b) SBA-15_TBAPS after wet H_2S sorption. Sorption conditions: 10% H_2S in N_2 at 30 °C.	99
Figure 4.9	The S-H··· N and HS^{-}-NH_2^{+} intensity region during desorption for SBA-15_TBAPS after dry and wet H_2S adsorption. Desorption conditions: UHP He at 120 °C	100
Figure 4.10	(a) ^{29}Si MAS NMR spectra and (b) ^{13}C MAS NMR spectra of the fresh silica sorbents.	103
Figure 4.11	Amine efficiencies for SBA-15_TBAPS and SBA-15_DMAPS over 3 cycles of sorption-desorption under humid conditions (49% RH). Sorption conditions: 1% H_2S in N_2 at 30 °C and desorption with (a) dry Helium at 120 °C (b) humid Helium at 80 °C	105
Figure 5.1	Unhindered and sterically hindered amines investigated for CO_2 and H_2S capture.	112
Figure A. 1	^{13}C CP-MAS Solid State NMR for SBA-15-MAPS before and after adsorption in 10% H_2S in N_2 at 30 °C	126
Figure A. 2	XPS, S2p data (a) before and (b) after H_2S adsorption in 10% H_2S in N_2 at 30 °C	127
Figure B. 1	Nitrogen adsorption/desorption isotherms at 77 K for bare and functionalized SBA-15 adsorbents	128
Figure B. 2	Pore size distributions of SBA-15 and all SHA calculated from the N_2 physisorption isotherms using the BdB-FHH method	128
Figure B. 3	Schematic of fixed bed setup for multicomponent adsorption experiments.	129
Figure B. 4	Normalized CH_4 breakthrough profile shows that it is non-adsorbing on all hindered amines with a similar breakthrough curve as the empty bed on all sterically hindered amines.	129
Figure B. 5	TGA vs. Fixed bed H_2S adsorption capacities for 1% H_2S in N_2 at 30 °C	130
Figure B. 6	The normalized H_2S breakthrough profile of SBA-15_TBAPS shows no significant change before and after the addition of CO_2, which confirms its feasibility for the selective removal of H_2S from biogas streams.	130

Figure B. 7	Single component adsorption isotherm for (a) CO_2 (b) H_2S at varying temperatures and concentrations.	131
Figure C. 1	Fixed bed adsorption system schematic	142
Figure C. 2	Nitrogen physisorption isotherms for SBA-15, SBA-15_TBAPS and SBA-15_DMAPS.	143
Figure C. 3	Pore size distribution of bare and amine functionalized SBA-15 calculated from N_2 physisorption isotherms using the BdB-FHH analysis method.	143
Figure C. 4	The normalized CO_2 and CH_4 breakthrough profiles for (a) SBA-15_TBAPS and (b) SBA-15_DMAPS shows CO_2 is non-adsorbing using 1% H_2S/30% CO_2/ 69% CH_4 with 49% RH.	144
Figure C. 5	Water sorption isotherms of the sorbents studied.	145
Figure C. 6	Computationally optimized structures for sorption complexes of H_2S and H_2O on one amine site of the SBA15-DMAPS sorbent through (a–c) H_2S-amine interactions and (d–f) H_2O-amine interactions. Sorption energies of the molecules (in kJ/mol) and main atomic distances (in Å) are shown.	146
Figure C. 7	Computationally optimized structures for sorption complexes of H_2S and H_2O on two amine sites of the SBA15-DMAPS sorbent through (a–c) H_2S-amine interactions and (d–f) H_2O-amine interactions. Sorption energies of the molecules (in kJ/mol) and main atomic distances (in Å) are shown.	146
Figure C. 8	FTIR spectra for SBA-15_DMAPS, (a) 4000−2000 wavenumbers and (b) 1800−1300 wavenumbers using 10% H_2S in N_2 under wet conditions.	147
Figure C. 9	FTIR spectra for SBA-15_DMAPS, (a) 4000−2000 wavenumbers and (b) 1800−1300 wavenumbers in 10% H_2S in N_2 under dry conditions.	148
Figure C. 10	FTIR spectra for 10% H_2S in N_2 sorption under dry and wet conditions on (a) SBA-15_TBAPS (b) SBA-15_DMAPS.	149
Figure C. 11	^{29}Si DP-MAS NMR spectra (solid line) of SBA-15. The dashed black lines indicate the deconvolution of the spectral line shapes summarized in Table S1.	151

Figure C. 12 ^{13}C DP-MAS NMR spectra of (a) SBA-15_TBAPS and (b) SBA-15_DMAPS 152

Figure C. 13 Nitrogen physisorption isotherms for (a) SBA-15_TBAPS and (b) SBA-15_DMAPS before and after humid H_2S sorption. 152

Figure C. 14 Sorption capacities for SBA-15_TBAPS and SBA-15_DMAPS over 3 cycles of sorption and desorption under dry conditions with 1% H_2S in N_2 at 30 ℃. 153

Figure C. 15 Sorption capacities for SBA-15_TBAPS and SBA-15_DMAPS over 3 cycles of sorption and desorption under humid conditions with sorption conditions: 1% H_2S in N_2 at 30 ℃ and desorption with (a) dry helium at 120 ℃ and (b) moist helium at 80 ℃ 153

SUMMARY

Hydrogen Sulfide (H_2S) is a pollutant that is odorous, poisonous and corrosive. It is a common contaminant in effluents associated with many industrial processes, including natural gas and biogas upgrading. Liquid phase chemical scrubbing with liquid amines and polymer membrane technology are the two current major acid gas removal techniques, with limitations arising in their high regeneration cost, excessive corrosion, or low selectivity, which lead to the loss of methane. Adsorption is an energy-efficient technology for both carbon dioxide (CO_2) and H_2S capture and requires materials with high and stable adsorption capacity and selectivity that operate under mild conditions. Solid amine adsorbents have been proposed for capture of such acid gases, owing to their basic character, imparted by the amines. This disserttaion investigates the effects of amine type (primary, secondary and tertiary amines), amine structure (hindered and unhindered amines) and humidity on the adsorption of H_2S. By developing amine- H_2S -silica structure-property relationships for these materials, the requisite fundamental understanding of the adsorption process will be obtained such that the rational design of improved adsorption materials, tailored for H_2S interactions, will be possible.

The first study assesses three adsorbents with similar textural and physical properties but with different amines grafted to the surface. Specifically, materials containing primary, secondary, and tertiary amines at the end of a propyl surface linker grafted on a silica support are explored (Chapter 2). H_2S adsorption isotherms and cyclic studies are presented for these materials, and it is shown that secondary amines have the best amine efficiency while tertiary amines are the most stable for H_2S capture, of the materials studied. The results suggest the

consideration of secondary and tertiary amines for the design of amine adsorbents suitable for H_2S removal in dilute gas streams over multiple cycles.

Next, three silica supported sterically hindered amines (SHA), two moderately hindered amines (containing primary and secondary amine groups) and one severely hindered amine (containing a secondary amine group), are evaluated for removal of H_2S from mixed $CH_4/CO_2/H_2S$ streams akin to those found in natural gas deposits or in biogas streams (Chapter 3). The results from in-situ infrared spectroscopy and both calculated and simulated heats of adsorption suggest a hydrogen bonding sorption mechanism for H_2S, involving two amine molecules and one H_2S molecule on all SHA adsorbents. Basicity calculations with a sterically hindered Lewis acid suggest that steric hindrance is responsible for the limited amine-CO_2 interactions on the hindered amines, but has less effect on the amine- H_2S interactions. Using a multicomponent gas mixture of $CH_4/CO_2/H_2S$, a range of experiments confirm that moderately sterically hindered amines can simultaneously remove CO_2 and H_2S while the most severely sterically hindered amine, based on a *tert*-butylaminopropylsilyl-grafted species, is the best adsorbent for the selective removal of H_2S in the presence of low and high CO_2 concentrations, offering facile regeneration. The H_2S selectivity achieved, with essentially no measurable CO_2 uptake, is the highest H_2S selectivity reported to date amongst similar gas mixtures for solid adsorbents.

Furthermore, the sorption of H_2S on a silica supported sterically hindered secondary amine and a supported unhindered tertiary amine is investigated. The sorption performance in dry and humid simulated biogas streams is explored using fixed bed breakthrough experiments. Furthermore, in situ Fourier-transform infrared spectroscopy and computational analysis is used to elucidate the structure of the surface species formed during humid H_2S sorption. Additionally,

the cyclic stability of the amine functionalized silica sorbent is assessed using NMR spectroscopy, N_2 physisorption and elemental analysis. For all sorbents under dry condition, physisorption led to low H_2S adsorption capacities but under humid condition, a strongly chemisorbed species is formed, which led to an increase in H_2S adsorption capacity. As a result of the strongly bound species, the sorbents are shown to require humid temperature swing sorption-desorption cycles for complete sorbent regeneration under the conditions studied, with temperature swings using dry gas failing to effectively desorb the H_2S. Overall, the structure of the silica framework and organic moieties are maintained for both sorbents after 6 hours humid H_2S exposure. The results in this work confirm the positive effect of humidity on the H_2S adsorption capacity of silica-supported sterically hindered and unhindered amines.

Lastly, a review of the relationship between adsorbents that have been evaluated in literature for CO_2 capture to similar adsorbents evaluated in this work for H_2S capture has been conducted (Chapter 5). This assessment shows the importance of evaluating the nature of the adsorbed species owing to its impact on capacity, amine efficiency and kinetics of the sorbent studied.

The results from this dissertation have confirmed the feasibility of using solid-supported amines for the selective or simultaneous removal of H_2S from dry or humid simulated biogas streams. Furthermore, the proton transfer mechanism proposed for H_2S absorption in aqueous amine solution has been suggested for the solid-supported analogues under humid conditions. This work also suggests that amine type and steric hindrance play a role in the adsorption of H_2S on solid-supported sorbents and should be considered when designing practical sorbents for biogas upgrading.

CHAPTER 1. AN INTRODUCTION TO H_2S CAPTURE USING AMINE-FUNCTIONALIZED SUPPORTS

1.1 Introduction

In recent years, natural gas has become one of the major sources of energy used in the United States, with an increase in shale gas reserves from 37.9% in 2009 to about 54% in 2015.[1,2] Although natural gas is a fossil fuel, it is a good alternative to crude oil or coal due to its lower carbon footprint.[3] Furthermore, renewable natural gas (RNG), an advanced biofuel, can be produced by the purification/upgrading of biogas produced in landfills (**Figure 1.1**). RNG can be used in all applications that utilize methane, most importantly in the transportation and electric power sector.[4]

Biogas is produced by the decomposition of organic matter in a digester, and the source of the organic matter determines the biogas composition. Some sources of biogas include landfills, agricultural waste and waste water. Specifically, landfills release bio-methane (CH_4) into the atmosphere, which has a global warming potential 23 times higher than carbon dioxide.[5,6] The typical biogas composition in landfills range from 50-80% CH_4, 20-50% CO_2, 0-3% H_2S, 0-10% H_2O and trace H_2 and O_2.[6]

Biogas can be used as an important energy source, but to inject it into natural gas pipelines, H_2S needs to be removed from the gas stream due to its corrosive and poisonous properties. A few techniques have been explored for the removal of corrosive gases such as H_2S from biogas. First, aqueous amine solutions have been used for the removal of acid gases, but the high regeneration cost associated with the high heat capacities of the aqueous solutions used

as well as high amine loss make this technique energy intensive and inefficient.[7] Second, membrane technologies have been used for the simultaneous separation of H_2S, CO_2 and CH_4, but poor selectivity for H_2S in the presence of CH_4 is observed owing to the comparable molecular diameters of H_2S (3.6 Å) to CH_4 (3.8 Å).[8] Furthermore, high H_2S selectivity is required because the end processing of hydrogen sulfide determines the required H_2S vs. CO_2/CH_4 selectivity; for example, the Claus process benefits from a High H_2S/CO_2 selectivity to recover elemental sulfur from gaseous hydrogen sulfide.[9]

The low regeneration energy and potential to fine tune the surface area and pore characteristics of solid-supported adsorbents make them components of promising adsorption based separation technologies for acid gas capture. Therefore, they should be explored as a potentially energy efficient separation method.[10,11] Supports such as metal oxides, silica, zeolites, metal organic frameworks (MOF's) and activated carbons (AC's) have been explored as solid adsorbents for H_2S capture. For MOF's and some solid supports, amine functionalization on such supports improves the H_2S adsorption capacities.[8,12–15] The effect of the type of amine(s) used, such as sterically hindered amines, unhindered amines or polymeric amines, has been investigated for H_2S capture in aqueous solutions, but limited information is available on the behavior of different types of amines on solid supports.[16–21] This gap in knowledge will be addressed in this dissertation to better understand how to design solid adsorbents as key components of a potential energy efficient adsorption method for biogas purification.

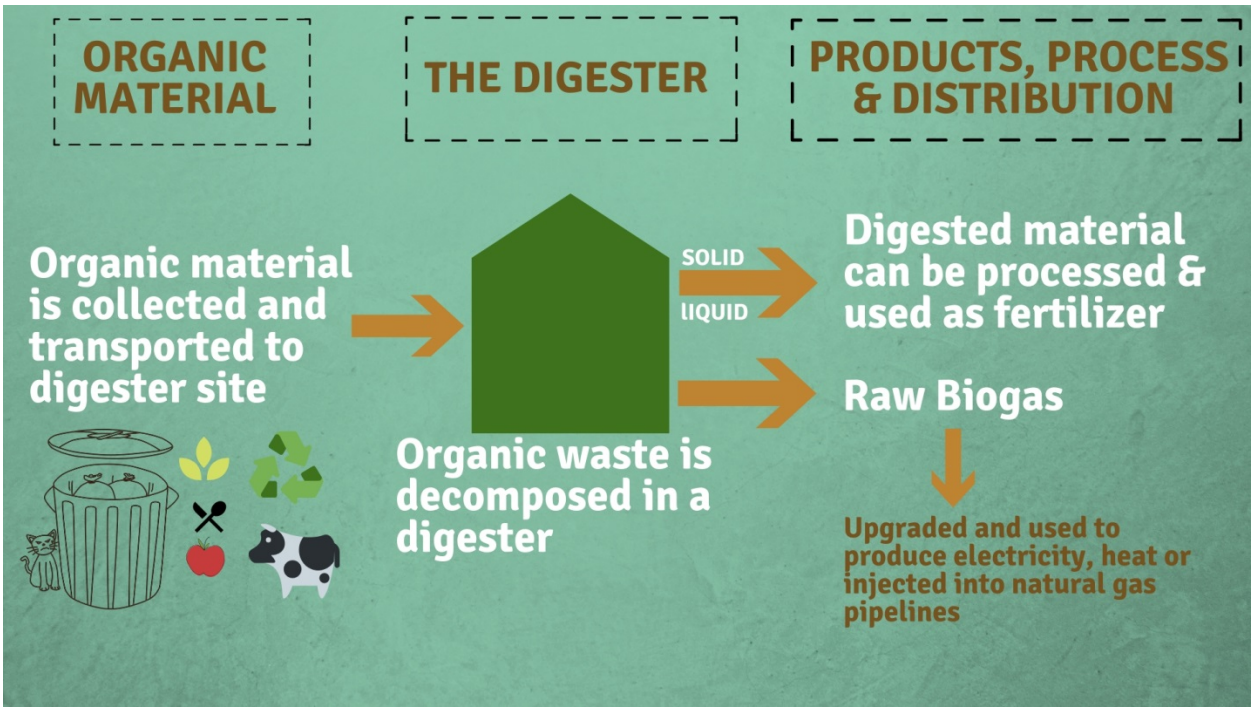

Figure 1.1. Biogas Processing

1.2 Amine-Modified Adsorbents for H_2S Capture

Adsorbents are key components of adsorption technologies, which often have lower regeneration cost and produce less waste compared to conventional aqueous amine solutions used for acid gas separations.[22] Several types of adsorbents such as activated carbons, zeolites, and metal oxides have been used for H_2S capture. However, these all have drawbacks such as low H_2S removal efficiency and high temperature requirements in metal oxides.[23–25] Supported amines, on the other hand, are an emerging class of hybrid organic-inorganic materials that is promising for CO_2 capture due to their high adsorption capacities, comparable to aqueous amine solutions in some cases. These amine-modified adsorbents are either impregnated into the pores of the support or chemically bound on the surface of the support. In addition to the potential of

supported amines as CO_2 capture materials, studies have shown that their application can be expanded and they can be used for H_2S capture.[11,26,27]

1.2.1 Classes of Amine-Modified Adsorbents

Solid-supported amines have been divided into four groups based on structural attributes and synthetic methods. The application of these three classes of adsorbents for CO_2 capture have been studied extensively.[28–37] Class 1 adsorbents were first introduced by the Song group in 2002. They are prepared by the physical impregnation of pre-synthesized amines onto or into the pores of solid supports. The advantages of class 1 amines lie in their low volatility when amine containing polymers are used; they also achieve high CO_2 capacities due to their high amine content. However, the non-covalent bonds that link the amine onto the support lead to amine/support degradation during repeated humid/steam CO_2 adsorption-desorption cycling.[38–40] Furthermore, class 1 adsorbents often have diffusion limitations as a result of crosslinking and aggregation of the polymer molecules used, such as low molecular weight branched poly(propylenimine) (PPI) and poly(ethelenimine) (PEI).[28,41]

Class 2 adsorbents contain covalent linkages between the amine and the support. These linkages are often created using aminosilanes, which are typically chemically grafted onto the surface of the porous support. Such materials were first prepared for CO_2 sorption by Tsuda following a co-condensation approach where the aminosilanes were incorporated into the oxide framework during the silica support synthesis.[29,42,43] Often being more well-defined than class 1 adsorbents, class 2 adsorbents have been used to understand the structure-property relationship of different amine types and how the amine sites interact with varying gas compositions. The covalent tethering of aminosilanes on the surface of the support improves the material's thermal

stability but provides lower amine loadings, which often leads to lower CO_2 adsorption capacities.[34]

Class 3 adsorbents are hyperbranched aminosilica materials (HAS), they were first reported by the Jones group in 2008.[37] Such adsorbents are synthesized by the *in situ* polymerization of monomers to create aminopolymers grafted to the support material, with the polymers fully or partially contained within the pores of the support. The covalent bonding to the surface improves the thermal stability of these adsorbents, while the high amine density provides high CO_2 adsorption capacities. Their limitations are associated with their more complex synthesis, as well as potential for pore diffusion limitations due to the large density of the amines in the pores.[44]

Class 4 adsorbents are categorized as a hybrid of class 1 and class 2 sorbents.[45,46] They are prepared by the chemical grafting of an aminosilane on the surface of the support and the physical impregnation of an aminopolymer into the porous support. These sorbents have shown increased CO_2 capacity compared to the class 1 and class 2 counterparts.[47] Furthermore, they have shown good water and CO_2 stability,[28] but the diffusion limitations associated with aggregation of amines, similar to the class 1 sorbents, appear inevitable.

Solid-supported adsorbents have recently been established as promising materials for H_2S capture. Specifically, class 1 and class 2 adsorbents have been the primary focus thus far for H_2S capture because of the ease of their lab scale synthesis and ability to control the structure, as well as to isolate the amines to perform fundamental studies. H_2S removal is most often performed using solid-supported adsorbents in a temperature swing adsorption (TSA) or pressure/vacuum

swing adsorption (PSA/VSA) process, which allows for the regeneration of the adsorbent material over multiple adsorption/desorption cycles.

Wang et. al studied H_2S adsorption using different mesoporous molecular sieves (MCM-48, MCM-41) and SBA-15 loaded with PEI, and they found that the 3-D mesoporous structure of MCM-48 improved the H_2S breakthrough capacity.[48] Their work showed that the structure of the support type used to synthesize solid-supported amines influences the kinetic capacity, stability and diffusional limitations of the adsorbent. Hence, it is important to consider support types with good thermal and hydrothermal stability, large surface areas and pore sizes.[48] Furthermore, studies have explored the effect of temperature, amine type, flow rates and varying H_2S concentrations on class 1 adsorbents, but there is limited information on H_2S removal using class 2 adsorbents, which are considered in this work. [49–53]

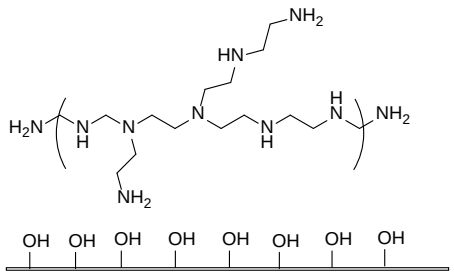

Class 1: Physical impregnation

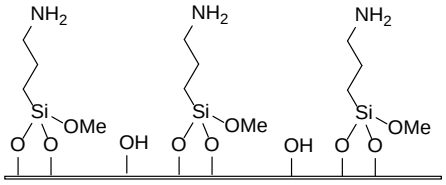

Class 2: Covalent tethering via silane linkage

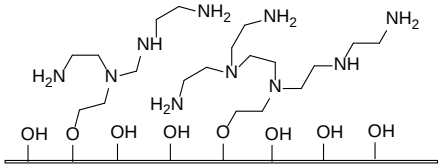

Class 3: Direct covalent tethering via *in situ* polymerization

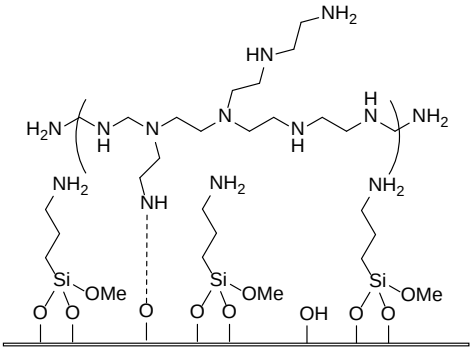

Class 4: A hybrid of class 1&2

Figure 1.2. Classes of Amine-Modified Adsorbents

1.2.2 CO_2 vs. H_2S Nature of Adsorbed Species

During adsorption, the species formed could be physisorbed (a weak bond) or chemisorbed (a strong bond) to the adsorbent material. It is important to understand the adsorption mechanism of solid supported amines because it influences the adsorption capacity and regeneration energy (or temperature) of the adsorbent. The adsorption mechanism influences the adsorbent's effectiveness for large scale applications and should be well understood in order to optimize the biogas upgrading process. In dry adsorption conditions (absence of water), it has been observed that CO_2 interacts with the solid-supported, primary and secondary amine groups to produce strongly bound carbamates and carbamic acid via a zwitterion mechanism on supported amines.[54–56] The formation of the alkylammonium carbamate species requires two

amines to capture one molecule of CO_2. This interaction is illustrated for primary amines in Figure 1.3 below.[29,44,57] Under dry conditions, tertiary amine adsorbents are not effective for CO_2 capture because they can only undergo a mechanism that requires water for CO_2 capture. The presence of water leads to the formation of bicarbonates with a ratio of 1 mol amine to 1 mol of CO_2, as illustrated in Figure 1.4.[58]

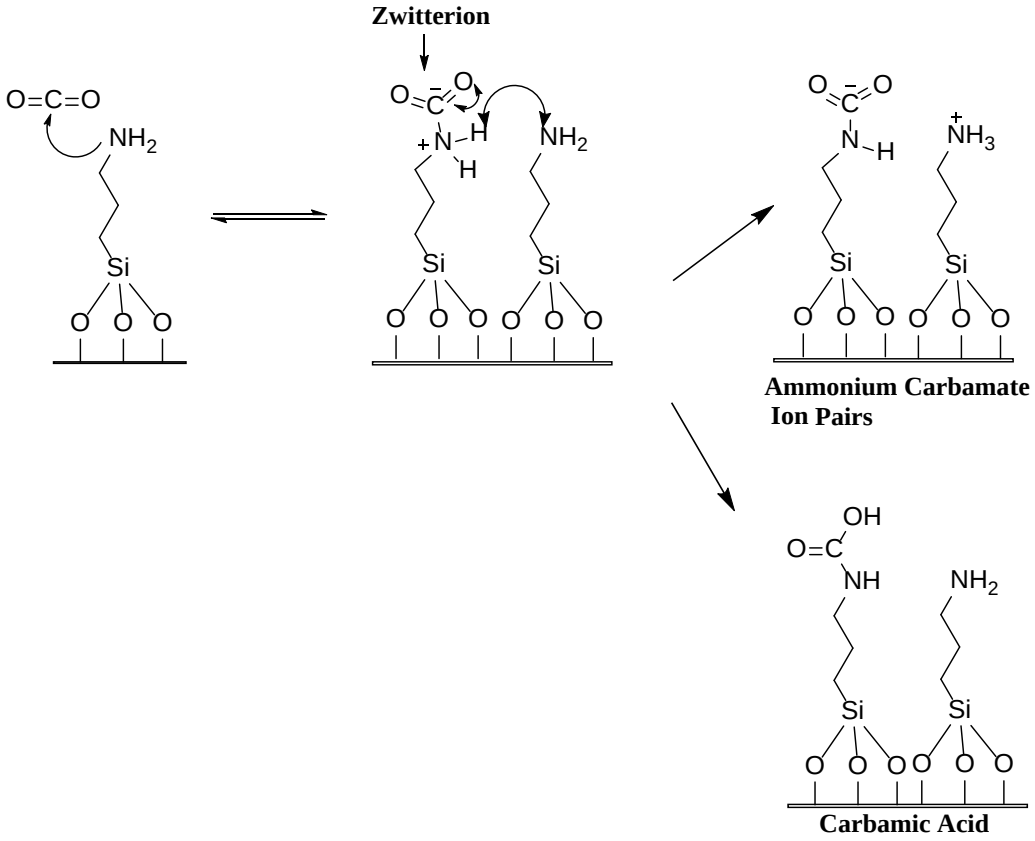

Figure 1.3. Zwitterion mechanism for CO_2 capture, valid for primary and secondary amines

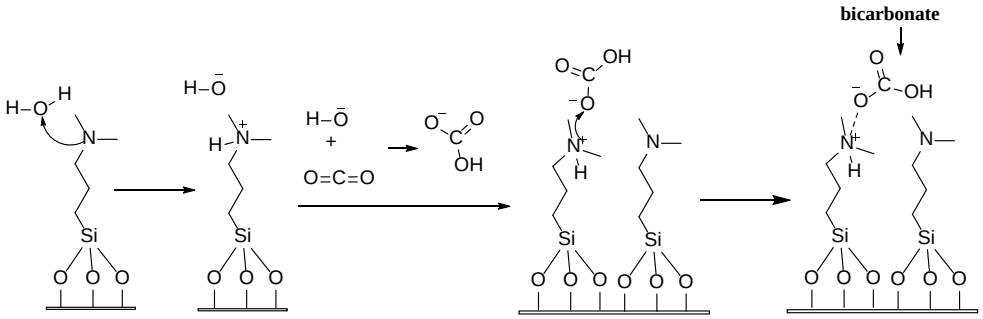

Figure 1.4. Reaction mechanism for CO_2 capture for tertiary amines in the presence of water. Manifold is also available for primary and secondary amines in the presence of water.

Currently, the mechanism for adsorption between amine-modified porous oxide adsorbents and H_2S is unclear; additionally, it is unclear how humidity, which varies substantially in different gas streams and in different regions of the world, affects H_2S adsorption. Although current technologies (liquid solutions, membranes) have benefited from years of research optimizing operating conditions and materials, the mechanism for H_2S adsorption in amine-adsorbent systems, notably between amine-modified mesoporous oxides and H_2S, is largely unknown. Also, the effects of water on H_2S adsorption are yet to be elucidated.

The interaction between solid-supported amines and H_2S may follow similar chemistry as in solution, corresponding to CO_2 adsorption/absorption theory considering the acid-base interactions that take place between both CO_2/H_2S and the amines.[19,59] So far, there are two proposed H_2S adsorption mechanisms: the formation of an H_2S-amine complex and a proton transfer mechanism. The latter mechanism is analogous to that observed in amine solution. [60,61] Figure 1.5 illustrates these H_2S adsorption mechanisms for a representative adsorbent. Figure 1.5 (a) illustrates a proton transfer between H_2S and NH_2 to form an ammonium ion (NH_3^+) and HS^- species, while Figure 1.5 (b) illustrates a hydrogen bonded H_2S-amine complex.

Although a few mechanisms have been proposed for H_2S absorption, there is limited research on the adsorption mechanism between H_2S and amines supported on solid adsorbents. In a study by the Chuang group, experimental IR and computational DFT calculations were used to elucidate the species formed during H_2S adsorption on tetraethylenepentamine (TEPA) thin films.[19] The formation of both a strongly bound ammonium ion (NH_3^+) and HS- species was observed, in addition to a weak hydrogen bonded amine complex to two amine molecules. Their work confirms that the adsorption chemistry between H_2S and amines on thin films are similar to those in solution, but very few studies discuss the adsorption mechanism for class 2 amines, which lack the translational mobility of amines in solution or in class 1 adsorbents.

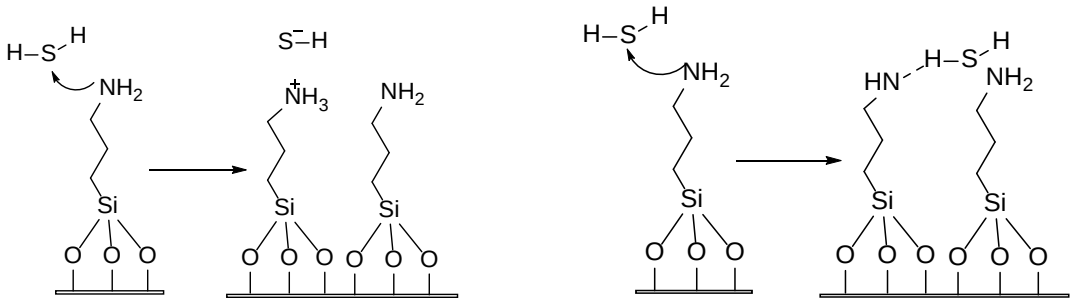

(a) Proton transfer (b) H_2S-amine complex

Figure 1.5. Proposed H_2S-amine reaction mechanism, suggested to be valid for primary, secondary and tertiary amines on solid adsorbents

1.2.3 Effect of Humidity

The presence of water vapor can act as a proton transfer agent in aqueous solutions[62] and because biogas contains up to 10% water vapor, it is crucial to assess its effects on solid-supported amines during H_2S capture.

Studies on H_2S capture using solid-supported sorbents have reported conflicting results on the effect of humidity. For example, a few studies using AC's have shown an increased H_2S adsorption capacity, when humidity is present.[63–65] Another study by Song et al. showed a

promoting effect of 3% water vapor on 50 wt% PEI/SBA-15. [66] To test the impact of moisture, H_2S adsorption was performed with a gas composition of 7300 ppmv of H_2S with 20% H_2 and 3% H_2O in N_2 at 22 °C. The H_2S saturation capacity increased from 2.53 mmol/g in dry conditions to 9.57 mmol/g in wet conditions. The authors posited several reasons behind the increase in H_2S capacity. First, they claimed that H_2S could absorb into the water film on the adsorbent, which will increases the H_2S capacity. Second, the amine-PEI interaction can change in the presence of water. Lastly, when PEI interacts with water, its flexibility increases, and this reduces diffusion limitations and enhances H_2S adsorption. In humid conditions, after three H_2S adsorption-desorption cycles, a 21% decrease in the H_2S adsorption capacity was reported. This reduction in cyclic H_2S capacity suggests that a higher regeneration temperature may be required for desorption, or the amine sites could degrade during H_2S adsorption, but this was not explored.

On the other hand, Huang et al. observed that humidity improved the CO_2-amine interaction on 3-aminpropytriethoxy-silane grafted MCM-48 and silica xerogel by examining TPD profiles and FTIR spectra, but no change was observed for H_2S. This finding was based on the claim that there was no change in the amount of H_2S desorbed in humid and dry conditions.[62] To provide more accurate information, quantitative results such as the H_2S adsorption capacity in the presence of humidity are required and are presented in this disserttaion.

The studies discussed above indicate that the presence of humidity could potentially impact the sorbent-H_2S interaction and should be assessed to determine the practicality of different sorbents for H_2S capture. In addition, the stability of adsorbents for H_2S capture in the presence of moisture is an area that has not been well studied and owing to the corrosive nature

of H_2S in humid conditions, it is important to assess the structural stability of varying sorbents under long term H_2S adsorption in humid gas streams.

1.3 Goals and Objectives

Silica supported amine adsorbents are promising materials for the removal of H_2S from gas mixtures based on their low regeneration temperatures unlike the use of aqueous amine solutions that require high energy for H_2S desorption due to the high heat capacity of water. This dissertation reports on a small family of amine-modified silica materials (class 2 adsorbents) for H_2S capture in both humid and dry conditions using single and multicomponent acid gas compositions. This work contributes to understanding the effects of amine type: primary, secondary and tertiary amines were studied; sterically hindered and unhindered amines were compared; and humid and dry streams were used in comprehensive studies of the adsorption of H_2S on amine-grafted mesoporous silica supports. Furthermore, the selective removal of H_2S was demonstrated in a complex, mixed gas stream, and adsorbent stability was assessed using simulated biogas streams. NMR was used to determine structural stability and *in situ* FTIR was used to identify the species that are formed during the interaction of H_2S with the supported amine materials, both in dry and humid conditions.

Chapter 2 reports on the efficacy of primary, secondary, and tertiary amine structures, as well as the effect of temperature and H_2S concentration, on the stability and regenerative ability of amine-oxide hybrid sorbents for H_2S capture. Here, the physicochemical characteristics of amines, specifically basicity and steric constraints, influence the H_2S adsorption capacity and stability at varying temperatures and concentrations. Chapter 3 reports investigations of the cyclic stability, H_2S selectivity and H_2S adsorption mechanism of sterically hindered amine

adsorbents in a simulated multicomponent biogas mixture using experimental and computational techniques. In Chapter 4, the effect of humidity on H_2S adsorption was investigated using silica supported sterically hindered secondary amine and an unhindered tertiary amine on a fixed-bed breakthrough adsorption system. Understanding the interaction of water with different amine-groups is essential to identify how different operating conditions might affect H_2S adsorption and desorption.

The structure-property relationships of the selected silica supported amines reported in this dissertation will help provide a detailed, fundamental understanding of how class 2 sorbents interact with H_2S at specific operating conditions. Furthermore, solid amine materials are also widely studied in membrane separations and in catalysis. The fundamental understanding of supported amine adsorbents is expected to impact the use of similar materials in membrane separations and catalysis. Additionally, this work will provide new information on amine-modified adsorbents for H_2S capture using materials that have been studied extensively for CO_2 capture.

1.4 References

(1) US Energy Information Administration. U.S. Crude Oil and Natural Gas Proved Reserves, 2011. **2013**, No. August, 1–54.

(2) US - Department of Labor and Statistics. The Effects of Shale Gas Production on Natural Gas Prices. *US - Dep. Labor Stat.* **2013**, *2* (13), 1–10.

(3) Gutierrez, J. P.; Ale Ruiz, E. L.; Erdmann, E. Energy Requirements, GHG Emissions and Investment Costs in Natural Gas Sweetening Processes. *J. Nat. Gas Sci. Eng.* **2017**, *38*, 187–194.

(4) NREL. *Biogas Potential in the United States*; **2013**.

(5) Favre, E.; Bounaceur, R.; Roizard, D. Biogas, Membranes and Carbon Dioxide Capture. *J.*

Memb. Sci. **2009**.

(6) Walker, S. B.; Sun, D.; Kidon, D.; Siddiqui, A.; Kuner, A.; Fowler, M.; Simakov, D. S. Upgrading Biogas Produced at Dairy Farms into Renewable Natural Gas by Methanation. *Int. J. Energy Res.* **2018**, 1–15.

(7) Gray T., R. Amine Scrubbing for CO_2 Capture. *Science (80-.).* **2010**, *325*, 1–28.

(8) Liu, G.; Cadiau, A.; Liu, Y.; Adil, K.; Chernikova, V.; Carja, I. D.; Belmabkhout, Y.; Karunakaran, M.; Shekhah, O.; Zhang, C. Enabling Fluorinated MOF-Based Membranes for Simultaneous Removal of H_2S and CO_2 from Natural Gas. *Angew. Chemie - Int. Ed.* **2018**, *57* (45), 14811–14816.

(9) Jagannathan N. Iyengar, Centreville, VA; David Perry, Alexandria, VA; Robert B. Fedich, Long Valley, N. Sulfur Recovery Plant Tail Gas Treatment Process, **2013**.

(10) Ünveren, E. E.; Monkul, B. Ö.; Sarıoğlan, Ş.; Karademir, N.; Alper, E. Solid Amine Sorbents for CO_2 Capture by Chemical Adsorption: A Review. 2017.

(11) Vilarrasa-García, E.; Cecilia, J. A.; Moya, E. M. O.; Cavalcante, C. L.; Azevedo, D. C. S.; Rodríguez-Castellón, E. "Low Cost" Pore Expanded SBA-15 Functionalized with Amine Groups Applied to CO_2 Adsorption. *Materials (Basel).* **2015**, *8* (5), 2495–2513.

(12) Sigot, L.; Fontseré Obis, M.; Benbelkacem, H.; Germain, P.; Ducom, G. Comparing the Performance of a 13X Zeolite and an Impregnated Activated Carbon for H_2S Removal from Biogas to Fuel an SOFC: Influence of Water. *Int. J. Hydrogen Energy* **2016**.

(13) Liu, J.; Wei, Y.; Li, P.; Zhao, Y.; Zou, R. Selective H_2S/CO_2 Separation by Metal-Organic Frameworks Based on Chemical-Physical Adsorption. *J. Phys. Chem. C* **2017**, *121* (24), 13249–13255.

(14) Joshi, J. N.; Zhu, G.; Lee, J. J.; Carter, E. A.; Jones, C. W.; Lively, R. P.; Walton, K. S. Probing Metal–Organic Framework Design for Adsorptive Natural Gas Purification. *Langmuir* **2018**, *34*, 8443–8450.

(15) Köchermann, J.; Schneider, J.; Matthischke, S.; Rönsch, S. Sorptive H_2S Removal by Impregnated Activated Carbons for the Production of SNG. *Fuel Process. Technol.* **2015**.

(16) Du, L.; Li, H.; Li, L.; Xu, J.; Li, Y. Investigation of Selective Desulfurization Performance of Sterically Hindered Amines. *Pet. Sci. Technol.* **2019**, *37* (1), 56–60.

(17) Bougie, F.; Iliuta, M. C. Sterically Hindered Amine-Based Absorbents for the Removal of CO_2 from Gas Streams. *J. Chem. Eng. Data* **2012**, *57* (3), 635–669.

(18) Sartorl, G.; Savage, D. W. Sterically Hindered Amines for CO_2 Removal from Gases. *Ind. Eng. Chem. Fundam.* **1983**, *22* (2), 239–249.

(19) Miller, D. D.; Chuang, S. S. C. The Effect of Electron-Donating Groups and Hydrogen

Bonding on H_2S Capture over Polyethylene Glycol/Amine Sites. *J. Phys. Chem. C* **2016**, *120* (2), 1147–1162.

(20) G.Sartori, W.S.Ho, D.W.Savage, G.R. Chludzinski, S. W. Sterically-Hindered Amines for Acid-Gas Absorption. *Sep. Purif. Methods* **1987**, *16*, 171–200.

(21) Guido Sartori, Linden; David W. Savage, Summit; Eugene L. Stogryn, Edison, all of N. J. Process for the Selective Removal of Hydrogen Sulfide from Gaseous Mixtures with Severely Sterically Hindered Secondary Aminoether Alcohols., 1983.

(22) Rezaei, F.; Rownaghi, A. a; Monjezi, S.; Lively, R. P.; Jones, C. W. SOx/NOx Removal from Flue Gas Streams by Solid Adsorbents: A Review of Current Challenges and Future Directions. *Energy & Fuels* **2015**, *2040* (x), 1–65.

(23) Ozekmekci, M.; Salkic, G.; Fellah, M. F. Use of Zeolites for the Removal of H_2S: A Mini-Review. *Fuel Processing Technology*. 2015.

(24) Bollini, P.; Didas, S. A.; Jones, C. W. Amine-Oxide Hybrid Materials for Acid Gas Separations. *J. Mater. Chem.* **2011**, *21* (39), 15100.

(25) Montes, D.; Tocuyo, E.; Gonzaĺez, E.; Rodriǵuez, D.; Solano, R.; Atencio, R.; Ramos, M. A.; Moronta, A. Reactive H_2S Chemisorption on Mesoporous Silica Molecular Sieve-Supported CuO or ZnO. *Microporous Mesoporous Mater.* **2013**, *168*, 111–120.

(26) Anbia, M, M. B. Novel Amine Modified Nanoporous SBA-15 Sorbent for the Removal of H_2S from Gas Streams in the Presence of CH_4. *Int. J. Eng., Trans.* **2014**, *27* (11), 1697–1704.

(27) Belmabkhout, Y.; Heymans, N.; De Weireld, G.; Sayari, A. Simultaneous Adsorption of H_2S and CO_2 on Triamine-Grafted Pore-Expanded Mesoporous MCM-41 Silica. *Energy & Fuels* **2011**, *25* (3), 1310–1315.

(28) Wilfong, W. C.; Kail, B. W.; Jones, C. W.; Pacheco, C.; Gray, M. L. Spectroscopic Investigation of the Mechanisms Responsible for the Superior Stability of Hybrid Class 1/Class 2 CO_2 Sorbents: A New Class 4 Category. *ACS Appl. Mater. Interfaces* **2016**, *8* (20), 12780–12791.

(29) Didas, S. A.; Choi, S.; Chaikittisilp, W.; Jones, C. W. Amine-Oxide Hybrid Materials for CO_2 Capture from Ambient Air. *Acc. Chem. Res.* **2015**, *48* (10), 2680–2687.

(30) Lee, J. J.; Sievers, C.; Jones, C. W. Silica-Supported Hindered Aminopolymers for CO_2 Capture . *Ind. Eng. Chem. Res.* **2019**.

(31) Xue, Q.; Liu, Y. Mixed-Amine Modified SBA-15 as Novel Adsorbent of CO_2 Separation for Biogas Upgrading. *Sep. Sci. Technol.* **2011**, *46* (4), 679–686.

(32) Bollini, P.; Brunelli, N. A.; Didas, S. A.; Jones, C. W. Dynamics of CO_2 Adsorption on Amine Adsorbents. 2. Insights Into Adsorbent Design. **2012**.

(33) Alkhabbaz, M. A.; Bollini, P.; Foo, G. S.; Sievers, C.; Jones, C. W. Important Roles of Enthalpic and Entropic Contributions to CO_2 Capture from Simulated Flue Gas and Ambient Air Using Mesoporous Silica Grafted Amines. *J. Am. Chem. Soc.* **2014**, *136* (38), 13170–13173.

(34) Didas, S. A.; Kulkarni, A. R.; Sholl, D. S.; Jones, C. W. Role of Amine Structure on Carbon Dioxide Adsorption from Ultradilute Gas Streams Such as Ambient Air. *ChemSusChem* **2012**, *5* (10), 2058–2064.

(35) Belmabkhout, Y.; Pillai, R. S.; Alezi, D.; Shekhah, O.; Pang, M.; Suetin, M.; Cairns, A. J.; Solovyeva, V. Metal – Organic Frameworks to Satisfy Gas Upgrading Demands : Fi Ne-Tuning the Soc-MOF Platform for the Operative Removal of H 2 S †. **2017**, 3293–3303.

(36) Drese, J. H.; Choi, S.; Lively, R. P.; Koros, W. J.; Fauth, D. J.; Gray, M. L.; Jones, C. W. Synthesis-Structure-Property Relationships for Hyperbranched Aminosilica CO_2 Adsorbents. *Adv. Funct. Mater.* **2009**, *19* (23), 3821–3832.

(37) Hicks, J. C.; Drese, J. H.; Fauth, D. J.; Gray, M. L.; Qi, G.; Jones, C. W. Designing Adsorbents for CO_2 Capture from Flue Gas-Hyperbranched Aminosilicas Capable of Capturing CO2 Reversibly. *J. Am. Chem. Soc.* **2008**, *130* (10), 2902–2903.

(38) Hammache, S.; Hoffman, J. S.; Gray, M. L.; Fauth, D. J.; Howard, B. H.; Pennline, H. W. Comprehensive Study of the Impact of Steam on Polyethyleneimine on Silica for CO_2 Capture. *Energy and Fuels* **2013**, *27* (11), 6899–6905.

(39) Wilfong, W. C.; Kail, B. W.; Gray, M. L. Rapid Screening of Immobilized Amine CO_2 Sorbents for Steam Stability by Their Direct Contact with Liquid H_2O. *ChemSusChem* **2015**, *8* (12), 2041–2045.

(40) J. Fauth, D.; L. Gray, M.; W. Pennline, H.; M. Krutka, H.; Sjostrom, S.; M. Ault, A. Investigation of Porous Silica Supported Mixed-Amine Sorbents for Post-Combustion CO_2 Capture. *Energy & Fuels* **2012**, *26* (4), 2483–2496.

(41) Sarazen, M. L.; A. Sakwa-Novak, M.; W. Ping, E.; W. Jones, C. Effect of Different Acid Initiators on Branched Poly(Propylenimine) Synthesis and CO_2 Sorption Performance. *ACS Sustain. Chem. & Eng.* **2019**, *7* (7), 7338–7345.

(42) Tsuda, T. and F. T. Polyethyleneimine and Macrocyclic Polyamine Silica Gels Acting as Carbon Dioxide Absorbents. **1992**, 1659–1661.

(43) Tsuda, T.; Fujiwara, T.; Taketani, Y.; Saegusa, T. Amino Silica Gels Acting as a Carbon Dioxide Absorbent. *Chemistry Letters*. 1992, pp 2161–2164.

(44) Bollini, P.; Didas, S. A.; Jones, C. W. Amine-Oxide Hybrid Materials for Acid Gas Separations. *J. Mater. Chem.* **2011**, 15100–15120.

(45) Wilfong, W. C.; Kail, B. W.; Jones, C. W.; Pacheco, C.; Gray, M. L. Spectroscopic Investigation of the Mechanisms Responsible for the Superior Stability of Hybrid Class

1/Class 2 CO_2 Sorbents: A New Class 4 Category. *ACS Appl. Mater. Interfaces* **2016**, *8* (20), 12780–12791.

(46) Choi, S.; Gray, M. L.; Jones, C. W. Amine-Tethered Solid Adsorbents Coupling High Adsorption Capacity and Regenerability for CO2capture from Ambient Air. *ChemSusChem* **2011**, *4* (5), 628–635.

(47) Sanz, R.; Calleja, G.; Arencibia, A.; Sanz-Pérez, E. S. Development of High Efficiency Adsorbents for CO_2 Capture Based on a Double-Functionalization Method of Grafting and Impregnation. *J. Mater. Chem. A* **2013**, *1* (6), 1956–1962.

(48) Wang, X.; Ma, X.; Xu, X.; Sun, L.; Song, C. Mesoporous-Molecular-Sieve-Supported Polymer Sorbents for Removing H_2S from Hydrogen Gas Streams. *Top. Catal.* **2008**, *49* (1–2), 108–117.

(49) Chu, X.; Cheng, Z.; Zhao, Y.; Xu, J.; Zhong, H.; Zhang, W.; Lü, J.; Zhou, S.; Zhu, F.; Zhou, Y.; et al. Study on Sorption Behaviors of H_2S by Triethanolamine-Modified Mesoporous Molecular Sieve SBA-15. *Ind. Eng. Chem. Res.* **2012**, *51* (11), 4407–4413.

(50) Xue, Q.; Liu, Y. Removal of Minor Concentration of H_2S on Mdea-Modified SBA-15 for Gas Purification. *J. Ind. Eng. Chem.* **2012**, *18* (1), 169–173.

(51) Xu, X.; Novochinskii, I.; Song, C. Low-Temperature Removal of H_2S by Nanoporous Composite of Polymer - Mesoporous Molecular Sieve MCM-41 as Adsorbent for Fuel Cell Applications. **2005**, No. 7, 2214–2215.

(52) Ma, X.; Wang, X.; Song, C. "Molecular Basket" Sorbents for Separation of CO_2 and H_2S from Various Gas Streams. *J. Am. Chem. Soc.* **2009**, *131* (13), 5777–5783.

(53) Quan, W.; Wang, X.; Song, C. Selective Removal of H_2S from Biogas Using Solid Amine-Based "Molecular Basket" Sorbent. *Energy and Fuels* **2017**, *31* (9), 9517–9528.

(54) Danon, A.; Stair, P. C.; Weitz, E. FTIR Study of CO_2 Adsorption on Amine-Grafted SBA-15: Elucidation of Adsorbed Species. *J. Phys. Chem. C* **2011**, *115* (23), 11540–11549.

(55) Shimon, D.; Chen, C. H.; Lee, J. J.; Didas, S. A.; Sievers, C.; Jones, C. W.; Hayes, S. E. ^{15}N Solid State NMR Spectroscopic Study of Surface Amine Groups for Carbon Capture: 3-Aminopropylsilyl Grafted to SBA-15 Mesoporous Silica. *Environ. Sci. Technol.* **2018**, *52* (3), 1488–1495.

(56) Chen, C. H.; Shimon, D.; Lee, J. J.; Didas, S. A.; Mehta, A. K.; Sievers, C.; Jones, C. W.; Hayes, S. E. Spectroscopic Characterization of Adsorbed $^{13}CO_2$ on 3-Aminopropylsilyl-Modified SBA-15 Mesoporous Silica. *Environ. Sci. Technol.* **2017**, *51* (11), 6553–6559.

(57) Lee, J. J.; Yoo, C.; Chen, C.; Hayes, S. E.; Sievers, C.; Jones, C. W. Silica-Supported Sterically Hindered Amines for CO_2 Capture. *Langmuir* **2018**, *34*, 12279–12292.

(58) Lee, J. J.; Chen, C. H.; Shimon, D.; Hayes, S. E.; Sievers, C.; Jones, C. W. Effect of

Humidity on the CO_2 Adsorption of Tertiary Amine Grafted SBA-15. *J. Phys. Chem. C* **2017**, *121* (42), 23480–23487.

(59) Waddington, J. D. C. and T. . Liquid Hydrogen Sulphide as an Ionising Solvent. Part I. Base Analogues and Their Neutralisation with Hydrogen Halides. *J. Am. Chem. Soc.* **1966**, *0*, 785–789.

(60) Huang, H. Y.; Yang, R. T.; Chinn, D.; Munson, C. L.; Yoosuk, B.; Wongsanga, T.; Prasassarakich, P.; Wang, X.; Ma, X.; Sun, L.; et al. Amine-Grafted MCM-48 and Silica Xerogel as Superior Sorbents for Acidic Gas Removal from Natural Gas. *Energy & Fuels* **2009**, *25* (23), 13275–13278.

(61) Jaiboon, V.; Yoosuk, B.; Prasassarakich, P. Amine Modified Silica Xerogel for H_2S Removal at Low Temperature. *Fuel Process. Technol.* **2014**, *128*, 276–282.

(62) Huang, H. Y.; Yang, R. T.; Chinn, D.; Munson, C. L. Amine-Grafted MCM-48 and Silica Xerogel as Superior Sorbents for Acidic Gas Removal from Natural Gas. *Ind. Eng. Chem. Res.* **2003**, *42* (10), 2427–2433.

(63) Bagreev, A.; Bandosz, T. J. On the Mechanism of Hydrogen Sulfide Removal from Moist Air on Catalytic Carbonaceous Adsorbents. *Ind. Eng. Chem. Res.* **2005**, *44* (3), 530–538.

(64) Adib, F.; Bagreev, A.; Bandosz, T. J. Effect of Surface Characteristics of Wood-Based Activated Carbons on Adsorption of Hydrogen Sulfide. *J. Colloid Interface Sci.* **1999**.

(65) Sitthikhankaew, R.; Chadwick, D.; Assabumrungrat, S.; Laosiripojana, N. Effects of Humidity, O_2, and CO_2 on H_2S Adsorption onto Upgraded and KOH Impregnated Activated Carbons. *Fuel Process. Technol.* **2014**, *124*, 249–257.

(66) Wang, X.; Ma, X.; Sun, L.; Song, C. A Nanoporous Polymeric Sorbent for Deep Removal of H_2S from Gas Mixtures for Hydrogen Purification. *Green Chem.* **2007**, *9* (6), 695.

CHAPTER 2. ROLE OF AMINE STRUCTURE ON HYDROGEN SULFIDE CAPTURE FROM DILUTE GAS STREAMS USING SOLID ADSORBENTS

Parts of this chapter are adapted from 'Okonkwo, N. C.; Okolie, C.; Sujan, A.; Zhu, G.; Jones, C. W. Role of Amine Structure on Hydrogen Sulfide Capture from Dilute Gas Streams Using Solid Adsorbents. *Energy & Fuels* **2018**, *32*, 6926-6933 with permission from The American Chemical Society.

2.1 Background

Biomass derived biogas is mainly composed of methane and can potentially supplement natural gas in regions with limited supply.[1,2]As an example, the methane supply from different biogas sources in the United States is about 7.9 million tonnes per year and can supplement 5% of natural gas in the electric power sector and 56% in the transportation sector. [3–5] However, upgrading biogas to renewable natural gas (RNG) to meet the same specifications as conventional natural gas requires the removal of impurities composed of 30-50% of carbon dioxide (CO_2) and 0-5% hydrogen sulfide (H_2S). H_2S is a highly poisonous, corrosive, flammable and explosive molecule[1] and is mitigated via chemical scrubbing, water scrubbing, pressure swing adsorption (PSA), and membrane based separation.[6] Liquid phase chemical scrubbing with amines is one of the major acid gas removal techniques. Limitations to this technique include high absorption regeneration costs, loss of amine via oxidative or other chemical degradation, and corrosion of the metallic components of the equipment due to the acidic nature of H_2S.[7] Adsorption on solid materials, on the other hand, is a potentially more

energy-efficient technique for both CO_2 and H_2S capture. This technique requires materials with high and stable adsorption capacity, as well as selectivity under mild conditions.[8]

Preliminary studies have shown that amine-modified adsorbents are promising materials for H_2S capture.[9–12] They have been explored for CO_2 capture over the years due to their rapid adsorption kinetics, low temperature operating conditions and regenerative capabilities.[13] We have defined three classes of amine-oxide hybrid adsorbents and two have been widely studied for CO_2 separation. Class 1 adsorbents are based on the physical impregnation of amines, often polyamines, into a porous support. class 2 adsorbents are based on the covalent grafting of small amine-containing molecules onto the surface of the support. An overview by Bollini et al. has described how these amine/oxide adsorbents can be applied to capture acid gases.[14]

This chapter considers the adsorption properties of primary, secondary and tertiary amine materials and seeks to identify the most promising amine type for H_2S capture. For CO_2 adsorption, it was determined that primary amines, with high heats of adsorption, show a greater amine efficiency (moles CO_2 captured per mole of amine) than secondary and tertiary amines.[15,16] However, similar information is not available for H_2S capture. Prior studies that explored the structure-property relationships of amine-oxide adsorbents for H_2S capture utilized polyamines, such as poly(ethyleneimine) (PEI), that contain a mixture of amines, including primary, secondary and tertiary amines.[8,9,1217–20] However, there is limited literature on the effects of specific amine types on H_2S capture. Abdouss et al.[21,22] explored how grafting three different aminosilanes with mono, di and tri amine structures on different support types (MCM-41, SBA-15, and UVM-7) would affect H_2S adsorption. Mono, di and tri amine materials were made using 3-aminopropyltriethoxysilane, N-[3-(trimethoxysilyl) propyl] ethylenediamine and (3-trimethoxysilylpropyl) diethylenetriamine, respectively. The work of Song et al.[23] also

explored primary, secondary and tertiary amines in class 1 adsorbents and this study showed that the tertiary class 1 amine material, tetramethyl hexanediamine supported on SBA-15 (TMHDA/SBA-15), was most suitable of the sorbents studied for the selective adsorption of H_2S in a highly concentrated CO_2 stream. However, the use of these class 1 adsorbents for H_2S capture can be limited by their slow kinetics, limited stability and incomplete regeneration. Class 1 adsorbents can also pose diffusion limitation through the aggregation and crosslinking of the polymers in the pores of the adsorbents, which lead to a slower rate of adsorption.[14]

Compared to class 1 adsorbents using polyamines, class 2 adsorbents have more open porosity, which is expected to lead to fewer diffusion limitations within the pores and improve the adsorption and desorption kinetics during H_2S capture.[14] The large surface area of the SBA-15 support employed will enable good control over the grafting of aminosilanes on the surface, allowing for the study of amine laoding such that only the amine type is varied from sample to sample. Hence, in this chapter, we explored how (i) the amine type: 3-aminopropyltrimethoxysilane (APS), (N-methylaminopropyl) trimethoxysilane (MAPS) and (N, N-dimethylaminopropyl) trimethoxysilane (DMAPS), (ii) adsorption temperature and (iii) H_2S concentration impact the performance and structure of these adsorbents. The stability and regenerability of these adsorbents after multiple cycles are also examined.

2.2 Experimental Section

2.2.1 Materials

The following chemicals were used as received from Sigma–Aldrich: Pluronic ((EO) 20(PO) 70(EO) 20)), tetraethyl orthosilicate (TEOS, 98%), hexane (BDH), methanol (ACS grade, >99.8%), toluene (ACS grade, >99.5%). For the grafting procedure, the following

chemicals from Gelest were used: 3-aminopropyltrimethoxysilane (APS), N-methylaminopropyl-trimethoxysilane (MAPS), 3-(N, N-dimethylaminopropyl)-trimethoxysilane (DMAPS). Specialty gases were purchased as a certified grade mixture from Airgas and include the following: 10% H_2S in N_2. Inert UHP nitrogen was also purchased from Airgas.

2.2.2 Material Synthesis

The synthesis of SBA-15 silica follows a previous procedure in literature;[24] this procedure was scaled up to produce 18 g of material. In a 2 L flask, 36 g of Pluronic P123 block copolymer ((EO) 20(PO) 70(EO) 20)) was dissolved in 180 mL of 12.1 M hydrochloric acid and 954 g of distilled water. The components were stirred for 3 h and 69.4 mL of tetraethyl orthosilicate (TEOS) was added dropwise to the aqueous mixture and stirred at 40 °C for 20 h, during which time a white precipitate was formed. The solution was heated to 100 °C and maintained for 24 h under constant stirring. The reaction was quenched with 400 mL of distilled water, and the white precipitate was filtered and washed with 4 L of distilled water. The filtered precipitate was dried overnight in an oven at 75 °C. The dried product was calcined in a calcination oven using the following temperature program: ramp to 200 °C at 1.2 °C/min, hold at 200 °C for 1 h, ramp to 550 °C at 1.2 °C/min, hold at 550 °C for 12 h, cool to room temperature at 10 °C/min. The calcined solid was then stored at room temperature in a jar before use.

2.2.3 Grafting of aminosilanes on SBA-15

First, SBA-15 was dried overnight in a vacuum line at 110 °C under a pressure of 10 mTorr. The silica, SBA-15, was then stirred with 200 mL toluene for a minimum of 1 hour after which 600 µL of DI water was added. The solution was equilibrated at room temperature for 3 hours. Next, to compare the three different structures, similar amine densities were grafted on the

surface of SBA-15; see Table 2.1 and Table 2.2 for nomenclature and amine loading values, respectively. Figure 2.1 shows the chemical structures of the aminosilanes used during this study. To obtain a similar amine density on SBA-15_DMAPS, more aminosilane was required, as the tertiary amine has the highest molecular weight of the three aminosilanes and it less effectively catalyzes its own surface grafting.[25,26] The solution was stirred at 85 °C for 24 h under nitrogen. The product was then filtered with 300 mL of toluene, 300 mL hexane and 300 mL methanol consecutively. The filtered product was dried under vacuum overnight at 75 °C under a pressure of 10 mTorr.

Table 2.1. Aminosilanes Used to Functionalize Silica Adsorbents

Aminosilane	Amine type	Sample name
3-aminopropyltrimethoxysilane (APS)	primary	SBA-15_APS
(N-methylaminopropyl) trimethoxysilane (MAPS)	secondary	SBA-15_MAPS
(N,N-dimethylaminopropyl) trimethoxysilane (DMAPS)	tertiary	SBA-15_DMAPS

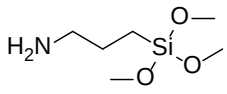

(3-Aminopropyl)trimethoxysilane

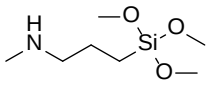

Trimethoxy[3-(methylamino)propyl]silane

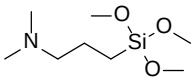

(N,N-Dimethylaminopropyl)trimethoxysilane

Figure 2.1. Chemical names and structures of aminosilanes used in this study

2.2.4 Material Characterization

The BET surface area, mean pore size, and pore volumes, were measured on a Micromeritics Tristar II at 77 K. To calculate the surface area and mean pore size from the isotherm data, the Brunauer-Emmett–Teller (BET) and Broekhoff-de Boer method with the

Frenkel-Halsey-Hill equation (BdB-FHH method)[27] were used. Elemental analyses (C,H,N,Si) were used to determine the amine loading of the functionalized materials. This analysis was performed by Galbraith Laboratories Inc. (Knoxville, TN, USA). ^{13}C CP-MAS solid-state NMR was performed on a Bruker DSX-300 spectrometer with a spinning frequency of 10 kHz. Powder X-ray diffraction patterns were obtained by using a PANalytical X-ray diffractometer using Cu Kα radiation. X-ray photoelectron spectroscopy (XPS) was performed on a Thermo K-alpha using Al X-ray source with binding energy of 1486.6 eV on adsorbent samples before and after H_2S adsorption.

2.2.5 Adsorption Measurements

A TA Instruments Q500 thermogravimetric analyzer (TGA) was used to measure dry H_2S adsorption capacities at different temperatures and H_2S concentrations. First, the adsorbent was pretreated in nitrogen at 120 °C for 2 h to remove adsorbed water or other impurities on the surface. The temperature was then set to the desired temperature and equilibrated in nitrogen for 10 min. The gas was then switched to H_2S for adsorption measurements until pseudo equilibrium was attained. The equilibrium time was dependent on the amine type and concentration of H_2S in the furnace, and the flowrate for all experiments was set to 90 mL/min. To obtain an adsorption isotherm at varying H_2S concentrations, the 10% H_2S in balance N2 was mixed with UHP nitrogen to obtain subsequent concentrations of 5%, 3.5%, 1% and 0.5%. Lastly, to determine the stability of these adsorbents, multiple adsorptions-desorption cycles were performed. To assess reproducibility, all experiments were repeated three times and the average adsorption capacities and amine efficiencies are shown below.

2.3 Results and Discussion

2.3.1 Textural Properties of Materials

The textural characteristics and amine loading of all materials used in this study, including the bare mesoporous silica support and amine-modified mesoporous support, are listed in Table 2.2**.** For the amine-grafted adsorbents, a reduction in pore size moving from SBA-15_APS to SBA-15_MAPS to SBA-15_DMAPS was observed, which can be attributed to their progressively bulkier head groups. The textural properties were studied by nitrogen physisorption at 77 K. Figure 2.2. Nitrogen adsorption/desorption isotherms at 77 K for bare and functionalized SBA-15 materials shows the N_2 physisorption isotherms of the materials, which are type IV isotherms with a hysteresis similar to those observed in the literature for SBA-15 materials.[28]

To determine the effect of amine types on H_2S adsorption and enable fair comparison between the adsorbents, the samples were synthesized with similar amine loadings. The grafting of amines on the support yields a decrease in the BET surface area and pore volume of the material, as expected. The functionalized supports all have similar surface areas and pore-volume. Figure 2.3 displays the X-ray diffraction pattern of the bare SBA-15 and amine-modified SBA-15 materials. The observed peaks are characteristic of the 2-D hexagonal structure of SBA-15, with a well ordered mesoporous structure.[29] The hexagonal structure of SBA-15 was maintained after grafting with amines, as these reflection peaks were not displaced. On the other hand, a change in the peak intensity was observed after the grafting of APS, MAPS and DMAPS on SBA-15. For example, SBA-15_MAPS and SBA-15_DMAPS had similar peak

intensities, but a larger peak change was observed for the SBA-15_APS adsorbent, which was reproducible in multiple batches.

Table 2.2. Structural Properties of Amine-Modified Silica Adsorbents

Sample	Amine loading mmol (N/g silica)	Surface area (m^2 /g)	Mean pore size (nm)	Pore volume (cm^3/g)	Mesopore volume (cm^3/g)
SBA-15	-	796	6.0	1.20	1.15
SBA-15_APS	2.0	399	5.7	0.67	0.67
SBA-15_MAPS	2.0	392	5.5	0.67	0.67
SBA-15_DMAPS	1.7	454	5.3	0.70	0.70

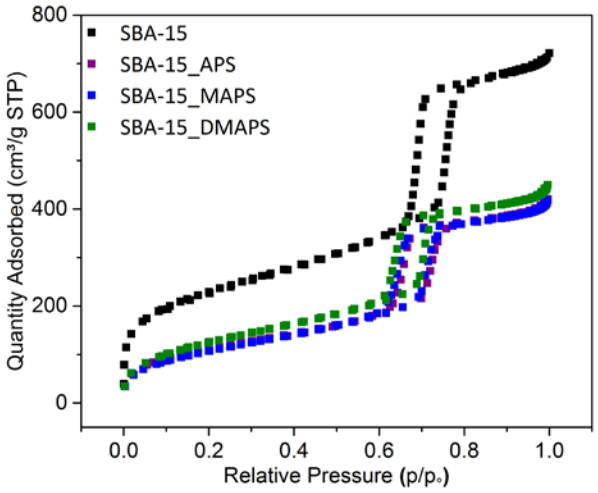

Figure 2.2. Nitrogen adsorption/desorption isotherms at 77 K for bare and functionalized SBA-15 materials

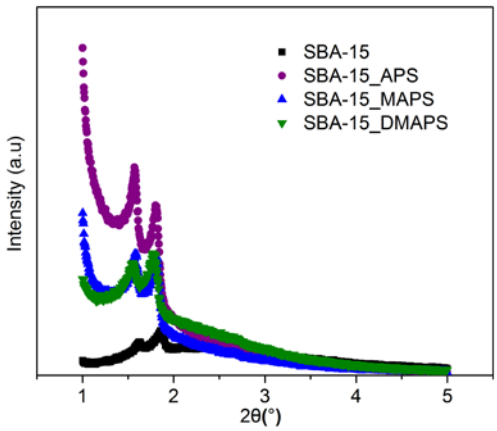

Figure 2.3. Low angle X-ray diffraction patterns for bare and functionalized SBA-15 materials.

.

2.3.2 Baseline H_2S Adsorption Performance

Two control experiments were performed to ensure accuracy of H_2S uptake measurements. First, to ensure no significant influence of the diluent gas in the H_2S in N_2 gas mixture, adsorption studies were performed using UHP N_2 and negligible adsorption capacities were observed. Secondly, H_2S adsorption experiments were performed on bare SBA-15 and there was no appreciable adsorption of H_2S at the operating conditions explored.

2.3.3 Impact of Amine Type on Cyclic Stability

The cyclic stability of an adsorbent upon repeated exposure to H_2S is important to improve the efficiency of the separation process. To this end, the structure and performance of SBA-15_APS, SBA-15_MAPS and SBA-15_DMAPS were evaluated after multiple adsorption-desorption cycles. Specifically, both the adsorption performance and the cyclic stability of these adsorbents were assessed to determine the effect of amine type on the efficacy of H_2S capture.

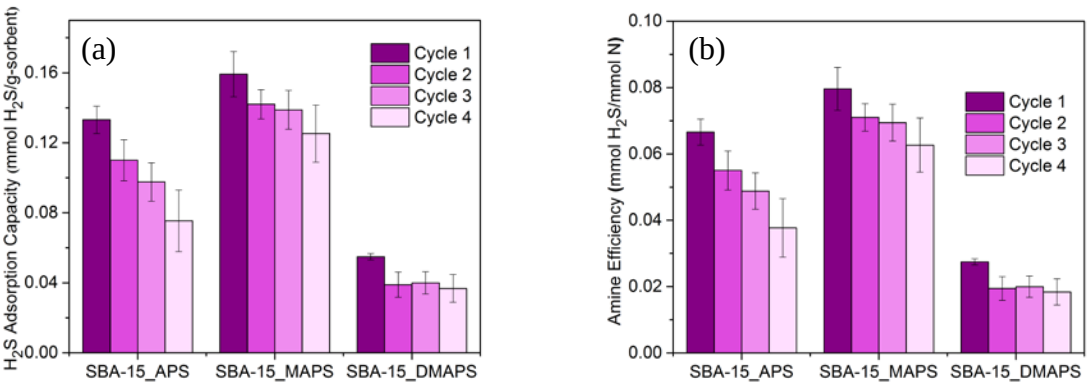

Figure 2.4. H_2S (a) adsorption capacities and (b) amine efficiencies of amine-modified adsorbents over four adsorption-desorption cycles using 1% H_2S in N_2 and 30 °C
error bars from standard deviation of three runs

Figure 2.4 (a) shows the adsorption capacity and cyclic stability of these amine-modified adsorbents in 1% H_2S in N_2 at 30°C. SBA-15_MAPS showed the highest adsorption capacity of 0.16 mmol H_2S/g sorbent and SBA-15_DMAPS showed the lowest adsorption capacity of 0.055 mmol H_2S/g. Figure 2.4 (b) shows the amine efficiency of the adsorbents, with the highest efficiency for SBA-15_MAPS at 0.08 mmol H_2S/mmol N. The adsorbents used for this study had low H_2S uptake but good stability for H_2S capture compared to the literature. [11,19,26] For all amine types, the most significant decrease in H_2S adsorption capacity occurred after the first cycle due to the strong binding of H_2S on the amine sites, and in subsequent cycles the materials remained relatively stable. A total capacity loss of 12% and 5% between cycles 2-4 was calculated for SBA-15_MAPS and SBA-15_DMAPS, respectively. Conversely, SBA-15_APS had more modest stability, with a 35% loss in H_2S adsorption capacity between cycles 2-4. Thus, further adsorption experiments were focused on SBA-15_MAPS and SBA-15_DMAPS sorbents because of their relatively higher adsorption capacity and cyclic stability.

The basicity and steric hindrance of amine moieties influence their stability and adsorption capacities in the presence of H_2S.[31,32] In solution, the strong basicity of secondary amines leads to a higher adsorption capacity as a result of the stronger H_2S-amine interactions. For tertiary amines, the inductive effect of the 3 alkyl groups leads to increased stability but lower basicity, which corresponds to the low adsorption capacity and increased stability for tertiary amines.[31,32]

Figure 2.5 shows the weight change of SBA-15_MAPS and SBA-15_DMAPS during cyclic adsorption with 10% H_2S in N_2 at 30°C in a TGA. The drop in the baseline during desorption can likely be attributed to the loss in trace adsorbed water over multiple cycles. At high H_2S concentrations, SBA-15-MAPS showed relatively stable cyclic performance after 4 cycles with a total H_2S capacity of 0.3 mmol H_2S/ g sorbent. The cyclic capacity loss is comparable to what was observed at lower H_2S concentrations, which confirms the good stability of secondary amine adsorbents for H_2S capture. The SBA-15_DMAPS had an adsorption capacity of 0.15 mmol H_2S/ g sorbent with relatively good stability at 10% H_2S concentration as well.

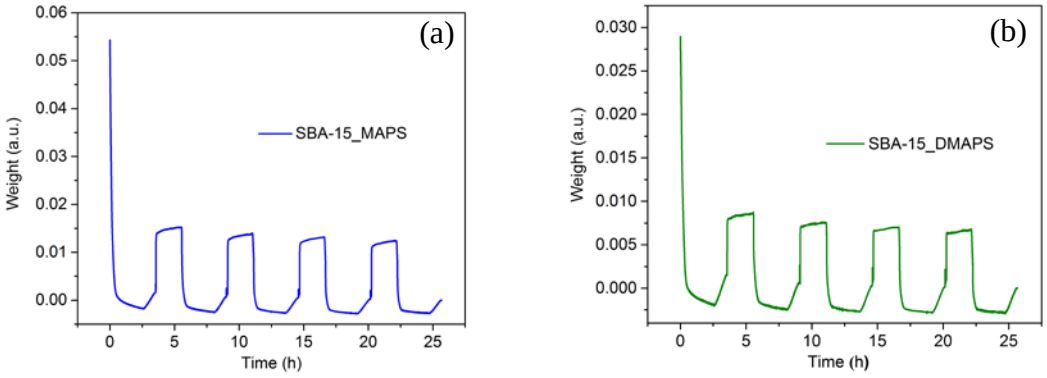

Figure 2.5. Cyclic performance of (a) SBA-15_MAPS and (b) SBA-15_DMAPS at 10% H_2S in N_2 and 30 °C

2.3.4 Effect of Adsorption Temperature

To determine the effect of temperature on the adsorption performance and amine efficiency of these amine-modified materials, measurements were performed at different adsorption temperatures. The H_2S adsorption capacities and amine efficiencies for SBA-15_MAPS and SBA-15_DMAPS with similar amine loadings are shown in Figure 2.6 (a) and Figure 2.6 (b) at three temperatures (30, 50, and 60) for MAPS and 4 temperatures of (30, 50, 60 and 75°C) for DMAPS using 10% H_2S in N_2 flowing at 90 mL/min. At the higher temperature of 75 °C, SBA-15_MAPS displayed a slow, linear increase in adsorption capacity over time. This prolonged time to reach equilibrium did not provide suitable operating conditions to obtain adsorption isotherms and hence, the results at this temperature for this sample are not shown.

From the plots, it can be seen that an increase in temperature led to a decrease in H_2S adsorption capacity and efficiency, as expected from thermodynamics. The MAPS adsorbent with an amine loading of 2.0 mmol N/g (SBA-15_MAPS) showed an H_2S capacity decrease from 0.36 to 0.28 and 0.27 mmol H_2S/g when the temperature was increased from 30 to 50 to 60 °C respectively. The DMAPS adsorbent with an amine loading of 1.7 mmol of N/g showed a H_2S capacity decrease from 0.2 mmol/g at 30 °C to a low capacity of 0.09 mmol/g at 75 °C. The amine efficiency for MAPS and DMAPS showed a similar trend as temperature increased. From these plots, the optimal operating temperature for these adsorbents to yield high capacities and amine efficiencies in the range studied appears to be 30 °C, which indicates that a lower temperature favors H_2S adsorption, as has been observed in other studies using dynamic adsorption methods.[19,23]

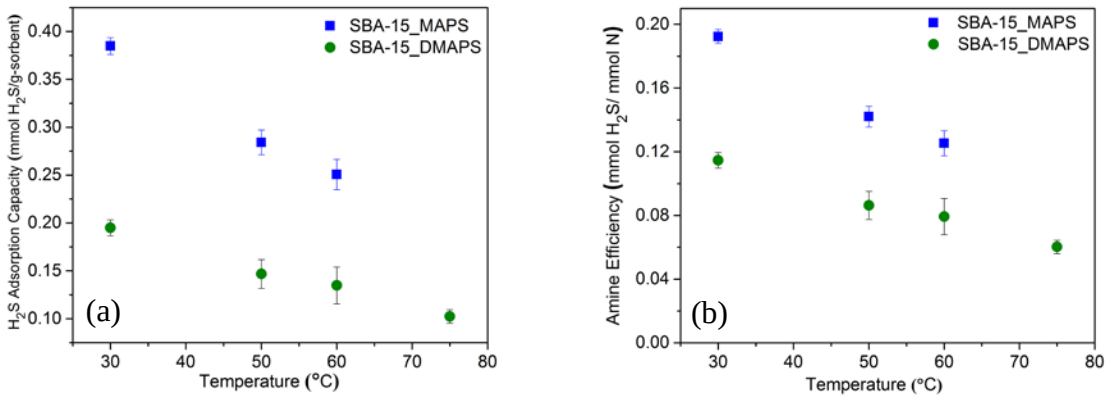

Figure 2.6. (a) H_2S adsorption capacity (b) amine efficiency of secondary and tertiary amine adsorbents at different temperatures using 10% H_2S in N_2
error bars from standard deviation of three runs

2.3.5 Effect of H_2S Concentration

Figure 2.7 (a) and Figure 2.7 (b) shows the H_2S adsorption capacities and amine efficiencies of the secondary and tertiary amine adsorbents with comparable amine loadings after exposure to 0-10% H_2S in N_2 at 30 °C. The plots indicate a significant increase in H_2S capacities with H_2S concentration at these low partial pressures, as expected. The SBA-15_MAPS sample containing secondary amines had the highest affinity toward H_2S at H_2S concentrations from 0.5-10% while SBA-15_DMAPS, the tertiary amine adsorbent, showed the lowest capacity for H_2S. At 0.5% H_2S, the H_2S capacity of SBA-15_MAPS material was 0.07 mmol H_2S/g sorbent and with further increase to 10% H_2S, the adsorption capacity increased to 0.4 mmol H_2S/g sorbent, which is twice the capacity of SBA-15_DMAPS at 10% H_2S in N_2.

Additionally, an increase in amine efficiency from 0.07 to 0.2 mmol H_2S/mmol N and 0.03 to 0.1 mmol H_2S /mmol N was observed for SBA-15_MAPS and SBA-15_DMAPS, respectively. At dilute H_2S concentrations, SBA-15_MAPS had four times the amine efficiency of SBA-15_DMAPS and at higher gas concentrations of 3.5-10%, the amine efficiency of SBA-

15_MAPS was twice that of SBA-15_DMAPS. In comparison, Song et. al., [19] assessed the effect of different H_2S concentrations (2000-6000 ppmv) on 50 wt% PEI/SBA-15, which contains primary, secondary and tertiary amines, using a fixed bed. The saturation capacities varied from 1.5-2.38 mmol H_2S/g sorbent for this class 1 amine material. The higher adsorption capacity can be attributed to the presence of a higher density of amine molecules, which is generally advantageous unless it leads to diffusion limitations and lower amine efficiencies at higher amine loadings.

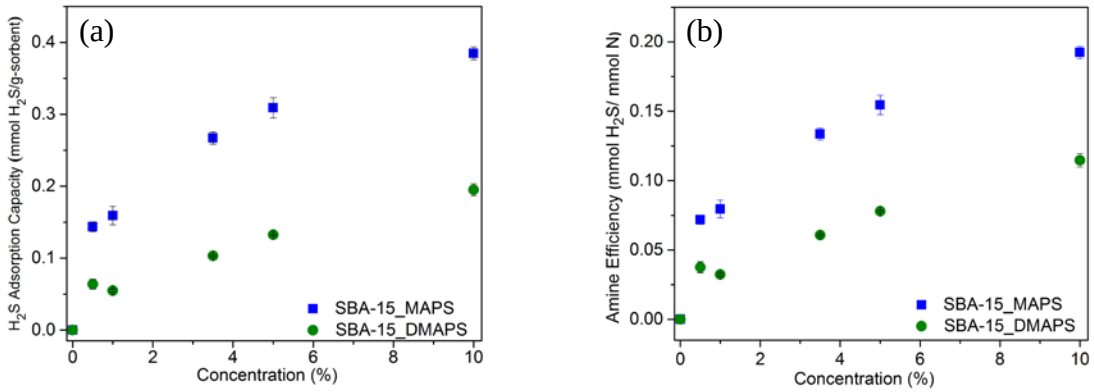

Figure 2.7. (a) H_2S adsorption capacity (b) amine efficiency of secondary and tertiary amines at different H_2S concentrations and 30 °C *error bars from standard deviation of three runs*

2.3.6 Estimated Heats of Adsorption

The measured adsorption isotherms were fit using the temperature dependent Toth isotherm, which has been typically used for heterogeneous materials in both high and low pressure ranges. [33,34] Figure 2.8 shows the adsorption isotherms, displayed in the form of adsorption capacities and amine efficiencies, for H_2S adsorption using SBA-15_MAPS and SBA-15_DMAPS under dry operating conditions. An increase in temperature led to a reduction in adsorption capacity, which is typical for exothermic adsorption events. At low temperatures,

the interaction of H_2S with SBA-15_MAPS was more sensitive to a change in temperature compared to SBA-15_DMAPS, which showed more sensitivity at higher temperatures.

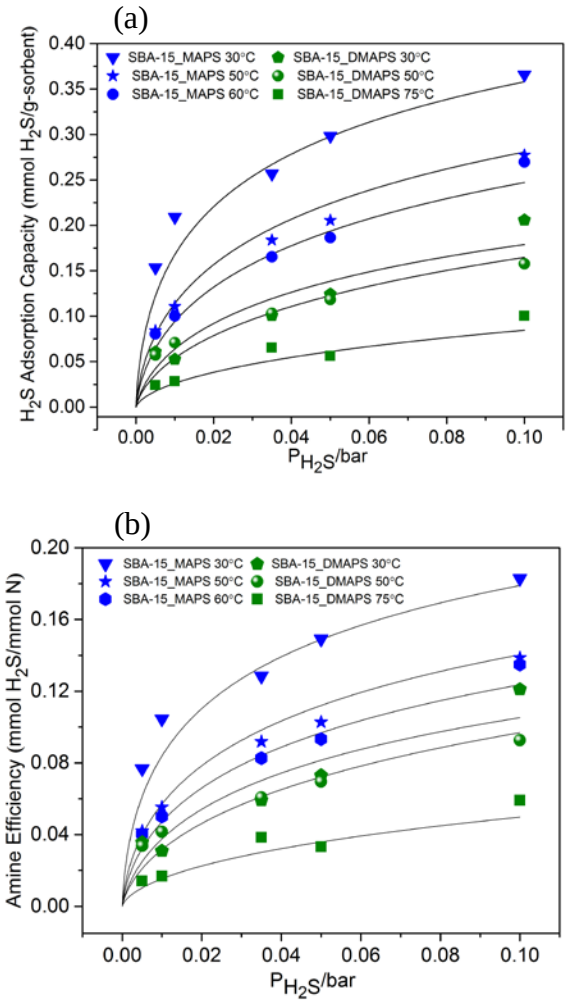

Figure 2.8. (a) H_2S adsorption isotherms (b) amine efficiency of secondary and tertiary amines at different temperatures

Figure 2.9 shows the isosteric heats of adsorption as a function of H_2S surface coverage calculated using the fitted isotherms. At zero surface coverage the isosteric heats were calculated to be ~45 and ~35 kJ/mol for the SBA-15_MAPS and SBA-15_DMAPS, respectively. The tertiary amine containing SBA-15_DMAPS, showed a higher heat of adsorption compared to the tertiary class 1 amine, TMHDA/SBA-15, studied by the Song group, which had a low heat

of adsorption of 15.4 kJ/mol. [23] Comparing the adsorption capacities, it is observed that at a H_2S concentration of 0.5%, the H_2S adsorption capacity at 50 °C is three times higher for SBA-15_DMAPS compared to TMHDA/SBA-15, but that could also be a result of the presence of CO_2 in the gas mixture in the latter case. A solution study using diethanolamine (DEA) and methyl diethanolamine (MDEA), which are secondary and tertiary amines, respectively, showed that the strong basicity of secondary amines led to a higher heat of adsorption.[32] A comparison of measured and calculated heats of (ab,ad)sorption in liquids and solid sorbents, respectively, are shown in Table 2.3. Isosteric heat of amine containing molecules for H_2S capture, which shows comparable isosteric heats for secondary and tertiary amines in solution to those calculated for the adsorbents used in this study.

Table 2.3. Isosteric heat of amine containing molecules for H_2S capture

	Amine	**Amine type**	**Weight (%)**	**Heat absorption/ adsorption (kJ/mol)**	**Reference**
liquid	DEA	secondary	35	40	[32]
solid	MAPS	secondary	2.8	45	this study
liquid	MDEA	tertiary	35	36	[32]
solid	DMAPS	tertiary	2.4	35	this study

The results obtained here show higher heats of adsorption at low surface coverages for SBA-15_MAPS compared to SBA-15_DMAPS, as expected from the higher H_2S uptake and amine efficiencies of SBA-15_MAPS. Hence, SBA-15_MAPS containing secondary amines would be more efficient for adsorption at dilute H_2S concentrations.[35]

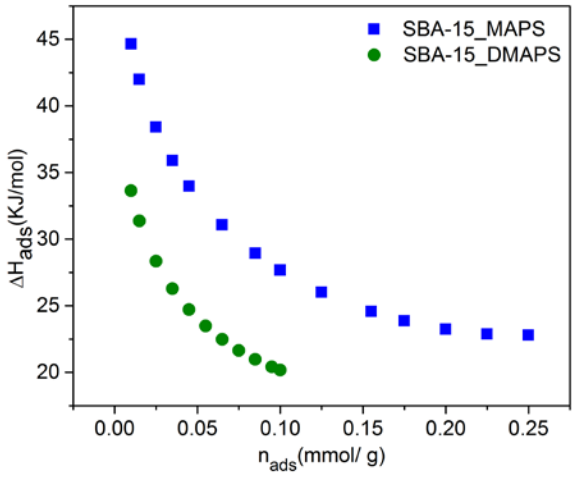

Figure 2.9. Isosteric heat of adsorption for H_2S on secondary and tertiary amine-modified mesoporous oxides

After the adsorption studies, the H_2S exposed samples were characterized ex-situ using an array of techniques to probe for possible material structure or textural property changes. Using ^{13}C MAS NMR the nature of the different carbon species in the amine adsorbents was probed with the expectation of potentially observing interactions between the C-N functional group and H_2S.[36] However, no visible changes in the NMR spectra were observed, suggesting no changes in the carbon species present in the aminosilane structure, as shown in **Fig. A-1**. XPS was used to probe for the presence of elemental sulfur after H_2S capture in 10% H_2S in N_2 at 30 °C. The XPS data did not show the formation of any sulfur peaks, as shown in **Fig. A-2**, though it should be noted that this may be due to the significant vacuum pretreatment required for the samples before analysis, which might remove any trapped H_2S.

Lastly, to test the limits of the cyclic stability of these amine-modified adsorbents, ten adsorption-desorption cycles were performed. After exposure to H_2S for ten cycles at 10% H_2S in N_2 and 30 °C, there was a significant drop in the H_2S adsorption capacity for SBA-15_APS

and SBA-15_MAPS functionalized materials, but SBA-15_DMAPS remained relatively stable in comparison, as shown in **Fig. 2.10**.

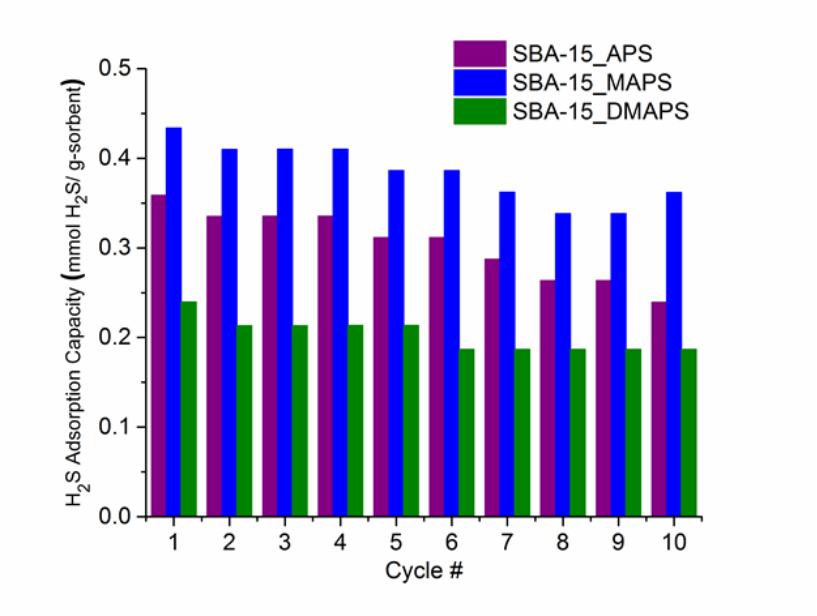

Figure 2.10. Adsorption capacities for SBA-15_APS, SBA-15_MAPS and SBA-15_DMAPS over 10 cycles of adsorption and desorption at 10% H_2S in N_2 and 30 °C.

To determine if a loss of amine content could lead to the drop in adsorption capacity after ten cycles, the combustible mass of the adsorbents was measured via oxidation in a TGA after H_2S exposure. **Fig. 2.11** displays the normalized weights before and after H_2S capture. The minimal difference in weight loss confirms that SBA-15_DMAPS is the most stable adsorbent even after ten cycles, with the greatest difference in weight loss after H_2S exposure observed for SBA-15_APS (**Fig. 2.11 (a)**).

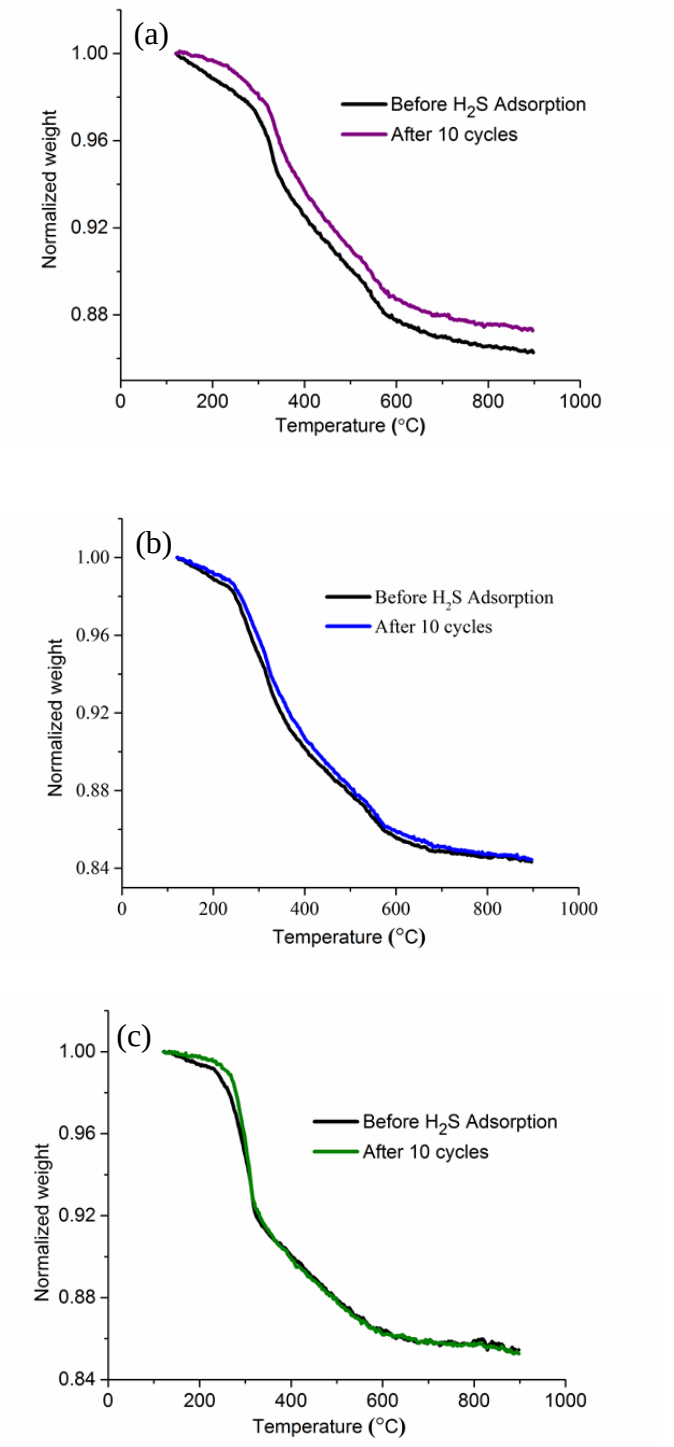

Figure 2.11. Normalized weight of (a) SBA-15_APS (b) SBA-15_MAPS (c) SBA-15_DMAPS after 10 cycles of adsorption and desorption at 10% H_2S in N_2 and 30 °C *normalized weight to 120 °C*

2.4 Conclusion

The adsorption performance and cyclic stability of three amine-modified adsorbents with similar amine loadings have been examined for H_2S capture at different temperatures and concentrations. Under the experimental conditions explored, SBA-15_MAPS adsorbed the most H_2S while SBA-15_DMAPS adsorbed smaller amounts of H_2S. SBA-15_APS had moderate H_2S uptake. While SBA-15_MAPS adsorbed the most H_2S, it was not the most robust material, with the cyclic stability of SBA-15_DMAPS at both high and low H_2S concentrations being more robust than the other two samples.

The adsorption isotherms and calculated isosteric heats of adsorption suggests that SBA-15_MAPS containing secondary amines is the most efficient for the capture of H_2S in dilute concentrations owing to its higher protonation energy. On the other hand, SBA-15_DMAPS containing tertiary amines may be most efficient for H_2S adsorption at higher H_2S concentrations. To obtain high adsorption capacities, a low temperature of 30 °C is suitable for both low and high concentration conditions. Further studies on the role of amine loading and the impact of CO_2 and other biogas components during H_2S capture are required to allow the design of high performing adsorbents for H_2S capture, and these parameters may be explored for class 2 adsorbents in our future work.

2.5 References

(1) Toledo-Cervantes, A.; Estrada, J. M.; Lebrero, R.; Muñoz, R. A Comparative Analysis of Biogas Upgrading Technologies: Photosynthetic vs Physical/chemical Processes. *Algal Res.* **2017**, *25*, 237–243.

(2) Walker, S. B.; Sun, D.; Kidon, D.; Siddiqui, A.; Kuner, A.; Fowler, M.; Simakov, D. S. Upgrading Biogas Produced at Dairy Farms into Renewable Natural Gas by Methanation. *Int. J. Energy Res.* **2018**, *42* (4), 1714-1728.

(3) American Gas Association. Preliminary Findings Concerning Natural Gas Reserves; 2017.

(4) US - Department of Labor and Statistics. The Effects of Shale Gas Production on Natural Gas Prices. *US - Dep. Labor Stat.* **2013**, *2* (13), 1–10.

(5) NREL. *Biogas Potential in the United States*; **2013**.

(6) Grande, C. A. Biogas Upgrading by Pressure Swing Adsorption. In *Biofuel's Engineering Process Technology*; **2011**; pp 65–84.

(7) Xue, Q.; Liu, Y. Removal of Minor Concentration of H_2S on MDEA-Modified SBA-15 for Gas Purification. *J. Ind. Eng. Chem.* **2012**, *18* (1), 169–173.

(8) Belmabkhout, Y.; De Weireld, G.; Sayari, A. Amine-Bearing Mesoporous Silica for CO_2 and H_2S Removal from Natural Gas and Biogas. *Langmuir* **2009**, *25* (23), 13275–13278.

(9) Ma, X.; Wang, X.; Song, C. "Molecular Basket" Sorbents for Separation of CO_2 and H_2S from Various Gas Streams. *J. Am. Chem. Soc.* **2009**, *131* (13), 5777–5783.

(10) Huang, Y. H.; Yang, R. T.; Chinn, D.; Munson, L. M. Amine-Grafted MCM-48 and Silica Xerogel as Superior Sorbents for Acidic Gas Removal from Natural Gas. *Ind. Eng. Chem. Res.* **2003**, *42*, 2427–2433.

(11) Anbia, M.; Babaei, M. Novel Amine Modified Nanoporous SBA-15 Sorbent for the Removal of H_2S from Gas Streams in the Presence of CH_4. *Int. J. Eng., Trans.* **2014**, *27* (11), 1697–1704.

(12) Belmabkhout, Y.; Heymans, N.; De Weireld, G.; Sayari, A. Simultaneous Adsorption of H_2S and CO_2 on Triamine-Grafted Pore-Expanded Mesoporous MCM-41 Silica. *Energy & Fuels* **2011**, *25* (3), 1310–1315.

(13) Rezaei, F.; Jones, C. W. Stability of Supported Amine Adsorbents to SO_2 and NO_X in Postcombustion CO_2 Capture. 2. Multicomponent Adsorption. *Ind. Eng. Chem. Res.* **2014**, *53*, 12103–12110.

(14) Bollini, P.; Didas, S. A.; Jones, C. W. Amine-Oxide Hybrid Materials for Acid Gas Separations. *J. Mater. Chem.* **2011**, 15100–15120.

(15) Didas, S. A.; Kulkarni, A. R.; Sholl, D. S.; Jones, C. W. Role of Amine Structure on Carbon Dioxide Adsorption from Ultradilute Gas Streams such as Ambient Air. *ChemSusChem* **2012**, *5* (10), 2058–2064.

(16) Didas, S. A.; Choi, S.; Chaikittisilp, W.; Jones, C. W. Amine-Oxide Hybrid Materials for CO_2 Capture from Ambient Air. *Acc. Chem. Res.* **2015**, *48* (10), 2680–2687.

(17) Chen, Q.; Fan, F.; Long, D.; Liu, X.; Liang, X.; Qiao, W. Poly (Ethyleneimine) -Loaded Silica Monolith with a Hierarchical Pore Structure for H_2S Adsorptive Removal. *Ind. Eng. Chem. Res.* **2010**, *49*, 11408–11414.

(18) Wang, X.; Ma, X.; Xu, X.; Sun, L.; Song, C. Mesoporous-Molecular-Sieve-Supported Polymer Sorbents for Removing H_2S from Hydrogen Gas Streams. *Top. Catal.* **2008**, *49* (1–2), 108–117.

(19) Wang, X.; Ma, X.; Sun, L.; Song, C. A Nanoporous Polymeric Sorbent for Deep Removal of H_2S from Gas Mixtures for Hydrogen Purification. *Green Chem.* **2007**, *9* (6), 695.

(20) Jaiboon, V.; Yoosuk, B.; Prasassarakich, P. Amine Modified Silica Xerogel for H_2S Removal at Low Temperature. *Fuel Process. Technol.* **2014**, *128*, 276–282.

(21) Abdouss, M.; Hazrati, N.; Miran Beigi, A. A.; Vahid, A.; Mohammadalizadeh, A. Effect of the Structure of the Support and the Aminosilane Type on the Adsorption of H_2S from Model Gas. *RSC Adv.* **2014**, *4* (12), 6337–6345.

(22) Shah, M. S.; Tsapatsis, M.; Siepmann, J. I. Hydrogen Sulfide Capture: From Absorption in Polar Liquids to Oxide, Zeolite, and Metal-Organic Framework Adsorbents and Membranes. *Chem. Rev.* **2017**, *117* (14), 9755–9803.

(23) Quan, W.; Wang, X.; Song, C. Selective Removal of H_2S from Biogas Using Solid Amine-Based "molecular Basket" Sorbent. *Energy and Fuels* **2017**, *31* (9), 9517–9528.

(24) Moschetta, E. G.; Sakwa-Novak, M. A.; Greenfield, J. L.; Jones, C. W. Post-Grafting Amination of Alkyl Halide-Functionalized Silica for Applications in Catalysis, Adsorption, and ^{15}N NMR Spectroscopy. *Langmuir* **2015**, *31* (7), 2218–2227.

(25) White, L. D.; Tripp, C. P. An Infrared Study of the Amine-Catalyzed Reaction of Methoxymethyasilanes with Silica. *J. Colloid Interface Sci.* **2000**, *227* (1), 237–243.

(26) Kanan, S. M.; Tze, W. T. Y.; Tripp, C. P. Method to Double the Surface Concentration and Control the Orientation of Adsorbed (3-Aminopropyl)dimethylethoxysilane on Silica Powders and Glass Slides. *Langmuir* **2002**, *18* (17), 6623–6627.

(27) Ravikovitch, P. I.; Neimark, A. V. Characterization of Micro- and Mesoporosity in SBA-15 Materials from Adsorption Data by the NLDFT Method. *J. Phys. Chem. B* **2001**, *105* (29), 6817–6823.

(28) Rezaei, F.; Sakwa-Novak, M. A.; Bali, S.; Duncanson, D. M.; Jones, C. W. Shaping Amine-Based Solid CO_2 adsorbents: Effects of Pelletization Pressure on the Physical and Chemical Properties. *Microporous Mesoporous Mater.* **2015**, *204* (C), 34–42.

(29) Li, Q. F.; Yue, D.; Lu, W.; Zhang, X.; Li, C.; Wang, Z. Hybrid Luminescence Materials Assembled by [Ln(DPA) 3]3-and Mesoporous Host through Ion-Pairing Interactions with High Quantum Efficiencies and Long Lifetimes. *Sci. Rep.* **2015**, *5*, 1–9.

(30) Hongyun,Y.; Tatarchuk, B. Novel-Doped Zinc Oxide Sorbents for Low Temperature Regenerable Desulfurization Applications. *AIChE* **2010**, *56* (11), 2898–2904.

(31) Hall, H. K. Correlation of the Base Strengths of Amines. *J. Am. Chem. Soc.* **1957**, *79* (20), 5441–5444.

(32) Bullin, J. A.; Polasek, J. C.; Fitz, C. W. The Impact of Acid Gas Loading on the Heat of Absorption and VOC and Btex Solubility in Amine Sweetening Units. *Proceedings, Annu. Conv. - Gas Process. Assoc.* **2007**, *1*, 385–399.

(33) Do, D. D. Adsorption Analysis: Equilibria and Kinetics. *In Adsorption Analysis: Equilibria and Kinetics;* Imperial College Press: London, U.K, 1998.

(34) Alkhabbaz, M. A.; Bollini, P.; Foo, G. S.; Sievers, C.; Jones, C. W. Important Roles of Enthalpic and Entropic Contributions to CO_2 Capture from Simulated Flue Gas and Ambient Air Using Mesoporous Silica Grafted Amines. *J. Am. Chem. Soc.* **2014**, *136* (38), 13170–13173.

(35) Lively, R. P.; Realff, J. M. On Thermodynamic Separation Efficiency: Adsorption Processes. *AIChE* **2016**, *62* (10), 3699–3705.

(36) Darbeau, R. Nuclear Magnetic Resonance (NMR) Spectroscopy: A Review and a Look at Its Use as a Probative Tool in Deamination Chemistry. *Appl. Spectrosc. Rev.* **2006**, *41* (4), 401–425.

CHAPTER 3. SELECTIVE REMOVAL OF HYDROGEN SULFIDE FROM SIMULATED BIOGAS STREAMS USING STERICALLY HINDERED AMINE ADSORBENTS

Parts of this chapter are adapted from 'Okonkwo, N. C.; Lee, J. J.; De Vylder, A.; Chiang, Y.; Joris W. Thybaut; Jones, C. W. Selective removal of hydrogen sulfide from simulated biogas streams using sterically hindered amine adsorbents. Chemical Engineering Journal **2020**, 379, 122349 with permission from Elsevier.

All computational work in this chapter was carried out by Dr. Anton De Vylder, Thybaut group, Ghent University. Sorbent synthesis was performed in collaboration with Dr. Jason Lee, Jones group, Georgia Tech and Yadong Chiang, Nair group, Georgia Tech performed the pyIAST calculations.

3.1 Background

Renewable natural gas (RNG), an advanced biofuel can be produced by the upgrading of biogas produced in landfills.[1] Such a resource can be used in all applications that utilize methane, such as the transportation and electric power sectors.[1,2]

A variety of experimental and computational studies have been reported in focusing on the design of efficient acid gas removal techniques to upgrade biogas to renewable natural gas standards.[3–7] A typical biogas stream contains methane (CH_4), carbon dioxide (CO_2) and hydrogen sulfide (H_2S).[2] H_2S corrodes the operating equipment and in most cases poisons the sorption material, while posing environmental hazards to operating personnel and the

environment.[8] These harmful effects lead to an increase in the industrial operating costs and therefore, selective H_2S removal is beneficial. Furthermore, a high H_2S/CO_2 selectivity ratio can facilitate use of the captured stream in a sulfur recovery unit via the Claus process.[9]

The use of solid-supported adsorbents has been proposed as a potentially effective method for acid gas removal due to the low heat capacities of most solid materials relative to water, which is used in many liquid absorption processes, and the concomitantly improved energy costs.[10] While this method of acid gas removal could potentially lead to an economically beneficial biogas upgrading process, a better understanding of H_2S interactions with solid supports is needed to improve the design of an adsorbent that can selectively remove H_2S in the presence of CO_2 and CH_4.

The use of conventional aminosilica sorbents for sorption of gases containing both H_2S vs. CO_2 has been investigated by the Sayari group.[11,12] They explored the simultaneous adsorption of H_2S and CO_2 over a triamine-grafted, pore-expanded mesoporous silica material, TRI-PE-MCM-41. They concluded that H_2S has a weaker interaction with the amine group than CO_2, with decreasing H_2S selectivity at increasing CO_2 concentrations. Huang et al.[13] investigated the single component adsorption of CO_2, H_2S and CH_4, using 3-aminopropyl-functionalized MCM-48, but they did not determine the effect of multicomponent adsorption on these materials. Ma et al.[14] proposed a two stage separation of CO_2 and H_2S by taking advantage of the difference in the optimum temperature (75 °C) of CO_2 adsorption versus H_2S at 22 °C, although at low temperatures, CO_2 limits the adsorption of H_2S. The Song group[6] explored the performance of a tertiary-amine based sorbent, TMHDA/SBA-15, which could selectively remove H_2S in the presence of CO_2. However, the tertiary-amine had very modest H_2S

adsorption capacities. They also showed that the presence of H_2O did not affect the H_2S adsorption capacity in the presence of CO_2.

The performance of metal-organic frameworks (MOFs) for selective H_2S separation from CO_2 has been extensively explored. Zou et. al[15] screened 11 MOFs and found that MIL-101(Cr) had good H_2S adsorption capacity and relatively high selectivity in the presence of CO_2, though the effect of CH_4 was not considered in this study. Walton et. al[16] explored the effect of amine functionalized UiO-66(Zr), MIL-125(Ti) and MIL-101(Cr) on the H_2S adsorption capacity and selectivity in a multicomponent gas mixture of $H_2S/CO_2/CH_4$. Their results showed that functionalizing MOFs with linker-based primary amines improves H_2S adsorption, but the presence of CO_2 and CH_4 decreased the H_2S adsorption capacity in the investigated MOFs. Belmabkhout et. al[17] reported fluorinated MOF membranes that could simultaneously remove H_2S and CO_2 in natural gas and a recent study[8] reported different fluorinated MOF structures that could selectively remove H_2S with an H_2S/CO_2 selectivity between 3.3 and 7 and simultaneously remove H_2S and CO_2 in the presence of CH_4.

In solution, sterically hindered amines (SHA) are used commercially for the selective removal of H_2S in the presence of CH_4 and CO_2.[18] These SHA have a bulky alkyl group attached to their amine group and fall into two distinct categories: a primary amine with an amino group attached to a tertiary carbon or a secondary amine with the amino group attached to at least one secondary or tertiary carbon.[19–21] With primary and secondary alkanolamines, the carbamates formed during CO_2 capture are stable and this limits the CO_2 theoretical capacity to 1 mol of CO_2 per 2 mol of amines.[21] With SHA, their steric hindrance reduces the stability of carbamates and increases the CO_2 theoretical capacity to 1 mol of CO_2 per mol of amine regardless of whether the amines have primary, secondary or tertiary structures.

Furthermore, solution studies show that an increase in the number of alkyl groups next to the alpha carbon leads to a severely sterically hindered amine, which causes a decrease in the absorption rate for CO_2. On the other hand, the proposed proton transfer mechanism[22,23] between H_2S and the amino group in solution is not affected by the bulky substituent in hindered amines. Hence, hindered amines do not affect the rate of absorption of H_2S in solution, but rather severely hindered amines kinetically favor the selective removal of H_2S in the presence of CO_2.[20,24] SHA in solution have been shown to have good H_2S selectivity, high absorption capacity, good chemical stability, low volatility, high solubility and no corrosivity.[20,24]

As a result of the promising characteristics of hindered amines for H_2S capture in solution, we have evaluated the use of SHA grafted onto solid supports as solid adsorbents. Owing to the limited knowledge associated with sterically hindered amines traditionally used in industrial solutions when they are affixed to solid support,[25] the hindered amines investigated here are chosen from structures that have been recently studied for their CO_2 sorption properties (in the absence of H_2S).[10] Such structures have yet to be reported in the literature as either absorbents/adsorbents for H_2S capture. To this end, these amine structures are being reported for selective removal of H_2S for the first time, to the best of our knowledge. The selected amines are hereby deployed to explore the effect of steric hindrance on the selectivity of H_2S in the presence of CO_2 and CH_4.

Using a breakthrough apparatus, in-situ infrared spectroscopy and thermogravimetric analysis, we report on (i) the H_2S selectivity in multicomponent gas mixtures, (ii) the nature of the species formed during H_2S adsorption and (iii) the effect of changing concentration and temperature on H_2S adsorption performance and stability using three types of amines (a) a hindered primary amine, (3-amino-3-methylbutyl)trimethoxysilane (AMBS) and two hindered

secondary amines, (b) (N-cyclohexylaminopropyl)trimethoxysilane (CHAPS) and (c) (*tert*-butylaminopropyl) trimethoxysilane (TBAPS) grafted on mesoporous silica, SBA-15 at similar amine loadings.

3.2 Methods

3.2.1 Materials

The following chemicals were used as received from Sigma–Aldrich: Pluronic ($(EO)_{20}(PO)_{70}(EO)_{20}$), tetraethyl orthosilicate (TEOS, 98%). Hexane (98.5%), methanol (ACS grade, >99.8%) and toluene (ACS grade, >99.5%) were purchased from BDH. For the grafting procedure, the following chemicals purchased from Gelest were used: (N-cyclohexylaminopropyl)trimethoxysilane and *tert*-butylaminopropyltrimethoxysilane. All materials used for the synthesis of (3-amino-3-methylbutyl)triethoxysilane and (E)-2-methyl-4-(triethoxysilyl)but-3-en-2-amine were purchased from Sigma-Aldrich. Specialty gases were purchased as a certified grade mixture from Airgas and include the following: 1% H_2S in N_2, 10% H_2S in N_2, 1% H_2S/ 10% CO_2 / 89% CH_4. 1% H_2S/ 30% CO_2/ 69% CH_4, Inert UHP nitrogen and helium were also purchased from Airgas.

3.2.2 Material Synthesis

The synthesis of SBA-15 silica follows a previous procedure in literature; [26] 18 g of product was calcined using the following temperature program: ramp to 200 °C at 1.2 °C/min, hold at 200 °C for 1 h, ramp to 550 °C at 1.2 °C/min, hold at 550 °C for 12 h, cool to room temperature at 10 °C/min. The calcined solid was then stored at room temperature before use.

Synthesis of (E)-2-Methyl-4-(triethoxysilyl)but-3-en-2-amine.

Synthesis of (E)-2-Methyl-4-(triethoxysilyl)but-3-en-2-amine and (3-Amino-3-methylbutyl) triethoxysilane was based on a previous procedure.[10] First, 2 wt% Platinum(0)-1,3-divinyl-1,1,3,3-tetramethyldisiloxane complex (Pt-DVDS) in xylenes (3.43 mL, 0.3 mmol Pt, 1 mol% catalyst) and 0.6 mL (0.5 M) of triisobutyl base solution (0.103 g of 2,8,9-triisobutyl-2,5,8,9-tetraaza-1-phosphabicyclo[3.3.3]undecane in 0.6 mL of diethyl ether) was added to a dried 100 mL three-neck round-bottom flask equipped with a condenser. The mixture was then stirred at 60 °C for 10 min. The mixture was cooled to room temperature and 20 mL of inhibitor-free anhydrous tetrahydrofuran was added into the flask. The mixture was then cooled to -10 °C using an ice and brine bath. Triethoxysilane (5.54 mL, 30 mmol) was added dropwise into the mixture subsequently and was stirred for 5 min. Next, 2-methyl-3-butyn-2-amine (2.5 mL, 23.75 mmol) was added into the mixture. The mixture was then warmed to room temperature and was stirred overnight. The mixture was then concentrated using a rotary evaporator and vacuum distillated (200 mTorr) at 60 °C to produce (E)-2-methyl-4-(triethoxysilyl)but-3-en-2-amine. ^{1}H NMR (400 MHz, $CDCl_3$): δ (ppm) 6.52 (d, J = 5.6 Hz, 1H) 6.47 (d, 1H), 3.82 (q, 6H), 1.23 (t, 9H), 1.19 (s, 6H). ^{13}C NMR (100 MHz, $CDCl_3$): δ (ppm) 162.21, 112.44, 58.41, 52.29, 29.73, 18.15.

Synthesis of (3-Amino-3-methylbutyl)triethoxysilane.

(E)-2-methyl-4-(triethoxysilyl)but-3-en-2-amine (2.5 g, 10 mmol), anhydrous ethanol (10 mL), and 5 wt% Pd/C (30 mg) was added into a dried 50 mL round-bottom flask. The flask was then purged under He flow for 15 min followed by H_2 flow for 20 min. The flask was then pressurized with H_2 using a two layered balloon and stirred for room temperature for 18 h. The

mixture was then filtered and washed with anhydrous ethanol and concentrated by rotary evaporation. The final product, (3-amino-3-methylbutyl) triethoxysilane, was purified by vacuum distillation (200 mTorr) at 60 °C. ^{1}H NMR (400 MHz, $CDCl_3$): δ (ppm) 3.84 (q, 6H) 1.45 (m, 2H), 1.25 (t, 9H), 1.08 (s, 6H), 0.64 (m, 2H). ^{13}C NMR (100 MHz, $CDCl_3$): δ (ppm) 58.40, 49.89, 37.66, 29.57, 18.31, 4.75.

3.2.3 Grafting of Aminosilanes on SBA-15

Aminosilane grafting on SBA-15 follows a previous procedure from a prior study.[26] To compare the three different hindered amines, similar amine densities were grafted on the surface of SBA-15; Fig. 3.1 shows the chemical structures of the aminosilanes used during this study. The solution containing added aminosilane was stirred at 85 °C for 24 h under nitrogen. Aminosilane to silica ratios (g aminosilane:g silica) used to achieve the amine loadings reported here for SBA-15_CHAPS, SBA-15_AMBS, and SBA-15_TBAPS were 3:1, 1:1, 2.5:1 respectively. Next, the final product was filtered with copious amounts of toluene, hexane and methanol consecutively. The filtered product was dried under vacuum overnight at 75 °C under a pressure of 10 mTorr.

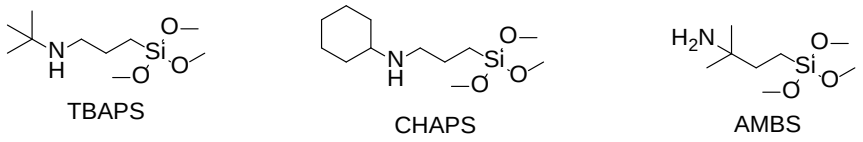

Figure 3.1. Chemical names and structures of aminosilanes used in this study

3.2.4 Material Characterization

The BET surface area, mean pore size, and pore volumes, were obtained from nitrogen sorption isotherm data obtained on a Micromeritics Tristar II at 77 K. To calculate the surface

area and mean pore size from the isotherm data, the Brunauer-Emmett–Teller (BET) and Broekhoff-de Boer method with the Frenkel-Halsey-Hill equation (BdB-FHH method)[27] were used, respectively. Elemental analyses (C,H,N) were used to determine the amine loading of the functionalized materials. This analysis was performed by Atlantic Microlab.

3.2.5 Dynamic Adsorption Measurements

Breakthrough measurements were carried out in a fixed bed made of quartz glass with dimensions 6 mm x 4 mm (O.D x I.D). A schematic is given in **Figure B.3.** A sample of the effluent gas concentrations was measured using an Omnistar QMG 220 mass spectrometer. Each run used 80-100 mg of sample, pelletized at 1000 psi and sieved at a mesh size between 425-850 μm.[28] All breakthrough experiments were performed at ~1 atm total pressure.

First, each sample was pretreated by flowing UHP He at a rate of 50 mL/min through the bed for 2 h at 120 °C, after which the temperature was cooled to 30 °C and allowed to equilibrate for 10 min. All dynamic adsorption studies were performed at a flowrate of 20 mL/min at 30 °C and before each experiment, the mass spectrometer was calibrated with each gas used and the dead volume measured using an empty bed (a bed with no adsorbent) as the baseline.

During adsorption, the gas was switched to 1% H_2S in N_2, 1% H_2S/10% CO_2/89% CH_4 or 1% H_2S/30% CO_2/69% CH_4. Desorption was initiated when the outlet stream concentration of H_2S reached the inlet gas concentration. During the desorption step, the temperature remained at 30 °C till the concentration of H_2S was below 100 ppm, after which the temperature was ramped up to 120 °C and maintained isothermal until the H_2S concentration observed was below 5 ppm.

The adsorption capacities were calculated by integrating the area above the breakthrough at the breakthrough point (the time at which the gas outlet concentration was 5% of the feed concentration) and at saturation.

3.2.6 CO_2 Adsorption Isotherm Measurements

A Micromeritics ASAP 2020 was used to measure the CO_2 adsorption isotherms of the materials, volumetrically, at 30 °C and 50 °C. All samples were activated at 120 °C for 12 h under vacuum (<5 mTorr) before measuring adsorption isotherms.

3.2.7 H_2S Adsorption Isotherm Measurements

A TA Instruments Q500 thermogravimetric analyzer (TGA) was used to measure dry H_2S adsorption capacities at different temperatures between 30 and 75 °C and H_2S concentrations from 0.5-10%. The procedure used can be found in a previous study.[29] To assess reproducibility, especially at very low H_2S concentrations, experiments were repeated three times on fresh sorbents.

3.2.8 In Situ Fourier-Transform IR (FTIR) Spectroscopy

A diffuse reflectance Harrick Praying Mantis High Temperature Reaction Chamber coated with Siliconert was used for *in situ* IR spectroscopy experiments. The IR spectrometer used for these experiments was a Thermo Nicolet is10 with a mercury cadmium telluride (MCT) detector. All flow rates were held constant at 20 mL/min. All samples were activated at 120 °C under He flow. The samples were then exposed to 10% H_2S/N_2 for an hour. All H_2S adsorption spectra were taken with the activated sample as the background. Spectra were taken at a resolution of 4 cm^{-1} at 64 scans.

*3.2.9 Computational Methods***

To keep the size of the computational model limited, only the organic group on the adsorbents was modeled. The accuracy of this approach for calculating the effects of steric hindrance of amine functionalized silicas has been demonstrated in previous work.[30] All of the electronic structure calculations were performed using the Gaussian 09 package.[31] Global minimum energy conformations for reactants and complexes were determined in vacuo by a first scan of all freely rotating dihedral angles at the B3LYP/6-31G* level of theory. For the proton and TMB basicity scale, the CBS-QB3 composite method was used for a full geometry optimization and free energy calculation of the lowest energy conformer, as this method has proven to accurately describe the proton basicity scale with a maximum deviation of 4.4 kJ mol^{-1} and the TMB basicity scale with a maximum deviation of 2.1 kJ mol^{-1}.[30] The amine-H_2S interactions have been calculated with the B3LYP/6-31G** level of theory, as has previously been successfully used for these kind of interactions.[22] A tight optimization criterion and an ultrafine integration grid were always used. Minimum energy conformations were confirmed to have zero imaginary frequencies. Coordinates of all optimized structures can be found in **Table B.4**. Partition functions were calculated using statistical thermodynamics, based on the scaled frequency calculations. These are evaluated by using the rigid-rotor and harmonic oscillator (HO) approximation, assuming separation of translational, external rotational, rovibrational, and electronic contributions. All thermal contributions were calculated in the (quasi)harmonic oscillator approach, which means that any frequencies below 30 cm^{-1} were raised to this value.[30]

The proton basicity (PB) and proton affinity (PA), determined via the Gibbs energy and the enthalpy of the deprotonation reaction, respectively, were calculated according to **Equation B.1** and **Equation B.2** at 298.15 K and 1 atm. The trimethylborane basicity (TMBB) and affinity

**All computational work in this chapter was carried out by Dr. Anton De Vylder, Thybaut group, Ghent University

(TMBA), respectively, were calculated according to **Equation B.3** and **Equation B.4**, at 298.15 K and 1 atm. The adsorption enthalpy was determined at 303.15 K and 1 atm.

3.3 Results and Discussion

3.3.1 Material Characterization

N_2 physisorption was used to determine the surface area and pore volume of the amine loaded silicas. The type IV hysteresis of the adsorbents in **Figure B.1** confirms the mesoporous structure of these adsorbents. The reduction in pore volume (**Figure B.1**) and surface area (**Table 3.1)** confirm the successful grafting of the aminosilanes on the surface of the silica support. An estimated 80-90% surface coverage was estimated from the reduction in BET surface area and pore volume after grafting, suggesting evenly distributed aminosilanes on the silica support. Similar amine loadings of 1.7-2.0 mmol N/g were achieved to make appropriate comparisons between the adsorbents studied.

Table 3.1. Structural Properties of Materials

Sample	Amine loading (mmol N/g)	Surface area (m^2/g_{SiO2})	Mean pore size (nm)	Pore volume (cm^3/g)
SBA-15	-	778	5.4	0.95
SBA-15_TBAPS	1.8	354	4.3	0.40
SBA-15_CHAPS	1.7	323	4.4	0.36
SBA-15_AMBS	2.0	326	4.2	0.36

3.3.2 FTIR Spectra of Adsorbed H_2S on SHA Sorbents

In-situ IR spectroscopy was used to determine the nature of the adsorbed H_2S-amine species. In **Figure 3.2** we show the intensities of isolated surface hydroxyl groups decreased upon exposure to H_2S for all samples, including the bare silica support, indicating that hydroxyl groups adsorbed some H_2S. Residual amounts of COS gas were observed as well, indicating that there were small amounts of COS in the gas cylinder used. For the aminosilane grafted sorbents, a reduction of peaks associated with stretching modes of $NH_{1\text{-}2}$ and $CH_{2\text{-}3}$ was observed, indicating that the H_2S interacted with the aminosilane **(Table 3.2)**. Hydrogen bonded NH arose and CH stretching modes intensities decreased upon exposure to H_2S for all the aminosilanes, indicating that some H_2S was interacting with the support and the amines through physisorption. Symmetrical and unsymmetrical stretching modes for H-S-H and a broad peak associated with both the asymmetrical and unsymmetrical stretching modes of HS were observed for all the sorbents, including the silica support. This mode is associated with physisorbed H_2S. The results suggest that H_2S physisorbs on all silica supported hindered amines under dry conditions, rather than protonating the hindered amines as is observed in solution.[22,23]

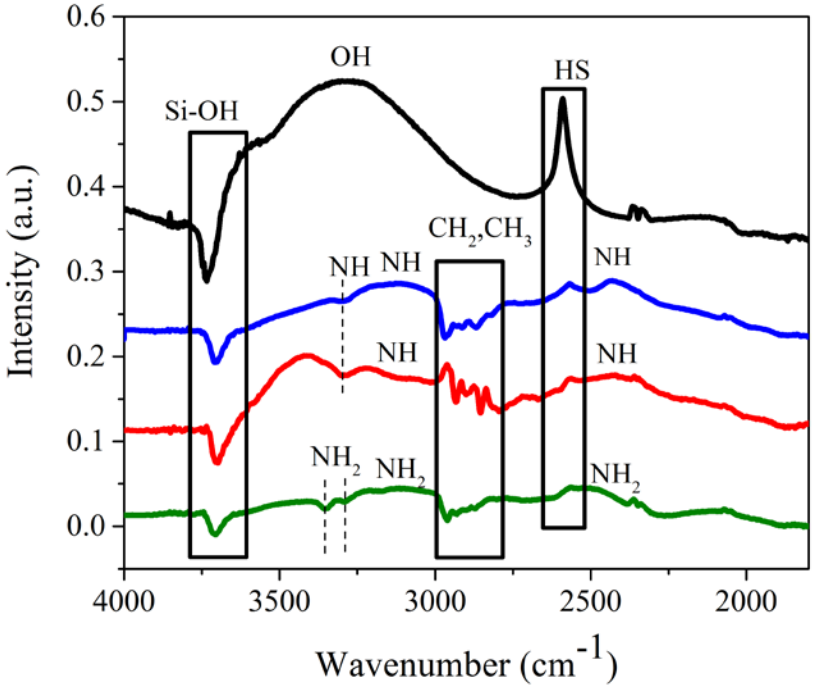

Figure 3.2. FTIR spectra for 10% H_2S in N_2 adsorption on (a) bare silica, SBA-15 (b) SBA-15_TBAPS (c) SBA-15_CHAPS (d) SBA-15_AMBS with activated sample as background.

Table 3.2. Assignments of FTIR absorption bands [22]

Assignment	Wavenumber (cm^{-1})
Isolated Si-OH stretch	3800-3700
NH_{1-2} stretch	3500-3300
NH_{1-2}, OH stretch (hydrogen bonded)	3500-3000
NH_{1-2} stretch (hydrogen bonded)	2500-2400
CH_{2-3} stretch	3000-2800
HS stretch	2600-2500

3.3.3 Understanding the Effects of Steric Hindrance on H_2S Selectivity

To evaluate which amine displays the highest steric hindrance for an incoming CO_2 molecule, the three hindered amine sites were computationally evaluated on both a steric-free proton basicity scale as well as a basicity scale constructed with the sterically demanding Lewis

acid trimethylborane (TMB).[30] The results w compared to the best performing unhindered secondary amine group for H_2S capture, i.e., 3-methylaminopropyl-trimethoxysilane (MAPS).[29] **Figure 3.3 and Table B.3** show that all the amines evaluated in this chapter exhibit a TMB basicity that is much lower than that of MAPS, indicating that they are indeed all more sterically hindered. The TBAPS and CHAPS groups display a similar proton basicity, but TBAPS has a much lower TMB basicity than CHAPS. This indicates that the steric hindrance encountered by the incoming Lewis acid is much more pronounced for TBAPS than for CHAPS. Comparatively, an incoming CO_2 molecule will also encounter more steric hindrance by TBAPS and, hence, its adsorption will be reduced, as compared to CHAPS. In fact, previous experimental work from our group suggests that severely hindered amines such as TBAPS cannot form amine-CO_2 species at all in the absence of water.[10]

The primary amine AMBS, on the other hand, exhibits a lower proton basicity than CHAPS, but the TMB basicity of AMBS is found to be higher than that of CHAPS. This shows that while AMBS is intrinsically a weaker base for protons, it exhibits a less pronounced steric hindrance as compared to CHAPS.

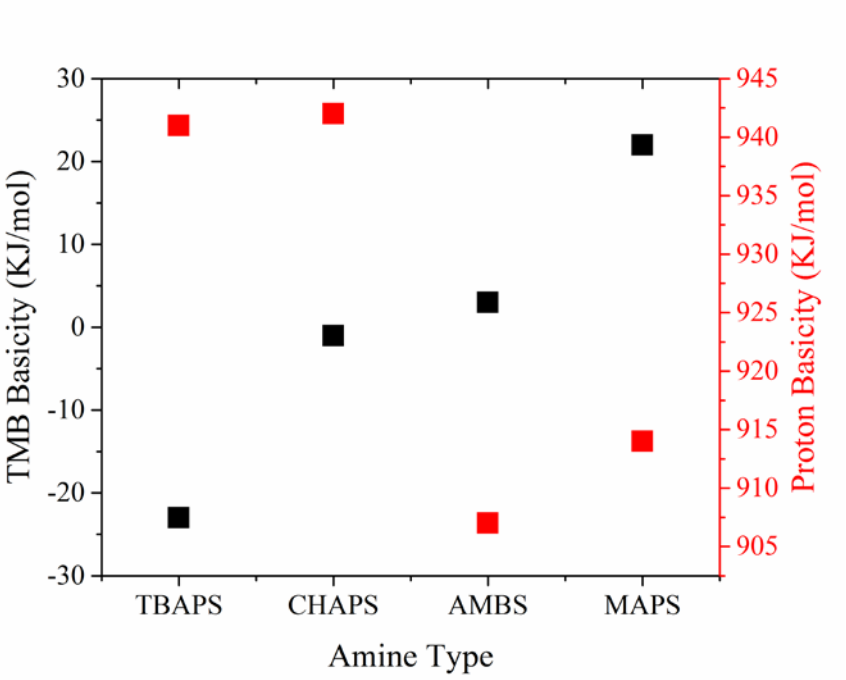

Figure 3.3. CBS-QB3 calculated TMB basicity and proton basicity at 298.15K and 1 atm of different hindered amines. Previous work with this model indicated a maximum deviation from experimental values of 2.1 kJ mol^{-1} for the TMB basicity and 4.4 kJ mol^{-1} for the proton basicity.

3.3.4 Multicomponent Adsorption Measurements

CO_2 and H_2S both interact with the free-electron pair in the amines, as a result, the difference between amine-H_2S interaction and the effect of steric hindrance on H_2S selectivity is elucidated experimentally. The performance and stability of the unhindered amine, SBA-15 supported 3-methylaminopropyl-trimethoxysilane (SBA-15_MAPS), in the presence of H_2S has been assessed in a prior study, [29] and its performance is compared to SHA in this study.

In **Figure 3.4(a) ,** SBA-15_MAPS shows a halving of the H_2S adsorption capacity from 0.2 mmol/g in 1% H_2S in N_2 stream to 0.1 mmol /g with the use of a 10% CO_2/1% H_2S/ balance CH_4 simulant biogas stream. This drastic decrease in H_2S adsorption capacity indicates competitive adsorption between CO_2 and H_2S. There was a less significant decrease of the H_2S adsorption capacity of the SHA studied here when compared to SBA-15_MAPS in the simulant

biogas stream. However, the SHA H_2S adsorption capacities were equivalent or lower than that of SBA-15_MAPS in the simulant biogas stream.

The composition of CO_2 in biogas streams is as high as 50%.[2] and to determine the effect of increasing CO_2 concentration on these SHA, a gas mixture containing 30% CO_2/1% H_2S and balance CH_4 was also deployed. In these conditions, the H_2S adsorption capacity of SBA-15_TBAPS was unchanged, while a decrease in H_2S sorption capacities was observed for SBA-15_CHAPS and SBA-15_AMBS.

Figure 3.4(b) shows the $H_2S/CO_2/CH_4$ breakthrough curves where the CH_4 is non-adsorbing on all hindered amines, as observed in **Figure B.4,** where it is shown there is no difference in the breakthrough profile for CH_4 through the sterically hindered amines and the empty bed. From these results, we see a correlation between steric hindrance and H_2S selectivity in the presence of CO_2 for the various amine materials. SBA-15_TBAPS, SBA-15_CHAPS and SBA-15_AMBS all have relatively stable H_2S adsorption capacities compared to the unhindered amine, SBA-15_MAPS, under the conditions studied. As we shift from moderately hindered amines, SBA-15_CHAPS and SBA-15_AMBS, to the more severely sterically hindered amine, SBA-15_TBAPS, the H_2S uptakes became stabilized, even with an increase in CO_2 concentration from 10-30%. This confirms a significant H_2S selectivity for SBA-15_TBAPS in the presence of CO_2. During adsorption processes where high H_2S selectivity is required the use of sterically hindered amine sorbents such as SBA-15_TBAPS could lead to high H_2S/CO_2 ratios, which could allow for H_2S recovery and further processing into elemental sulfur, coupled with secondary CO_2 removal to meet the required renewable natural gas standards.

It is interesting that the calculated proton basicity of the secondary amines, SBA-15_TBAPS and SBA-CHAPS, are equal but that SBA-15_TBAPS was experimentally observed to provide a more stable H_2S capacity even at high CO_2 concentrations. This suggests that the proton basicity of the hindered amines does not influence the H_2S selectivity in the presence of CO_2. Furthermore, with the understanding of the effects of steric hindrance and basicity on H_2S uptake in a multicomponent gas mixture, it is possible to design efficient solid-supported adsorbents for H_2S/CO_2 separations.

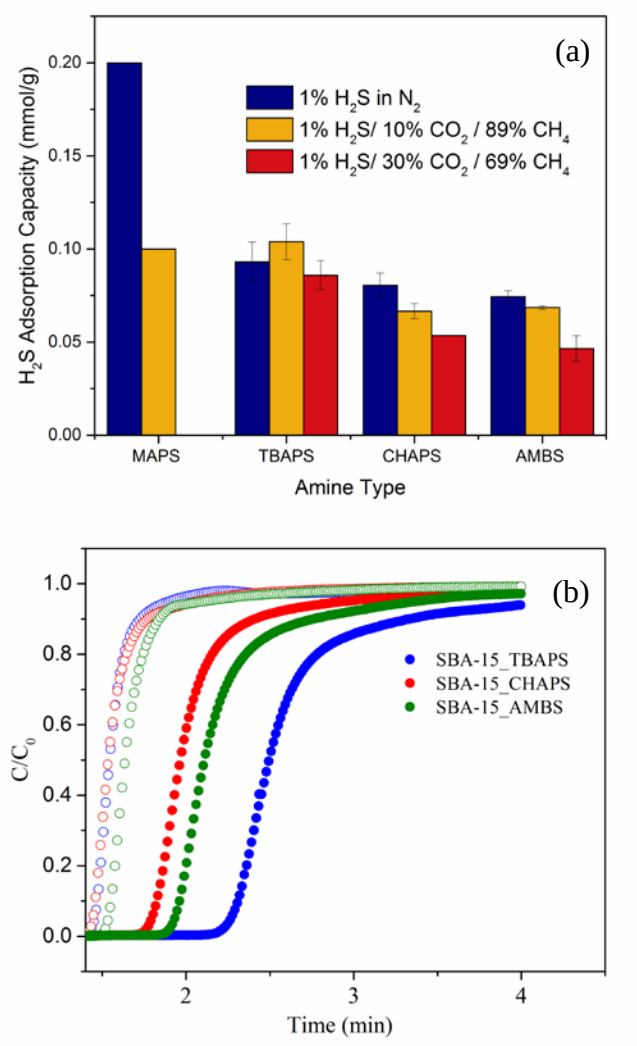

Figure 3.4. H_2S adsorption capacity with and without CO_2. The error bars were estimated with two independent experiments. (b) 1% H_2S/ 10% CO_2/89% CH_4 breakthrough curves on hindered amines with H_2S (filled circle) CO_2 (open circle).

3.3.5 Desorption Kinetics

Thermal desorption determines the extent of surface regeneration of the adsorbent. **Figure 3.5** illustrates the desorption profiles of all the supported hindered amines studied using a 1% H_2S/30% CO_2/89% CH_4 gas mixture at 30 °C. During the desorption step, UHP helium was passed through the fixed bed at 30 °C and a decrease in H_2S and CO_2 concentrations was observed, which shows the ease of regeneration of these adsorbents at low temperatures. An increase in temperature led to an increase in effluent H_2S for all the adsorbents between 70-80 °C. This increase in H_2S concentration at higher temperatures can be attributed to the stronger hydrogen bonded H_2S molecules. The CO_2 desorption profiles show an increased CO_2 concentration as temperature increased for SBA-15_AMBS and SBA-15_CHAPS, with no CO_2 released for SBA-15_TBAPS, as expected.[10] This temperature controlled desorption procedure illustrates the effect of steric hindrance in the selective removal of H_2S. SBA-15_TBAPS favors the adsorption of H_2S, while essentially completely blocking the adsorption of CO_2. The moderately sterically hindered amines, SBA-15_CHAPS and SBA-15_AMBS, mostly adsorbed H_2S with small amounts of CO_2, which make them suitable adsorbents for the simultaneous removal of CO_2 and H_2S. The stable H_2S adsorption capacities for SBA-15_TBAPS coupled with no CO_2 released during desorption demonstrates SBA-15_TBAPS as a promising adsorbent for the selective removal of H_2S in a dry multicomponent gas mixture. The obtained H_2S selectivity for SBA-15_TBAPS, with essentially no CO_2 or CH_4 uptake, makes this material akin to the most H_2S selective adsorbent material reported to date for similar gas mixtures (**Table B.1**).

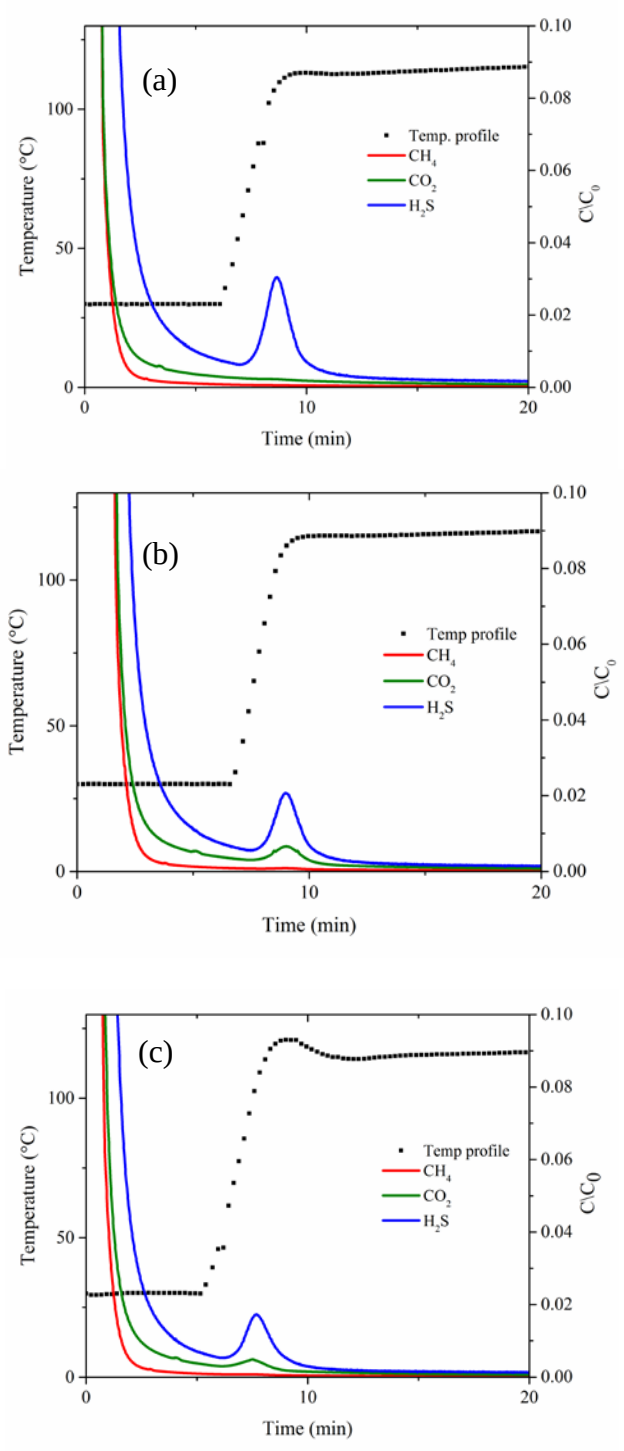

Figure 3.5. Desorption profile for hindered amines in 1% H_2S/ 30% CO_2/ 69% CH_4 for (a) SBA-15_TBAPS, (b) SBA-15_CHAPS and (c) SBA-15_AMBS.

3.3.6 CO_2 and H_2S Adsorption Isotherms

Figure B.10 shows the CO_2 and H_2S adsorption capacities for the SHA studied. As expected, the CO_2 and H_2S adsorption capacities decrease with an increase in temperature and increase with an increase in pressure for all SHA. At pressures between 0-100 mbar, the most severely sterically hindered amine, SBA-15_TBAPS has three times the H_2S adsorption capacity of SBA-15_AMBS, which has the highest CO_2 adsorption capacity. SBA-15_CHAPS and SBA-15_AMBS have comparable H_2S and CO_2 adsorption capacities at 50 °C while the H_2S adsorption capacities for SBA-15_TBAPS are higher at all temperatures.

Ideal adsorbed solution theory (IAST) has been applied to predict the uptakes of molecules and selectivity under multi-component conditions for both gas and vapor systems to support the experimental data.[32] The Toth adsorption model, as shown in **Equation 3.1**, was utilized to provide the parameters for IAST simulation.

Equation 3.1
$$q = q_{\max} \frac{bP}{(1+(bP)^{n}))^{\frac{1}{n}}}$$

The parameters used are summarized in **Table B.2**, where b and n are Toth model constants, q and q_{max} are the uptake and maximum uptake, respectively, and P is the partial pressure. This model has been applied for the analysis of multilayer and heterogeneous adsorption systems.[33] The fitting results (**Figure B.10**) show that the model can depict the data from the low to high pressure regime, and thus they are ideal for IAST calculation. The IAST calculations were performed with pyIAST.***[32]

***pyIAST calculations were performed by Yadong Chiang, Nair group, Georgia Tech.

Using the single component adsorption isotherms for CO_2 and H_2S, as shown in **Figure B.10,** predictions of selectivity from IAST were compared with the multicomponent experimental results. The correlation of experiments and the model is given in **Figure 3.6**. The predictions obtained with IAST are fairly comparable with the observed multicomponent gas sorption experiments, with the model being more accurate at lower CO_2 concentrations. This is attributed to the extrapolation of the IAST results to CO_2 pressures between 100 - 300 mbar, outside the experimental isotherm range. In correlation with the experimental results, SBA-15_TBAPS has the highest selectivity under all conditions explored. The selectivity of SBA-15_TBAPS is higher than the selectivity determined for hindered amines in solution,[24,25] and is the highest H_2S selectivity reported for adsorbent materials thus far in a $H_2S/CO_2/CH_4$ gas mixture as shown in **Table B.1**. [8,34]

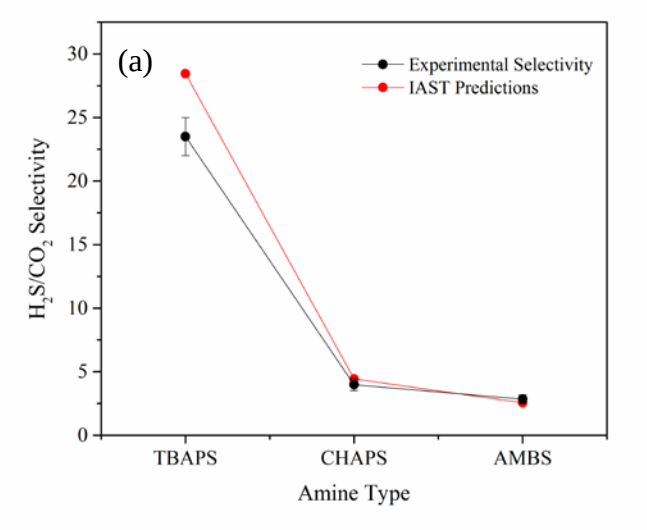

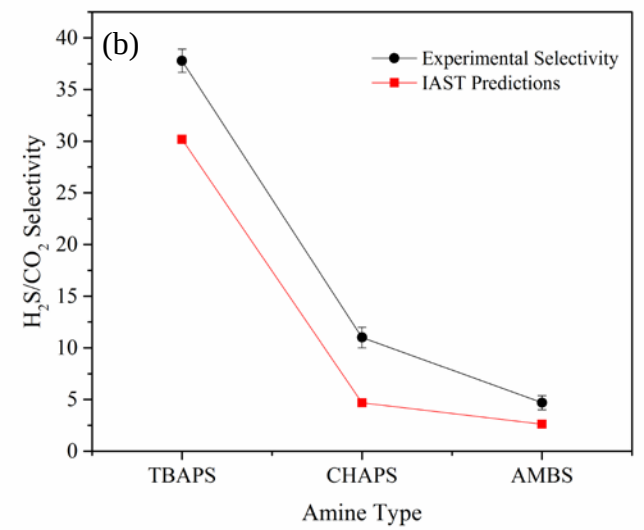

Figure 3.6. H_2S selectivity obtained from IAST predictions and experimental data using a multicomponent mixture at the following operating conditions (a) 1% H_2S/ 10% CO_2/ 89% CH_4 and (b) 1% H_2S/ 30% CO_2/ 69% CH_4 at 30 °C and 1 atm.

3.3.7 Discussion of H_2S-amine adsorption mechanism and CO_2 selectivity

The measured H_2S single component adsorption isotherms were fit using the temperature dependent Toth isotherm, as noted above. **Figure 3.7** displays the H_2S isosteric heat of adsorption as a function of surface coverage calculated using the fitted isotherms following a previous method.[29,35,36] **Table 3.3** compares these experimental initial isosteric heats of

adsorption, which are found to be typical values for physisorption,[37] to the computed values at the B3LYP/6-31G** level of theory. These computational results suggest that the experimentally observed isosteric heat of adsorption, which is in the range of 24 – 33 kJ/mol, can best be rationalized by a H_2S molecule hydrogen-bonding to two amine sites (illustrated in **Figure 3.8**). This is consistent with proposed amine-H_2S interactions in other solid adsorbents containing amines.[5,6,14,22]

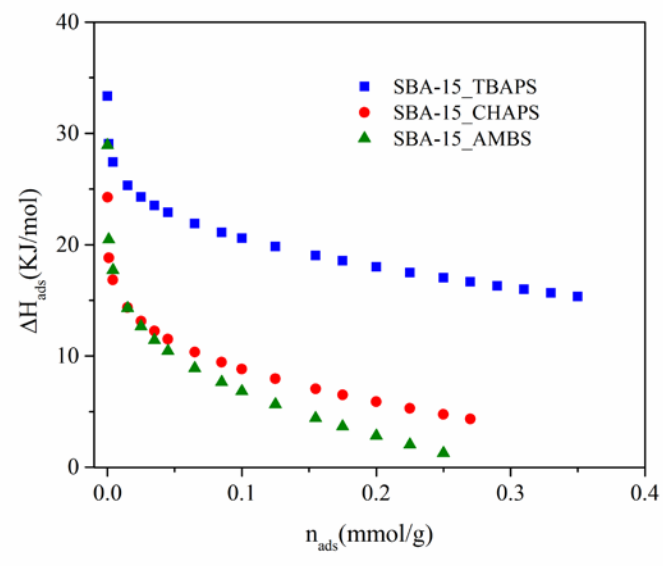

Figure 3.7. Calculated isosteric heats of adsorption of H_2S vs. surface coverage for all adsorbents at 30°C.

Table 3.3. Isosteric heat of Adsorption for Sterically Hindered Amine Adsorbents

Amine	**Heat of H_2S adsorption (Toth) (kJ/mol)**	**Heat of H_2S adsorption on one amine (B3LYP/6-31G**) (kJ/mol)**	**Heat of H_2S adsorption on two amines (B3LYP/6-31G**) (kJ/mol)**	**Heat of CO_2 adsorption (Calorimeter) (kJ/mol)[10,37]**	**Heat of CO_2 adsorption (Toth) (kJ/mol)**
TBAPS	33	16	27	46[10]	18
CHAPS	24	17	28	66[10], 40[37]	35
AMBS	29	18	29	70[10]	83

Moreover, because a hydrogen bond is a longer-range interaction, it is expected that steric hindrance around the amine has less effect on H_2S adsorption than on CO_2 adsorption, as observed in the multicomponent adsorption measurements where steric hindrance had essentially no effects on the H_2S adsorption capacity but restricted the adsorption of CO_2 in SBA-15_TBAPS.

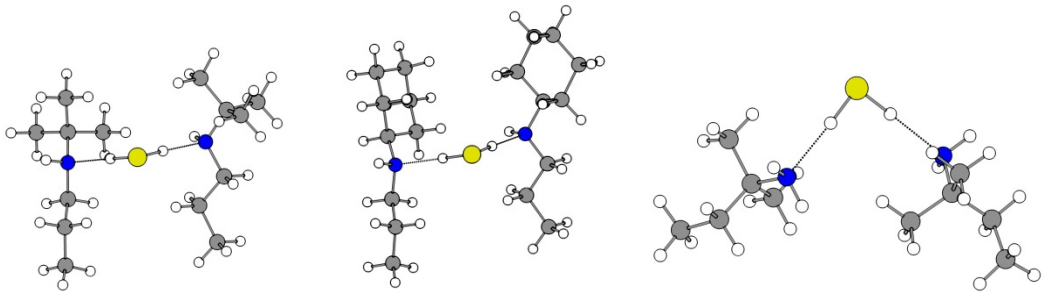

Figure 3.8. Computationally Optimized Structures at the B3LYP/6-31G** level of theory for H_2S-Amine Adsorbent Interaction in (a) SBA15-TBAPS (b) SBA-15_CHAPS (c) SBA-15_AMBS. (Grey = carbon, white = hydrogen, blue = nitrogen, yellow = sulfur)

3.3.8 Discussion on the Impact of heat of adsorption on CO_2 vs. H_2S selectivity

It was observed that the heat of CO_2 adsorption calculated using the Clausius Clapeyron equation applied to Toth isotherms at various temperatures differs from those measured using a calorimeter for all three sorbents (**Table 3.3**). This merits further analysis and discussion. In previous work, Alkhabbaz et al. noted that experimental heats from calorimetry differed from calculated heats from isotherms fit at various temperatures for CO_2 adsorption over supported amine materials similar to those used in chapter 2 of this dissertation.[37] Specifically, they noted that for secondary non-sterically hindered amines (MAPS, NBAPS), experimental heats of adsorption were similar to those measured for primary amines. However, the materials based on secondary amines adsorbed less CO_2 than the primary amine counterpart. This suggested that the entropy of adsorption was different between these cases, and they hypothesized that the

second alkyl chain attached to secondary amines introduced a steric hindrance that required additional chain ordering for CO_2 adsorption to occur via the cooperative carbamate formation mechanism, imparting an additional entropic penalty to adsorption for secondary amines. Thus, despite similar enthalpies of adsorption, the lower uptake, a result of a less favorable Gibbs free energy of formation, must have been associated with a greater entropic penalty for adsorption.

Two different calorimetric heats of adsorption values for CO_2 were identified for SBA-15_CHAPS in literature. A lower heat of adsorption of 40 kJ/mol was observed by Alkhabbaz et al. [37] at an amine loading of 1.97 mmol/g compared to the 66 kJ/mol observed by Lee et al., [10] at an amine loading of 1.86 mmol/g **(Table 3.3)**. The differences in the heats of adsorption could be attributed to the amine spacing of the moderately hindered amine molecules within the pores of the silica support, which could change the nature of the adsorbed species. For instance, materials with more paired amines might produce carbamates, whereas isolated amines can produce carbamic acid or bicarbonates when water is present. Bicarbonates and carbamic acid are suggested to offer lower enthalpies of adsorption compared to carbamates.[10,38] Thus, the enthalpies may differ due to the formation of different forms of adsorbed CO_2. An alternative explanation is that one of the values reflects some experimental error.

In this study, it was observed that the H_2S selectivity decreases for the SBA-15_CHAPS sample in the presence of CO_2 and the desorption profile showed the simultaneous adsorption of both CO_2 and H_2S (**Figure 3.5(b)**). Although the initial calorimetric heat of adsorption of CO_2 was higher than the calculated heats from Toth isotherm for H_2S, the H_2S adsorption capacity was higher than CO_2, as shown with the gas composition of 1% H_2S/30% CO_2/69% CH_4, where an adsorption capacity of 0.01 mmol/g and 0.05 mmol/g was observed for CO_2 and H_2S respectively. Drawing from prior work, SBA-15_CHAPS can adsorb traces of CO_2 via formation

of carbamates, consistent with an elevated enthalpy of adsorption, as well as carbamic acids.[10] However, we hypothesize that most CO_2 is adsorbed as carbamic acids via CO_2 sorption between an amine and a surface silanol. These species are formed with much lower enthalpies of adsorption.[38] Thus, the observed elevated H_2S selectivity relative to CO_2 may be rationalized by the form of the adsorbed CO_2, which may not directly correlate with a single enthalpy of adsorption value associated with the first CO_2 adsorbed to the material, as represented in **Table 3.3**. More importantly, noting high enthalpies of adsorption are strongly associated with carbamate formation, and that carbamate formation over secondary amines like MAPS, NBAPS, CHAPS comes with significant entropic penalties for adsorption, it is clear that Gibbs free energies of formation for CO_2 may not track directly with enthalpies of formation for secondary amine materials. Furthermore, it is noted that the hypothesized steric effects that lead to larger entropic penalties for adsorption in the CO_2 case are likely less important for H_2S, which forms hydrogen bonds with the amines, consistent with the higher capacities observed for H_2S. In addition, a gradual decrease in the heat of adsorption was observed as the H_2S coverage increases for SBA-15_CHAPS, while a steep decrease in the isosteric heat of adsorption was observed as the CO_2 coverage increases (**Figures 3.7 and 3.8(a)**). A steeper slope suggests a faster decline of the enthalpy of adsorption to a physisorbed region, with lower CO_2 uptakes where H_2S selectivity could improve.[38] Both SBA-15_CHAPS and SBA-15_AMBS are moderately sterically hindered sorbents, as evaluated in **Figure 3.3**, and similar conclusions on the impacts of heats of adsorption on selectivity are proposed for the SBA-15-AMBS sorbent.

Comparing the calculated enthalpies from isotherms fit at various temperatures for H_2S to those of CO_2, it was observed that the heat of H_2S adsorption is higher than the heat of CO_2 adsorption for SBA-15_TBAPS, which supports the experimentally observed high H_2S

selectivity under the conditions studied. However, the measured heats of CO_2 adsorption were higher than those calculated from the thermodynamic treatment of the Toth isotherm at various temperatures, with the measured enthalpies of adsorption being ~13 kJ/mol higher than observed for the calculated heats of H_2S adsorption. Building on the discussion above, it is proposed that the discrepancy in the measured heats of adsorption and calculated heats from isotherm fits for CO_2 was as a result of the severe steric hindrance of the *t*-butyl functional group of SBA-15_TBAPS. The entropic penalty presented by the bulky functional group was not accounted for in the calculated heats from the CO_2 isotherm at different temperatures, as previously discussed. The severe steric hindrance encountered by CO_2 via the *t*-butyl group limits CO_2 adsorption on SBA-15_TBAPS. Furthermore, the CO_2 heats of adsorption as a function of surface coverage show that the heat of adsorption decreases as surface coverage increases, with the lowest initial heat of adsorption and a steep slope observed for SBA-15_TBAPS (**Figure 3.9(a)**). Explicitly, the change in the measured heat of adsorption for CO_2 was compared to the slope for the calculated heats for H_2S (**Figure 3.9 (b)**), and the data show that at a certain surface coverage, there is a threshold where the heat of adsorption for H_2S is higher or the same as CO_2, though both are approximately similar throughout the range. The steric effects that provide a greater entropic penalty for CO_2 adsorption relative to H_2S adsorption, coupled with the change in heat of adsorption as a function of surface coverage, could provide a rationale behind the experimentally observed increased H_2S selectivity for SBA-15_TBAPS even with higher initial heats of adsorption for CO_2. Moreover, we note that using a single value of the initial heat of adsorption to represent the overall thermodynamic selectivity of CO_2 vs. H_2S does not provide a holistic interpretation of the thermodynamic impact on selectivity.

From the above discussion, it is evident that heats of adsorption measured experimentally via calorimetry can vary significantly from heats inferred from a thermodynamic treatment of adsorption isotherms at different temperatures for sorbents with mobile, flexible binding sites. This is hypothesized to be due to two related factors. First, the two sorbates in question, CO_2 and H_2S, can adsorb in differing ways over these sorbents. CO_2 can adsorb with enthalpic driving force using two amine sites forming covalent linkages but with hypothesized significant entropic penalties for adsorption or in 1:1 amine-CO_2 adducts with lower enthalpies and hypothesized less significant entropic penalties. In contrast, H_2S is hypothesized to adsorb only via hydrogen bonding, forming no new covalent bonds, with lower enthalpies of adsorption and hypothesized modest entropic penalties. The second key factor is what enables the behavior discussed above. The inherent mobility and flexibility of the binding sites in supported amine materials can lead to varying entropies of adsorption in comparison to conventional solid adsorbents with rigid surfaces and where the entropy of adsorption would be approximately constant across all materials within a sorbent family. Additionally, the assessment of heats of adsorption for H_2S is further complicated by the fact that we cannot directly measure calorimetric adsorption heats with the experimental equipment available (our calorimeters are not compatible with H_2S). Thus, heats of adsorption can only be derived from thermodynamic treatment of adsorption isotherms at multiple temperatures, and from theory. Further studies should explore the impact amine spacing and amine loading has on sterically hindered amines and their effect on CO_2 and H_2S heats of adsorption. Lastly, this discussion highlights the importance of maintaining a consistent method and criteria for evaluating and comparing different sorbents in order to make fair and accurate comparisons.

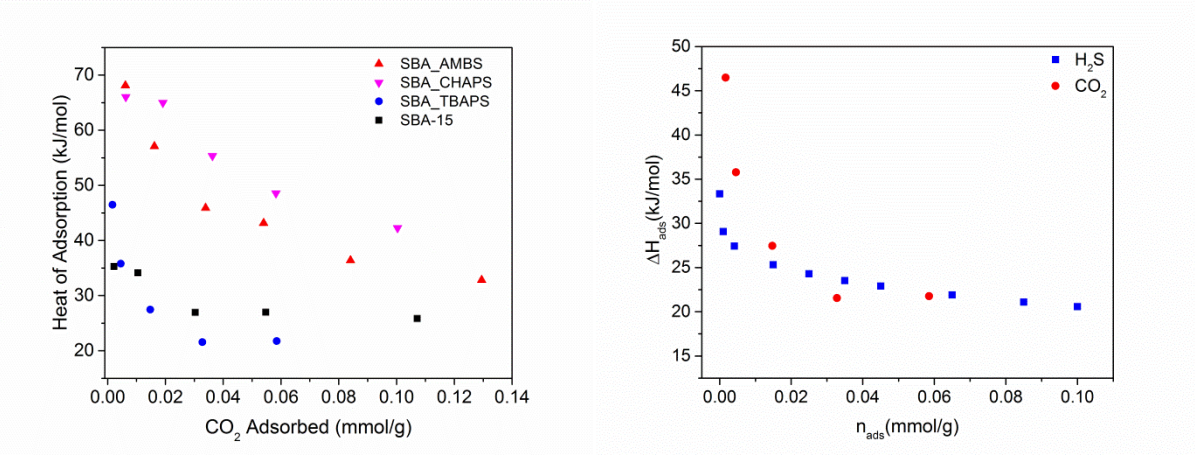

Figure 3.9. (a) Isosteric heats of CO_2 adsorption under dry conditions for all sorbents at 30 °C. Reprinted with permission from ref 10. Copyright (2018) American Chemical Society. (b) Measured isosteric heats of CO_2 adsorption and calculated heats of H_2S adsorption from Toth isotherm fits at different temperatures for SBA-15_TBAPS.

3.3.9 Cyclic Stability of Sterically Hindered Amines

To determine the cyclic stability of the SHA studied, the H_2S adsorption capacities were measured with a TGA at a high H_2S concentration (10% H_2S in N_2) for 10 cycles. The results in **Figure 3.9** show that the SHA maintained relatively stable H_2S adsorption capacities over 10 cycles of adsorption and desorption for all adsorbents studied. This confirms that the relative stability of sterically hindered amines observed in solution studies[24] is also observed in the silica-supported analogues. The organic amine loadings of the sterically hindered amines were measured after 10 H_2S adsorption cycles and the results showed no apparent loss of organic content (<0.01% change) for the sterically hindered amine adsorbents.

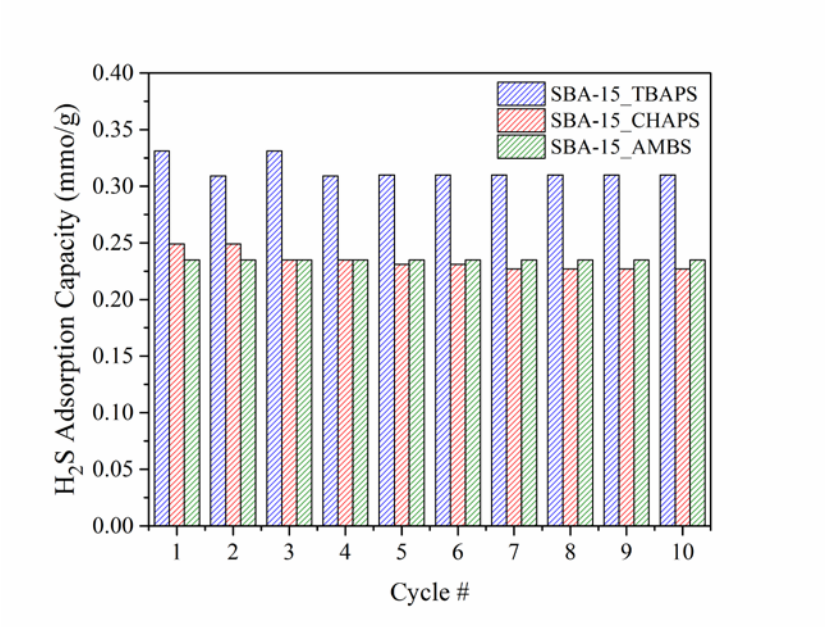

Figure 3.10. Adsorption capacities for SBA-15_TBAPS, SBA-15_CHAPS, and SBA-15_AMBS over 10 cycles of adsorption and desorption at 10% H_2S in N_2 at 30 °C

3.4 Conclusions

The effects of steric hindrance on H_2S selectivity in the adsorption of acid gases on sterically hindered amine adsorbents using a simulated biogas stream, containing H_2S and CO_2, has been explored in this chapter. In-situ IR studies and calculated heats of adsorption, both from computational chemistry and experimental adsorption isotherms, suggest the importance of hydrogen bonding on adsorption of H_2S. All hindered amine adsorbents displayed a good H_2S selectively when compared to unhindered amine sorbents. The SBA-15_TBAPS material exhibited the best H_2S selectivity of all the adsorbents studied here, which is attributed to the absence of amine-CO_2 chemisorption interactions under our nominally dry conditions due to the severe steric hindrance it experiences.

The hindered amine sorbents studied here had a similar H_2S capacity to that of an unhindered amine sorbent (SBA-15-MAPS) when exposed to a gas stream that also contained

10% CO_2 at 30 °C, which confirms the good performance of these adsorbents in the presence of CO_2. Further research must be conducted to enhance the H_2S adsorption capacities of the hindered amine sorbents for the materials to be used practically. Water, which is a component of biogas, is known to enhance the H_2S capacity of aminosilica sorbents.[5,6] Future studies will assess the effects of water on supported hindered amine sorbents. The SHA H_2S capacities were relatively stable at high H_2S concentrations (10%) over 10 cycles and it was also observed that the regeneration of these sorbents was relatively facile. These characteristics suggest that SHA could potentially be used for low energy, selective H_2S separations via adsorption.

3.5 References

(1) EPA, U.S. Greenhouse gas emissioms and sinks, 1990-2016, Epa 430-R-18-003. 106 (2002) 1323–1330. doi:EPA 430-R-12-001.

(2) NREL, Biogas potential in the United States, 2013. doi:NREL/FS-6A20-60178.

(3) N. Noramelya, Overview of H_2S removal technologies from biogas production, 11 (2016) 10060–10066.

(4) S. Lee, T. Lee, D. Kim, Adsorption of hydrogen sulfide from gas streams using the amorphous composite of α-FeOOH and activated carbon powder, Ind. Eng. Chem. Res. 56 (2017) 3116–3122. doi:10.1021/acs.iecr.6b04747.

(5) Q. Xue, Y. Liu, Removal of minor concentration of H_2S on MDEA-modified SBA-15 for gas purification, J. Ind. Eng. Chem. 18 (2012) 169–173. doi:10.1016/j.jiec.2011.11.005.

(6) W. Quan, X. Wang, C. Song, Selective removal of H_2S from biogas using solid amine-Based “molecular basket” sorbent, Energy and Fuels. 31 (2017) 9517–9528. doi:10.1021/acs.energyfuels.7b01473.

(7) X. Liu, R. Wang, Effective removal of hydrogen sulfide using 4A molecular sieve zeolite synthesized from attapulgite, J. Hazard. Mater. 326 (2017) 157–164. doi:10.1016/j.jhazmat.2016.12.030

(8) Y. Belmabkhout, P.M. Bhatt, K. Adil, R.S. Pillai, A. Cadiau, A. Shkurenko, G. Maurin, G. Liu, W.J. Koros, M. Eddaoudi, Natural gas upgrading using a fluorinated

MOF with tuned H_2S and CO_2 adsorption selectivity, Nat. Energy. 3 (2018) 1059–1066. doi:10.1038/s41560-018-0267-0.

(9) L. Du, H. Li, L. Li, J. Xu, Y. Li, Investigation of selective desulfurization performance of sterically hindered amines, Pet. Sci. Technol. 37 (2019) 56–60. doi:10.1080/10916466.2018.1490758.

(10) J.J. Lee, C. Yoo, C. Chen, S.E. Hayes, C. Sievers, C.W. Jones, Silica-supported sterically hindered amines for CO_2 Capture, Langmuir. 34 (2018) 12279–12292. doi:10.1021/acs.langmuir.8b02472.

(11) Y. Belmabkhout, G. De Weireld, A. Sayari, Amine-bearing mesoporous silica for CO_2 and H_2S removal from natural gas and biogas, Langmuir. 25 (2009) 13275–13278. doi:10.1021/la903238y.

(12) Y. Belmabkhout, N. Heymans, G. De Weireld, A. Sayari, Simultaneous adsorption of H_2S and CO_2 on triamine-grafted pore-expanded mesoporous MCM-41 Silica, Energy & Fuels. 25 (2011) 1310–1315. doi:10.1021/ef1015704.

(13) Y. H. Helen, R.T. Yang, D. Chinn, C. L. Munson, Amine-grafted MCM-48 and silica xerogel as superior sorbents for acidic gas removal from natural gas, Ind. Eng. Chem. Res. 42 (2003) 2427–2433.

(14) X. Ma, X. Wang, C. Song, “Molecular Basket” sorbents for separation of CO_2 and H_2S from various gas streams, J. Am. Chem. Soc. 131 (2009) 5777–5783. doi:10.1021/ja8074105.

(15) J. Liu, Y. Wei, P. Li, Y. Zhao, R. Zou, Selective H_2S/CO_2 separation by metal-organic frameworks based on chemical-physical adsorption, J. Phys. Chem. C. 121 (2017) 13249–13255. doi:10.1021/acs.jpcc.7b04465.

(16) J.N. Joshi, G. Zhu, J.J. Lee, E.A. Carter, C.W. Jones, R.P. Lively, K.S. Walton, Probing metal-organic framework design for adsorptive natural gas purification, Langmuir. 34 (2018) 8443–8450. doi:10.1021/acs.langmuir.8b00889.

(17) G. Liu, A. Cadiau, Y. Liu, K. Adil, V. Chernikova, I.D. Carja, Y. Belmabkhout, M. Karunakaran, O. Shekhah, C. Zhang, A.K. Itta, S. Yi, M. Eddaoudi, W.J. Koros, Enabling fluorinated MOF-based membranes for simultaneous removal of H_2S and CO_2 from natural gas, Angew. Chemie - Int. Ed. 57 (2018) 14811–14816. doi:10.1002/anie.201808991.

(18) J. N. Iyengar, D. Perry, R. B. Fedich, Sulfur recovery plant tail gas treatment process, U.S Patent 8,524,184, Sep. 3, 2013.

(19) F. Bougie, M.C. Iliuta, Sterically hindered amine-based absorbents for the removal of CO_2 from gas streams, J. Chem. Eng. Data. 57 (2012) 635–669. doi:10.1021/je200731v.

(20) B. E. Roberts, A. E. Mather, Solubility of CO_2 and H_2S in a hindered amine solution, Chem. Eng. Commun. 64 (1968) 105–111.

(21) G. Sartori, D.W. Savage, Sterically hindered amines for CO_2 removal from gases, Ind. Eng. Chem. Fundam. 22 (1983) 239–249. doi:10.1021/i100010a016.

(22) D.D. Miller, S.S.C. Chuang, The effect of electron-donating groups and hydrogen bonding on H_2S capture over polyethylene glycol/amine sites, J. Phys. Chem. C. 120 (2016) 1147–1162. doi:10.1021/acs.jpcc.5b11796.

(23) J. D. Cotton, T. C.Waddington, Liquid hydrogen sulphide as an ionising solvent. part I. base analogues and their neutralisation with hydrogen halides, J. Am. Chem. Soc. 0 (1966) 785–789.

(24) G. Sartori, W.S. Ho, D.W. Savage, G.R. Chludzinski, S.Wiechert, Sterically-hindered amines for acid-gas absorption, Sep. Purif. Methods. 16 (1987) 171–200.

(25) E. L. Stogryn, D.W. Savage, G. Sartori, Process for the selective removal of hydrogen sulfide from gaseous mixtures with severely sterically hindered secondary aminoether alcohols, U.S Patent 4,405,582, Sep 20, 1983.

(26) S.A. Didas, A.R. Kulkarni, D.S. Sholl, C.W. Jones, Role of amine structure on carbon dioxide adsorption from ultradilute gas streams such as ambient air, ChemSusChem. 5 (2012) 2058–2064. doi:10.1002/cssc.201200196.

(27) P.I. Ravikovitch, A. V. Neimark, Characterization of micro- and mesoporosity in SBA-15 materials from adsorption data by the NLDFT method, J. Phys. Chem. B. 105 (2001) 6817–6823. doi:10.1021/jp010621u.

(28) F. Rezaei, M.A. Sakwa-Novak, S. Bali, D.M. Duncanson, C.W. Jones, Shaping amine-based solid CO_2 adsorbents: Effects of pelletization pressure on the physical and chemical properties, Microporous Mesoporous Mater. 204 (2015) 34–42. doi:10.1016/j.micromeso.2014.10.047.

(29) C.N. Okonkwo, C. Okolie, A. Sujan, G. Zhu, C.W. Jones, Role of amine structure on hydrogen sulfide capture from dilute gas streams using solid adsorbents, Energy and Fuels. 32 (2018) 6926–6933. doi:10.1021/acs.energyfuels.8b00936.

(30) A. De Vylder, J. Lauwaert, M.K. Sabbe, M. Reyniers, J. De Clercq, P. Van Der Voort, J.W. Thybaut, Rational design of nucleophilic amine sites via computational probing of steric and electronic effects, Catal. Today. (2019) 1–8. doi:10.1016/j.cattod.2019.01.026.

(31) M. J. Frisch, G. W. Trucks, H. B. Schlegel, G. E. Scuseria, M. A. Robb, J. R. Cheeseman, G. Scalmani, V. Barone, G. A. Petersson, H. Nakatsuji, X. Li, M. Caricato, A. Marenich, J. Bloino, B. G. Janesko, R. Gomperts, B. Mennucci, H. P. Hratchian, J. V. Ort, Gaussian 09. (2016)

(32) C. M. Simon, B. Smit, M. Haranczyk, pyIAST: Ideal adsorbed solution theory (IAST) Python package, Comput. Phys. Commun. 200 (2016) 364–380.

(33) K. Wang, S. Qiao, X. Hu, Application of IAST in the prediction of multicomponent adsorption equilibrium of gases in heterogeneous solids: Micropore size distribution versus energy distribution, Ind. Eng. Chem. Res. 39 (2000) 527–532. doi:10.1021/ie990548i.

(34) Y. Belmabkhout, N. Heymans, G. De Weireld, A. Sayari, Simultaneous aadsorption of H_2S and CO_2 on triamine-grafted pore-expanded mesoporous MCM-41 silica, Energy & Fuels. 25 (2011) 1310–1315. doi:10.1021/ef1015704.

(35) P. Bollini, N.A. Brunelli, S.A. Didas, C.W. Jones, Dynamics of CO_2 adsorption on amine adsorbents. 2. insights into adsorbent design, Ind. Eng. Chem. Res. 51 (2012) 15153–15162. doi:10.1021/ie3017913.

(36) D.D. Do, Adsorption analysis: equilibria and kinetics, in: R. T. Yang (Eds) , Imperial College Press, London, **1998**, Vol 2, pp 64-69. doi:10.1142/9781860943829.

(37) M.A. Alkhabbaz, P. Bollini, G.S. Foo, C. Sievers, C.W. Jones, Important roles of enthalpic and entropic contributions to CO_2 capture from simulated flue gas and ambient air using mesoporous silica grafted amines, J. Am. Chem. Soc. 136 (2014) 13170–13173. doi:10.1021/ja507655x.

(38) C.J. Yoo, L.C. Lee, C.W. Jones, Probing Intramolecular versus Intermolecular CO_2 Adsorption on Amine-Grafted SBA-15, Langmuir. 31 (2015) 13350–13360. doi:10.1021/acs.langmuir.5b03657.

CHAPTER 4. EFFECT OF HUMIDITY ON THE SORPTION OF H_2S FROM MULTI-COMPONENT ACID GAS STREAMS ON SILICA-SUPPORTED STERICALLY HINDERED AND UNHINDERED AMINES

All computational work in this chapter was carried out by Dr. Hanjun Fang, Sholl group, Georgia Tech.

4.1 Background

Biogas streams are composed of methane (CH_4), carbon dioxide (CO_2), hydrogen sulfide (H_2S) and water vapor (H_2O) and to increase the calorific value of biogas, CO_2 and H_2S removal by biogas upgrading is required. CO_2 removal from biogas has been extensively explored but there is limited information on H_2S capture from this source.[1–3] H_2S is a poisonous and corrosive gas that releases sulfur oxides when combusted, leading to acid rain, causing environmental hazards.[4–7] Upgrading of biogas to biomethane makes it a potential source of renewable energy that can be injected into natural gas pipelines and used as fuels for heating or transportation.[8] This additional source of energy could help alleviate the current global energy demand and reduce waste and greenhouse gas (GHG) emissions.[9]

The use of aqueous amine absorbents has been implemented over the years for industrial scale sulfur removal, but limitations arise in the external heat required for regeneration, which increases operating costs.[10] Solid-supported amines have recently been explored as promising materials for the removal of H_2S from simulated biogas streams owing to their potentially lower regeneration requirements.[11–17] A recently studied class of solid-supported amines containing

covalent linkages between pendant aminosilanes and porous oxide supports provides a promising platform for the development of structure-property relationships for these model acid gas sorbents.[3,15,18]

To replicate practical biogas compositions, which often contain 5-10% water vapor, it is important to evaluate the impact of humidity on H_2S sorption.[19,20] Indeed, vapor/gas phase combinations of water and acidic species often behave substantially differently from dry acid gases in their interactions with catalytic and separations materials.[21–23] However, most likely due to equipment limitations on the lab scale, there is very limited published information on the effect of humidity on H_2S sorption on solid supports[14,24–30] and even less using chemically grafted solid-supported sorbents.[17,31–33]

Solid supports such as activated carbons and metal-organic frameworks (MOF's) have been evaluated for H_2S capture under humid conditions. Wood based activated carbons,[34] KOH impregnated activated carbons[35] and carbonaceous sorbents[28] have shown improvement in H_2S sorption capacities under such conditions. Additionally, the work of Petit et. al on MOF/GO composites showed that prehumidification of the bed promoted H_2S retention.[36] On the other hand, the A1FFIVE-1-Ni MOF studied by Belmabkhout et al., which was observed to simultaneously sorb H_2S and CO_2, showed negligible change in the H_2S/CO_2 sorption capacity under humid conditions.[37] Titanosilicates have also been considered for H_2S capture, though they require relatively high temperatures for sorption (75-950 °C).[38] The Cu-ETS-2 titanosilicate evaluated in the work of Roller et al. showed a reduction in the H_2S sorption capacity as the H_2O concentration increased.[38] Given the varied results obtained, these reports further confirm the need to assess the effect of humidity new solid supports that show the potential to capture H_2S.

The few studies that assessed the impact of humidity on H_2S sorption using solid-supported amines have reported conflicting results. For example, Song and coworkers reported that the H_2S sorption capacity under humid conditions did not improve with a tertiary amine based sorbent, tetramethyl hexanediamine (TMHDA) impregnated in SBA-15 in the presence of CO_2, but a slight increase in H_2S sorption capacity was observed in the absence of CO_2.[39] Another study using a chemically grafted primary amine, 3-aminopropyltriethoxysilane (APTES) functionalized on MCM-48, proposed that the presence of moisture had no effect on H_2S sorption.[31] While the functionalization of activated carbon with APTES led to an increase in the H_2S sorption capacity by four times relative to the H_2S capacity observed for bare activated carbon, the presence of moisture had a negative effect on H_2S removal using the material.[32] Another study by Wang et al. showed a promoting effect of 3% water vapor on 50 wt% PEI/SBA-15.[33] These reports show that the amine type and support type influences H_2S sorption in humid conditions and they confirm the importance of understanding how new combinations of solid-supported sorbents behave in the presence of humidity to help consider their practical use for H_2S removal in biogas streams. Most of these studies did not consider the effect of CO_2 in the gas composition during humid-H_2S sorption, which is likely to be an additional complicating factor, as many relevant streams contain CO_2, H_2S and water.

The H_2S sorption mechanism influences the sorption capacity and H_2S selectivity of sorbents under humid or dry multicomponent gas conditions. In solution, the mechanism of H_2S sorption on amine sites has been reported to follow a simple proton transfer mechanism where H_2S dissociates and protonates the amine. In the solid analogue under dry conditions, computational studies coupled with heat of sorption results have suggested that the H atom in H_2S hydrogen bonds to the basic amine group to form an H_2S-amine complex that requires two

amine molecules to interact with one H_2S.[40] Previously, it has been proposed that under both humid and dry conditions a hydrogen bonding interaction with a H_2S -amine-water complex occurs, with one amine interacting with one H_2S molecule. However, this proposed mechanism was not supported with spectroscopic or computational evidence, rather it was proposed based on quantitative comparisons to the theoretical H_2S sorption capacity.[39]

Sterically hindered amines (SHA), which have bulky alkyl groups attached to their primary/secondary amine site, and unhindered tertiary amines such as N-methyldiethanolamine (MDEA) have been widely researched in aqueous solutions for H_2S capture applications. They have been reported to have both high H_2S selectivities and good stability, but there is limited information available on their solid-supported analogues.[41–45] In our previous studies, H_2S sorption experiments confirmed similar promising performance characteristics for the solid-analogues. Specifically, a sterically hindered amine, based on a *tert*-butylaminopropylsilyl-grafted species, showed high H_2S selectivity and good stability in the presence of H_2S, CO_2 and CH_4. In addition, a tertiary amine, based on a dimethylaminopropylsilyl-grafted species showed good stability when exposed to high H_2S concentrations (10% H_2S in N_2).[40,46] To the best of our knowledge, the effect of humidity on H_2S sorption under single and multicomponent gas conditions is yet to be investigated for sterically hindered amine sorbents.

In this study, to provide more detailed understanding of the effect of humidity on H_2S sorption in a multicomponent gas stream, a sterically hindered amine [*tert*-butylaminopropyltrimethoxysilane (TBAPS)] and a tertiary amine, [N,N-dimethyl-3-aminopropyltrimethoxysilane (DMAPS)] grafted onto mesoporous silica SBA-15 are studied under dry and humid mixed gas conditions. Dry and humid H_2S uptakes, selectivities and amine efficiencies for the sterically hindered and unhindered amines were measured using fixed bed

breakthrough experiments. In-situ FTIR spectroscopy was implemented to elucidate any differences in species sorbed under humid and dry conditions and sorption energies were calculated using computational methods to probe possible sorption mechanisms under humid and dry H_2S conditions. Lastly, owing to the increased corrosiveness of H_2S in humid conditions, NMR spectroscopy, elemental analysis and N_2 physisorption were used to evaluate the potential for support or amine degradation after humid H_2S sorption.

4.2 Methods

4.2.1 Materials

The following chemicals were used as received from Sigma–Aldrich: Pluronic 123: $(EO)_{20}(PO)_{70}(EO)_{20}$), tetraethyl orthosilicate (TEOS, 98%). Hydrochloric acid (ACS grade, 36.5-38%), hexane (98.5%), methanol (ACS grade, >99.8%) and toluene (ACS grade, >99.5%) were purchased from BDH and. For the grafting procedure, the following chemicals purchased from Gelest were used: *tert*-butylaminopropyltrimethoxysilane and (N, N-dimethylaminopropyl) trimethoxysilane. Specialty gases were purchased from Airgas and include the following: 1% H_2S in N_2, 10% H_2S in N_2, 1% H_2S/ 10% CO_2 / 89% CH_4 and 1% H_2S/ 30% CO_2/ 69% CH_4. Inert gases such as UHP nitrogen and helium were also purchased from Airgas.

4.2.2 Material Synthesis

In a 2 L Erlenmeyer flask, 36 g of Pluronic 123 block copolymer was dissolved in 180 mL of hydrochloric acid and 950 g of distilled water. After stirring the solution for 3 h at room temperature, 70 mL of tetraethyl orthosilicate (TEOS) was added dropwise and stirred at 40 °C for 20 h after which a white precipitate formed. The solution was heated to 100 °C for 24 h

without stirring. The precipitate was filtered and washed with distilled water, after which it was dried in a 75 °C oven overnight. The dried product was calcined in an oven using the following temperature program: ramp to 200 °C at 1.2 °C/min, hold at 200 °C for 1 h, ramp to 550 °C at 1.2 °C/min, hold at 550 °C for 12 h, cool to room temperature at 10 °C/min.

4.2.3 Grafting of Aminosilanes on SBA-15

Silica SBA-15 was dried overnight at 110 °C on a high vacuum line at a pressure of 10 mTorr. To create a homogeneous mixture, the silica was stirred in 200 mL of toluene for an hour and then 600 µL of DI water was added with a pipette and stirred continuously at room temperature for 3 h. Next, 6 mL of the desired aminosilane was added to the mixture at loadings necessary to obtain similar amine densities on each material. **Figure 4.1** shows the chemical structures of the aminosilanes used during this study. The solution containing added aminosilane was stirred at 85 °C for 24 h under nitrogen. Next, the final product was filtered with 300 mL of toluene, hexane and methanol consecutively. The product was dried under vacuum overnight at 75 °C under a pressure of 10 mTorr.

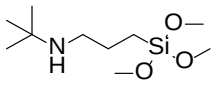

Tert-butylaminopropyltrimethoxysilane
(TBAPS)

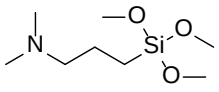

(N,N-Dimethylaminopropyl)trimethoxysilane
(DMAPS)

Figure 4.1. Chemical names and structures of aminosilanes used in this study.

4.2.4 Material Characterization

N_2 physisorption was performed on a Micromeritics Tristar II at 77 K were the BET surface area, mean pore size, and pore volumes were obtained. To calculate the surface area and

mean pore size from the isotherm data, the Brunauer-Emmett–Teller (BET) and Broekhoff-de Boer method with the Frenkel-Halsey-Hill equation (BdB-FHH method) were used, respectively. To determine the chemical composition of the sorbents, samples were sent to Galbraith for elemental analyses (C, H, N, S and Si).

4.2.5 Water Sorption Isotherms

The gravimetric water sorption measurements were performed on a TA VTI-SA+ automated vapor sorption analyzer (TA Instruments, New Castle, DE) at 30 °C with relative pressures ranging from 0 to 0.9. Before each test, the samples were dried in situ at 120 °C for 3 h under flowing nitrogen.

4.2.6 Dynamic Sorption Measurements

Dry and humid H_2S capacities were obtained using a 6 mm × 4 mm (outer diameter × inner diameter) fixed bed made of quartz. A schematic of the set-up is shown in **Figure C.1**. The outlet gas was analyzed using an Omnistar GSD 320 mass spectrometer. A typical run used 70−100 mg of sample, pelletized at 1000 psi for 30 seconds and then sieved at a mesh size between 425−850 μm.

Dry sorption measurements using the fixed bed followed a similar to chapter 3. For both humid and dry experiments, each sample was pretreated in flowing UHP He at 50 sccm and 120 °C for 2 h, after which the temperature of the bed was reduced to 30 °C for sorption. During humid sorption measurements, the bed was first pre-saturated; a humid He stream (49 % relative humidity (RH) at 30 °C) was introduced into the bed at 100 sccm until the outlet stream concentration matched the inlet stream concentration of water (2 mol%). Humidity was

generated by flowing UHP helium through a bubbler containing a saturated salt solution of potassium carbonate (K_2CO_3) in DI water that was maintained at 30 °C. Once the bed was saturated with water, the humid stream (100 sccm) was mixed with the dry H_2S containing gas streams flowing at 100 sccm (1% H_2S in N_2 or 1% H_2S/30% CO_2/69% CH_4) and then introduced to the bed. During dry and humid experiments, the desorption step was started when the outlet stream concentration of H_2S reached 98% of the inlet stream concentration of H_2S. The sorbed species were desorbed from the bed by flowing dry helium at 50 sccm through the bed at a temperature of 120 °C, conditions that were maintained until the outlet concentrations were below 5 ppm. The H_2S capacities were calculated by integrating the area above the breakthrough at the breakthrough point during the sorption step.

4.2.7 In Situ Fourier-Transform IR (FTIR) Spectroscopy

In situ IR spectroscopy experiments were preformed using a diffuse reflectance Harrick Praying Mantis high temperature reaction chamber coated with Siliconert. The IR spectrometer used for these experiments was a Thermo Nicolet is10 with a mercury cadmium telluride (MCT) detector. All flow rates were held constant at 20 mL/min. All samples used for dry sorption experiments were activated at 120 °C under UHP He flow. The samples were then exposed to 10% H_2S in N_2. All H_2S sorption spectra were taken with KBr as the background. The spectra were taken at both long (every minute for an hour) and short time scales (every 5 seconds for 5 minutes) at a resolution of 4 cm^{-1} at 64 scans.

4.2.8 NMR Spectroscopy

All solid-state ^{13}C and ^{29}Si NMR measurements were performed on a Bruker DSX- 300 spectrometer with a spinning frequency of 10 kHz. All sorbents were tested using a 4 mm

zirconia rotor. For solid-state ^{13}C and ^{29}Si experiments, both cross-polarization (CP) and direct polarization (DP) magic-angle spinning (MAS) experiments were performed. Quantitative NMR spectra, i.e. NMR spectra, where the relative peak intensity reflects the corresponding molar amount of corresponding species, were obtained be recurred using the DP (direct polarization experiments) recorded under a condition where the repetition delay between scans, T_R, was set significantly larger than the longitudinal relaxation time, T_1, of all species. Due to a poor signal to noise ratio and long relaxation times it was not feasible to conduct T_1 experiments for all samples. As a compromise, one representative sample was measured with increasing repetition delays to establish repetition delays where the ratio of peak intensities would not change upon increase of TR, leading to the conditions noted here. For DP-MAS experiments, ^{29}Si NMR spectroscopy data were acquired at a pulse length of 2.5 μs with a recycle delay of 600 s and 128 scans. ^{13}C spectra were collected with a 20 s recycle delay and 1028 scans. For CP-MAS experiments, the contact time was set to 3 ms with a 2048 and 4096 scans for ^{13}C and ^{29}Si NMR, respectively. ^{13}C and ^{29}Si NMR spectra chemical shifts were referenced relative to adamantane and tetramethylsilane, respectively. Furthermore, all DP-MAS spectra were deconvoluted with OriginPro and fit with Gaussian/Lorentzian curves.

*4.2.9 Computational Modeling Method***

As a complement to the experimental characterization, density functional theory (DFT) calculations were performed to investigate the effect of H_2O on H_2S sorption on the amine-modified sorbents, SBA15-TBAPS and SBA15-DMAPS. Following the strategy used in our previous work,[40] only the organic groups of the sorbents were modeled to reduce the computational cost. Geometry optimizations and energy calculations were performed at the B3LYP-D3/6-31+g(d, p) level of theory using Gaussian 16, where all atoms were relaxed during

geometry optimizations.[47] Compared to the B3LYP functional, the D3 version of Grimme's dispersion with Becke-Johnson damping was included to more reliably account for sorption energies,[48,49] where van der Waals interactions could play an important role in the sorption of molecules such as H_2S and H_2O in nanoporous materials.[50,51] It should be noted that there may be multiple local minimum energy states for each adsorption complex depending on the initial configuration used during energy minimization, especially on two amine sites. To find the global minimum energy states, we sampled different initial configurations for geometry optimizations and chose the most stable ones among them. Infrared normal vibrational frequencies were determined using analytic second derivatives of the energy with respect to nuclear displacement at the same level of theory as geometry optimizations, and frequencies were not corrected with scaling factors prior to comparison with the experimental infrared spectra. The sorption energies between molecules and amine sites were defined using,

$$E_{ads} = E_{complex} - \sum E_{amine} - \sum E_{molecule} \quad (1)$$

where: $E_{complex}$, $\sum E_{amine}$ and $\sum E_{molecule}$ are the total energies for the optimized sorption complex, isolated amine sites, isolated H_2S and (or) H_2O molecules, respectively.

4.3 Results & Discussion

4.3.1 Material Characterization

N_2 physisorption was used to determine the surface area and pore volume of the amine modified mesoporous silicas. **Figure C.2** shows isotherms with type IV hysteresis that are common for mesoporous structures**.** The aminosilanes were successfully grafted on the surface of the silica support, as observed by the reduced pore volumes (**Figure C.3, Table 4.1**) and

**All computational work in this chapter was carried out by Dr. Hanjun Fang, Sholl group, Georgia Tech

surface areas (**Table 4.1)**. Similar moderate amine loadings of 2.2-2.9 mmol N/g_{sio2} were achieved to make appropriate comparisons between the sorbents studied.

Table 4.1 Structural Properties of Sorbent Materials

Sample	Amine loading ($mmolN/g_{SiO2}$)	Surface area (m^2/g_{SiO2})	Mean pore size (nm)	Pore volume (cm^3/g)	Pore filling (%)
SBA-15	-	756	6.3	1.9	
SBA-15_TBAPS	2.2	303	5.6	0.42	78
SBA-15_DMAPS	2.9	286	5.4	0.45	80

4.3.2 Fixed Bed Sorption Measurements

Fixed bed measurements were conducted on the sterically hindered amine SBA-15_TBAPS and the tertiary unhindered sorbent, SBA-15_DMAPS, in H_2S gas mixtures with and without CO_2 to determine their H_2S sorption capacities under dry and humid conditions. Under dry conditions, SBA-15_DMAPS, was observed to have stable H_2S sorption capacities in the presence of 10% and 30% CO_2 **(Figure 4.2(a))**. Previously, it has been shown that negligible CO_2 is sorbed by SBA-15_DMAPS under dry conditions.[3,18] Additionally, SBA-15_TBAPS showed negligible change in H_2S sorption capacity with and without CO_2, as also demonstrated in chapter 3, where the thermodynamic selectivity of SBA-15_TBAPS for H_2S in the presence of CO_2 was evaluated based on ideal adsorption theory, measured heats of adsorption of CO_2 and the enthalpies from isotherms fit at different temperatures for H_2S under dry conditions. Briefly, it was proposed that the selectivity of SBA-15_TBAPS for H_2S is attributed to the impact of the severely sterically hindered *t*-butyl functional group, which hinders CO_2 adsorption by lowering the enthalpy of adsorption and/or providing a more severe entropic penalty for adsorption of

CO_2. From the negligible differences in H_2S sorption capacities with and without CO_2 in the mixture, it is evident that SBA-15_TBAPS and SBA-15_DMAPS are highly selective for H_2S in the presence of CO_2. However, the H_2S sorption capacities and amine efficiencies **(Figure 4.2)** were three times higher for SBA-15_TBAPS than SBA-15_DMAPS under dry conditions. The higher H_2S sorption capacities for SBA-15_TBAPS compared to SBA-15_ DMAPS are likely due to the higher proton basicity of the secondary amines in SBA-15_TBAPS compared to the weaker base of the tertiary amine sorbent.[46,52]

Both SBA-15_TBAPS and SBA-15_DMAPS exhibited a higher H_2S sorption capacity under humid conditions than in dry conditions (**Figure 4.3**). Under humid conditions, SBA-15_DMAPS had twice the H_2S sorption capacity of SBA-15_TBAPS. To compare the increase in H_2S capacity under humid conditions, the efficiency enhancement, defined as the ratio of the humid amine efficiency of the sorbent to the amine efficiency under dry conditions, was calculated (**Table 4.2**). Without CO_2 present, SBA-15_DMAPS had three times the efficiency enhancement of SBA-15_TBAPS, which means it had the largest increase in H_2S sorption capacity when comparing humid to dry conditions. In the presence of CO_2, negligible change in the H_2S sorption capacity was observed for SBA-15_DMAPS and SBA-15_TBAPS, with negligible CO_2 sorbed **(Figure 4.3 and Figure C.4)**. The adsorption enthalpies, which will provide insight on the impact of thermodynamics on the selectivity of H_2S in the presence of CO_2 under humid conditions, are further evaluated in section 4.3.3 using computational studies.

To better understand the correlation between H_2S uptake and time, the sorption kinetic curves under humid and dry conditions were compared (**Figure 4.4**). In dry conditions, the curves displayed a linear and fast approach to the equilibrium capacity, while under humid conditions, the curve showed a slow increase in H_2S uptake with time. Interestingly, SBA-

15_DMAPS showed a slower increase in H_2S uptake compared to SBA-15_TBAPS. It is evident from the shape of the kinetic curves that the presence of water slows down the kinetics during H_2S sorption but improves the total sorption capacity; a similar trend has been reported for the sorption of H_2S on KOH impregnated activated carbon with 70% relative humidity.[35]

Furthermore, water sorption isotherms were measured for all the sorbents and the amount of water sorbed at the humid fixed bed sorption conditions of 49% RH at 30 °C is shown in **Table 4.2, Figure C.5**. The isotherms demonstrate the hydrophilic nature of the amine-modified sorbents. SBA-15_DMAPS showed a higher H_2O sorption capacity compared to SBA-15_TBAPS. Some activated carbons that have high water sorption capacities have been reported to promote H_2S sorption.[53] Hence, the hydrophilicity of the sorbents studied could promote the condensation of water as a film on the sorbent surface. The formation of a water film, where H_2S is absorbed by water on either an amine containing sorbent such as PEI/SBA-15[33] or on activated carbon[28,32,54] has been reported to promote H_2S dissociation, thereby increasing the H_2S sorption capacity. Therefore, for both sorbents, the increase in H_2S sorption capacity in the presence of humidity may be due to the dissociation of H_2S promoted by the sorbed water to form chemisorbed HS^- and H^+ ions.[32,35] The effect of humidity on the H_2S sorption capacities for SBA-15_TBAPS and SBA-15_DMAPS were further assessed using in-situ IR and computational studies, as discussed below.

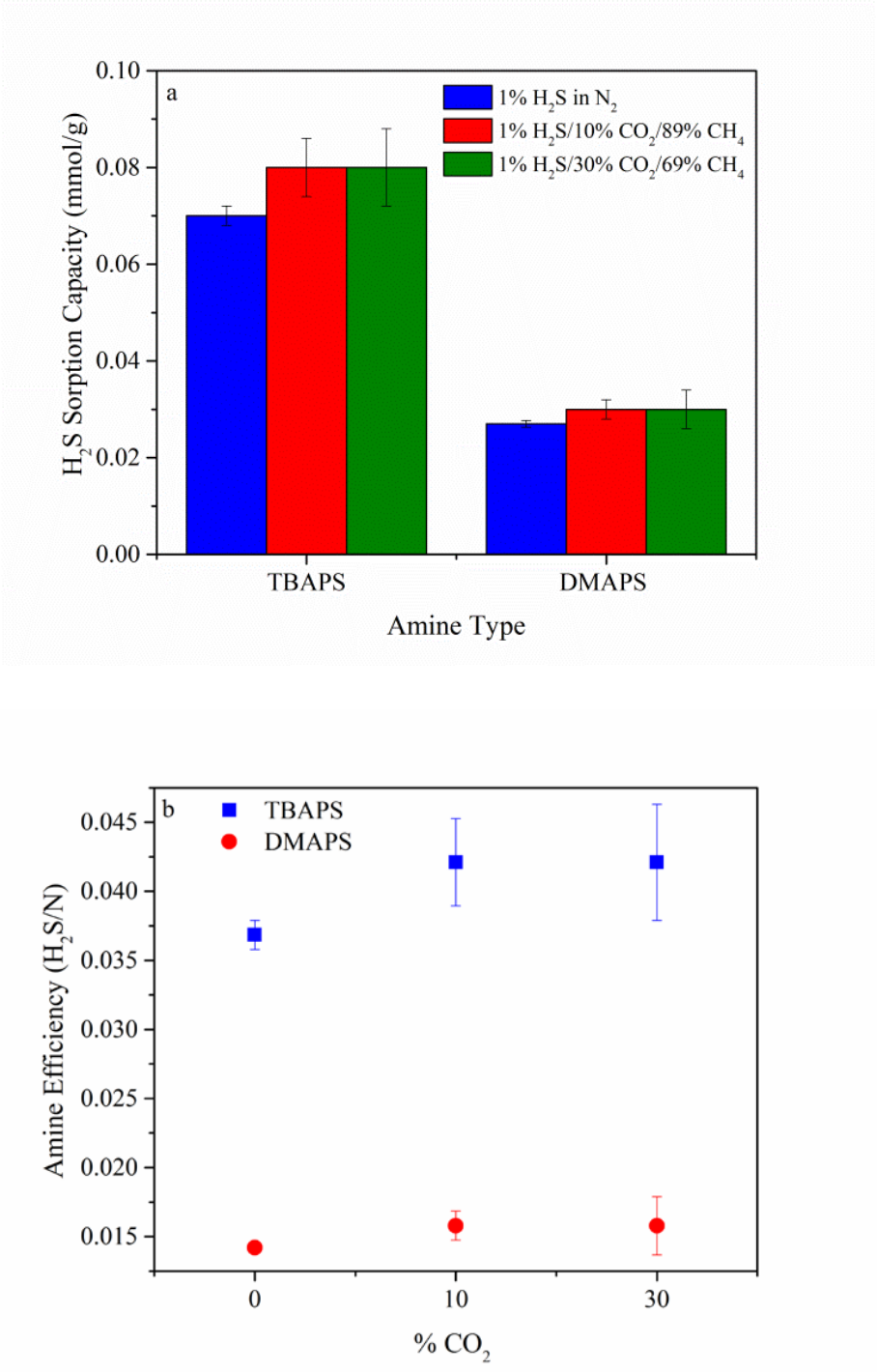

Figure 4.2. (a) H_2S sorption capacities and (b) amine efficiencies for hindered and unhindered amine sorbents with and without CO_2 under dry conditions at 30 °C. The error bars were estimated with three consecutive experiments

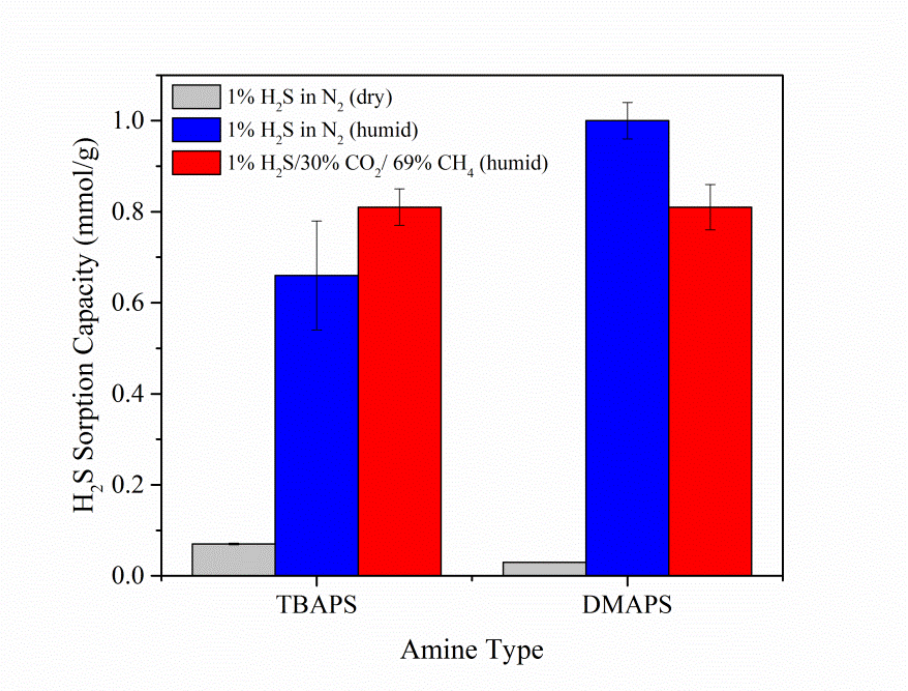

Figure 4.3. H_2S sorption capacities under dry and humid conditions (49% RH) at 30 °C. The reported error in the humid and dry runs is the standard deviation calculated from three independent runs.

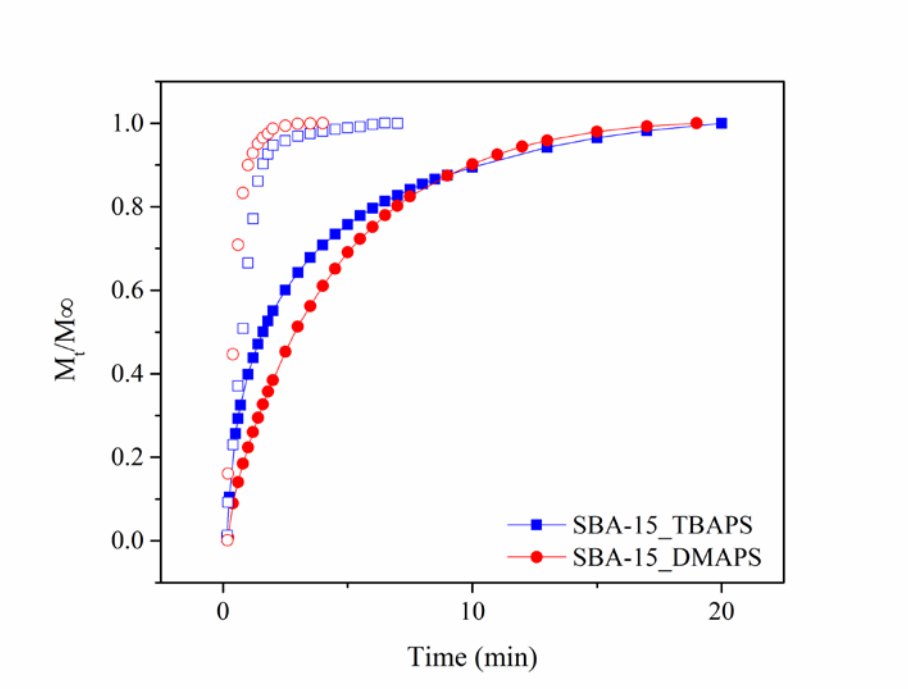

Figure 4.4. Comparison of normalized H_2S uptake profiles for SBA-15_TBAPS and SBA-15_DMAPS under humid (filled symbols) and dry (open symbols) conditions using 1% H_2S in N_2 at 30 °C.

Table 4.2. Dry and Humid H_2S Capacities using 1% H_2S in N_2 at 30 °C

Sorbent	H_2S capacity (dry) (mmol/g)	H_2S capacity (humid) (mmol/g)	Amine efficiency (dry) (H_2S/N)	Amine efficiency (humid) (H_2S/N)	Efficiency enhancement (humid A.E. /dry A.E.)	H_2O capacity (mmol/g)
SBA-15_TBAPS	0.07	0.66	0.03	0.3	10	1.3
SBA-15_DMAPS	0.03	1	0.01	0.3	30	1.7

4.3.3 Computational Analysis of H_2S Sorption Mechanism

Previous computational studies indicate that one H_2S molecule can sorb at both one amine site or two amine sites.[40,55] In this study, the H_2S interaction with one TBAPS amine site in the presence of different amounts of H_2O was initially evaluated. **Figure 4.5(a)-(c)** shows the DFT optimized structures of H_2S sorption complexes on TBAPS. When no H_2O is present, the H_2S molecule sorbs at the amine site via S-H ⋯ N hydrogen bonding with a sorption energy of -33 kJ/mol (**Figure 4.5(a)**). This is consistent with a physisorption interaction. When one H_2O molecule was present and coordinated to H_2S by O-H ⋯ S hydrogen bonding, one H atom of H_2S was found to readily transfer to the N atom of the TBAPS amine group (**Figure 4.5(b)**). During H transfer the S–H covalent bond is completely broken while a new N–H bond is formed, resulting in the formation of the chemisorbed HS^-–NH_2^+ species. Similar HS^- sorbed species have been observed and identified by Miller and Chang for H_2S sorption over tetraethylenepentamine (TEPA).[6] In the presence of two H_2O molecules (**Figure 4.5(c)**) the H atom of H_2S transfers even more effectively to the amine group, as indicated by the longer S-H distance (2.092 Å) and the shorter N-H bond length (1.075 Å) compared to the one H_2O case (1.911 and 1.121 Å, respectively). The additional H_2O molecule can help to stabilize the sorbed HS^- species via the O-H ⋯ S hydrogen bond.

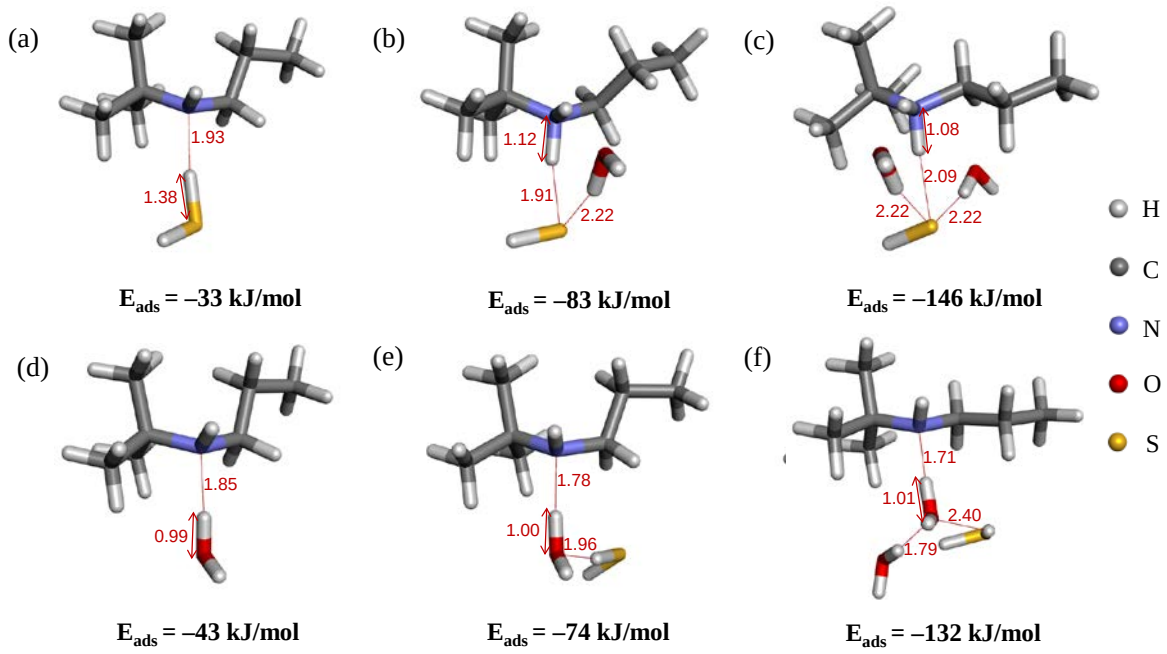

Figure 4.5. Computationally optimized structures for sorption complexes of H_2S and H_2O on one amine site of TBAPS through (a–c) H_2S-amine interactions and (d–f) H_2O-amine interactions. Sorption energies of the molecules (in kJ/mol) and main atomic distances (in Å) are shown.

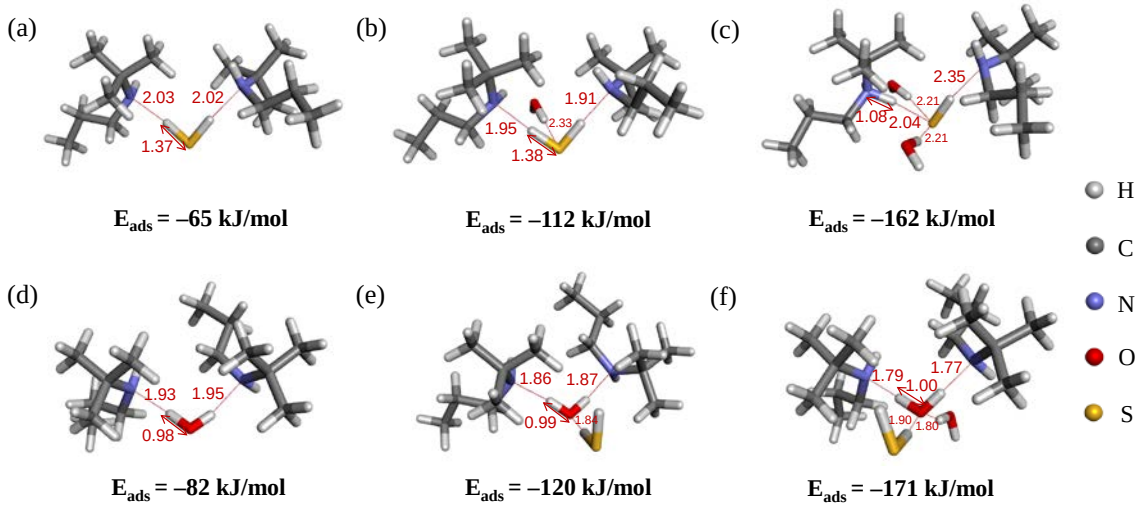

Figure 4.6. Computationally optimized structures for sorption complexes of H_2S and H_2O on two amine sites of TBAPS through (a–c) H_2S-amine interactions and (d–f) H_2O-amine interactions. Sorption energies of the molecules (in kJ/mol) and main atomic distances (in Å) are shown.

Under humid conditions, H_2S and H_2O competitively sorb on the amine sites. The possibility of the formation of H_2S or HS^- sorbed species on the amine sites can be evaluated by comparing their sorption energies with those of the sorption complexes where the binding is through H_2O-amine interactions (**Figure 4.5(d)-(f)**). While a single H_2S molecule binds more weakly than a single H_2O molecule by 10 kJ/mol (**Figure 4.5(a)** and **(d)**), the co-sorption complex of one H_2S and one H_2O via H_2S-amine interactions to form the chemisorbed HS^- species is energetically more favorable than that via H_2O-amine interaction by 9 kJ/mol (**Figure 4.5(b)** and **(e)**). For the case of one H_2S and two H_2O, H_2S sorbs even more preferentially on the amine site and forms the HS^- species over H_2O (by 14 kJ/mol, **Figure 4.5(c)** and **(f)**).

For H_2S interacting with two SBA15-grafted amine sites, we were not able to observe situations where the presence of one H_2O molecule led to H transfer from H_2S to the amine group (**Figure 4.6(b)**), However, two H_2O molecules can facilitate the H transfer from H_2S to the N atom of the amine site and form a chemisorbed HS^--NH_2^+ species (**Figure 4.6(c)**). The sorption energy of this HS^- sorption complex is only 9 kJ/mol weaker compared to the corresponding cosorption complex via H_2O-amine interactions (**Figure 4.6(f)**). As expected, transfer of two H atoms from H_2S to the two amine sites simultaneously was not observed in our DFT calculations. The interaction of H_2S with the amine sites of DMAPS was also explored, and the results are similar to that of H_2S on TBAPS discussed above (**see Figures C.6** and **C.7**).

To evaluate the thermodynamic selectivity of TBAPS for H_2S in the presence of CO_2, the adsorption enthalpy of the species formed when CO_2 adsorbs on TBAPS was calculated. The DFT optimized structures are shown in **Figure 4.7(a)-(f)**. When no H_2O is present, the CO_2 molecule sorbs at the amine site primarily via the electrostatic interaction between the C atom in CO_2 and the N atom of the amine with a sorption energy of -25 kJ/mol (**Figure 4.7(a)**). This is a

physisorption interaction. Similar adsorption configurations were observed by Ma et al.[55] The carbamic acid structure, which is a chemisorbed species of CO_2 with the amine site, was optimized and the sorption energy was calculated to be +3 kJ/mol, indicating it is an energetically unfavorable species; (**Figure 4.7(b)**) in fact, Lee et al. proposed that due to the severe steric hindrance of the *t*-butyl functional group on TBAPS, only bicarbonates were formed during CO_2 adsorption whereas carbamates and carbamic acids were not observed in their in-situ IR experiments. Furthermore, these bicarbonates were formed only in the presence of water via carbamate hydrolysis or a base catalyzed hydrolysis with one amine.[42] Interestingly, the DFT optimized structures show the formation of carbonic acid **(Figure 4.7(d))**. Carbonic acid could be formed by the direct reaction of CO_2 and H_2O, which is stabilized by the hydrogen bonding with the amine group of TBAPS, but this structure has not been observed under experimental conditions.

In the presence of one H_2O molecule, the bicarbonate structure during the interaction of CO_2 with one amine was found to be formed on TBAPS via two N-H ⋯ O hydrogen bonds at the B3LYP-D3/6-31+g(d,p) level of theory (**Figure 4.7(c)**). Its sorption energy (-76 kJ/mol) is larger than those of the carbonic acid and physisorbed complexes by 7-23 kJ/mol (**Figure 4.7(d)-(f)**). Furthermore, the co-sorption complex of one H_2S and one H_2O via H_2S-amine interactions to form the chemisorbed HS^- species is energetically more favorable than the bicarbonate by 7 kJ/mol (-83 vs -76 kJ/mol), which supports the high H_2S selectivity experimentally observed for TBAPS under humid conditions. However, the relatively small difference in sorption energy for CO_2 vs H_2S likely cannot account for the massive difference in uptake observed experimentally, suggesting that kinetic factors may also be at play.

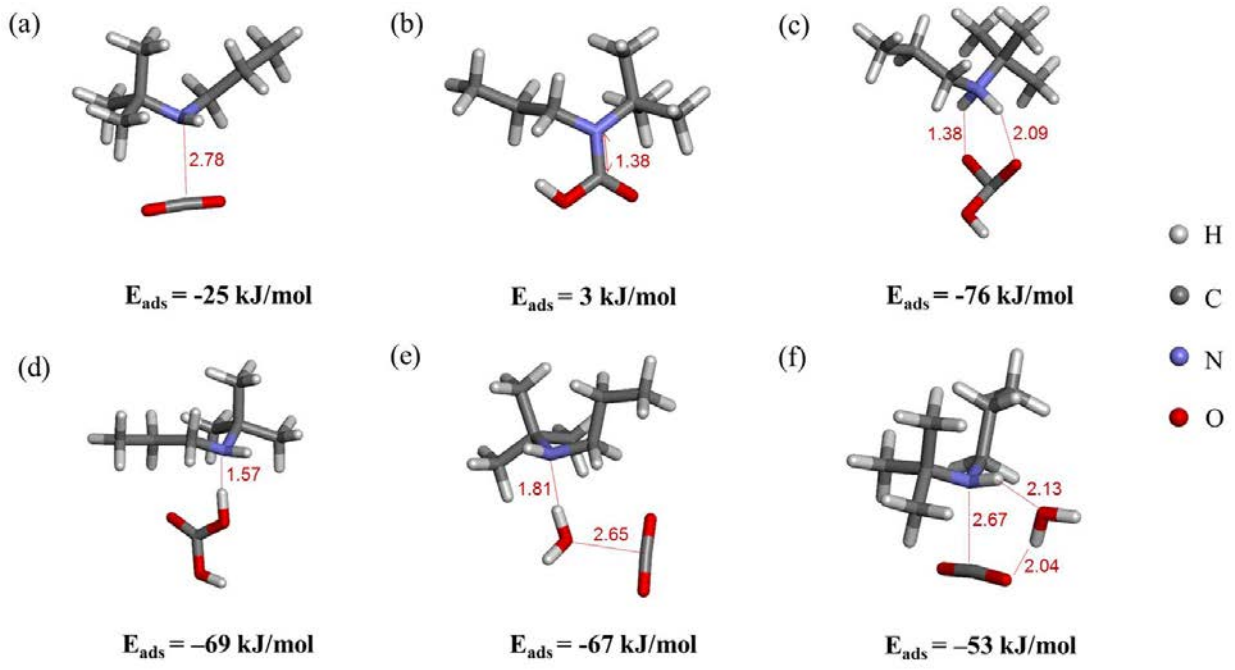

Figure 4.7. Computationally optimized structures for sorption complexes of CO_2 on one amine site of TBAPS (a–b) in the absence of H_2O and (c-f) in the presence of one H_2O molecule via physisorbed and chemisorbed interactions. Sorption energies of the molecules (in kJ/mol) and main atomic distances (in Å) are shown.

The DFT calculations demonstrate that the presence of H_2O facilitates proton transfer from H_2S to the amine group of the sorbent and the formation of chemisorbed HS^- species. These HS^- species are energetically more stable or comparable to the sorption complexes where the binding is through H_2O-amine interactions. These computational modeling results give insight into the experimental observation that the H_2S capacities increase when the sorption is performed under humid conditions and further establishes the thermodynamic selectivity of these sorbents for H_2S in the presence of CO_2.

4.3.4 FTIR Spectra of Sorbed H_2S in Humid and Dry Conditions

To further elucidate the nature of the H_2S-amine species formed on the sorbents under dry and wet conditions, in-situ FTIR spectroscopy experiments were conducted. For the wet experiments, the sorbents were saturated with a 1:1 ratio of sorbent to water. To ensure the sorbents were wet during the initial H_2S sorption step, activation of the sorbent at 120 °C in UHP He unlike under dry H_2S adsorption experiments. The wet sorption spectra for all sorbents showed a peak at 3214 cm^{-1} and 1649 cm^{-1}, which support the presence of Si-OH and OH deformation vibrations of physisorbed H_2O **(Figure C.8)**.[42,56] An additional peak at 1468 cm^{-1} was observed and could be attributed to a blueshift of the CH_3 deformation in wet conditions. As the sorption progressed with time, a decrease of the intensities for the Si-OH and OH bands was observed. This reduction can be attributed to sample drying as the dry H_2S gas is sorbed onto the sorbent. In fully dry conditions, minimal change in intensities for the Si-OH and OH bands was observed.

For the SBA-15_TBAPS sorbent under dry conditions, peaks observed for H_2S sorbed species were similar to those observed in a previous study (**Figure C.10(a)**).[40] Specifically, the stretching modes of the HS^{-}-NH_2^{+} stretch at 2568 cm^{-1} and the physisorbed S-H···N hydrogen bonded species at 2435 cm^{-1} are observed[6,57] (**Figure 4.8(a)**). A prior study has posited that small quantities of water are present on the surface of amine sorbents even in dry conditions, [58] hence; it is proposed that, the presence of the HS^{-}-NH_2^{+} intensity at 2568 cm^{-1} could be as a result of formation of some ammonium ions even in dry conditions. For SBA-15_DMAPS in dry conditions, the reduced CH stretching modes indicated an interaction of H_2S with the sorbent, though SBA-15_DMAPS showed no presence of the HS and hydrogen bonded NH stretching

modes (**Figure C.10(b)**). This is likely due to the low H_2S sorption capacity observed in dry conditions (0.03 mmol H_2S/g sorbent).

In wet conditions, both SBA-15_TBAPS and SBA-15_DMAPS showed a slight increase in intensity of the HS^{-}-NH_2^{+} stretch and a decrease in the physisorbed S-H···N hydrogen bonded species (**Figure 4.8(b**)).[6,57] The broader and increased intensity observed at 2568 cm^{-1} for SBA-15_TBAPS, could be as a result of the formation of more ammonium ions owing to the chemisorption of the amines with hydrogen sulfide under wet conditions. Furthermore, the presence of the reduced hydrogen bonded S-H···N peak under humid conditions is consistent with the computational results that showed the possibility of both a proton transfer mechanism between the amine and H_2S in the presence of water, as well as the hydrogen bonded cosorption complex via H_2O (**Figure 4.6 (c)** and **(f)**).

We calculated the vibrational frequencies of the chemisorbed HS^{-}–NH_2^{+} and physisorbed S-H···N hydrogen bonded species on the amine sites of TBAPS based on the DFT optimized structures (Figure 5), and compared the calculated frequencies of N-H and S-H stretches with the peaks observed in FTIR. The results are summarized in Table 3. For physisorbed S-H···N hydrogen bonded species, the calculated frequencies of the S-H stretch in these sorption complexes span the range of 2213-2409 cm^{-1} (**Figure 4.5(a)**, **4.6(a)** and **(b)**), which agree reasonably well with the experimental observation from FTIR (2435 cm^{-1}). For the chemisorbed HS–NH_2^{+} species, the frequency of N-H stretch was calculated to be 1954 cm^{-1} for the sorption complex with one H_2O molecule coordinated to H_2S (**Figure 4.5(b)**), much smaller than that observed in FTIR (2568 cm^{-1}). However, when two H_2O molecules were present, the calculated frequencies of the N-H stretches with both one and two amines (**Figure 4.5(c)** and 4.**6(c)**) agree much better with the experimental data.

Table 4.3. Comparison of the computed and experimental vibrational frequencies of the chemisorbed HS^-–NH_2^+ and physisorbed S-H···N hydrogen bonded species on the amine sites of TBAPS

Structure Name	ν (N-H) of $HS–NH_2^+$ (cm^{-1})	ν (S-H) of S-H···N (cm^{-1})	Note
TBAPS…H_2S	-	2250	Figure 4.5 (a)
TBAPS-H^+…HS^-+H_2O	1954	-	Figure 4.5 (b)
TBAPS-H^+…HS^-+2·H_2O	2595	-	Figure 4.5 (c)
2·TBAPS…H_2S	-	2387, 2409	Figure 4.6 (a)
2·TBAPS…H_2S+H_2O	-	2213, 2268	Figure 4.6 (b)
2·TBAPS-H^+…HS^-+2·H_2O	2451	-	Figure 4.6 (c)
Exp. in-situ FTIR	~ 2568	~ 2435	

Lastly, the strong chemisorbed species formed in wet conditions was also confirmed in the H_2S desorption spectra (**Figure 4.9**). During the desorption experiment, UHP He was flowed through the bed at 120 °C for both humid and dry experiments. Under dry conditions, the chemisorbed HS^--NH_2^+ and the physisorbed S-H···N hydrogen peaks disappeared, whereas these peaks were still visible in wet conditions, with a larger reduction in the hydrogen bonded peak even after 1 h of desorption. Furthermore, it is posited that higher regeneration temperatures, longer regeneration times or alternative desorption gas conditions are required to completely remove the sorbed species. To determine conditions that effectively regenerate the sorbents, different desorption conditions are evaluated below.

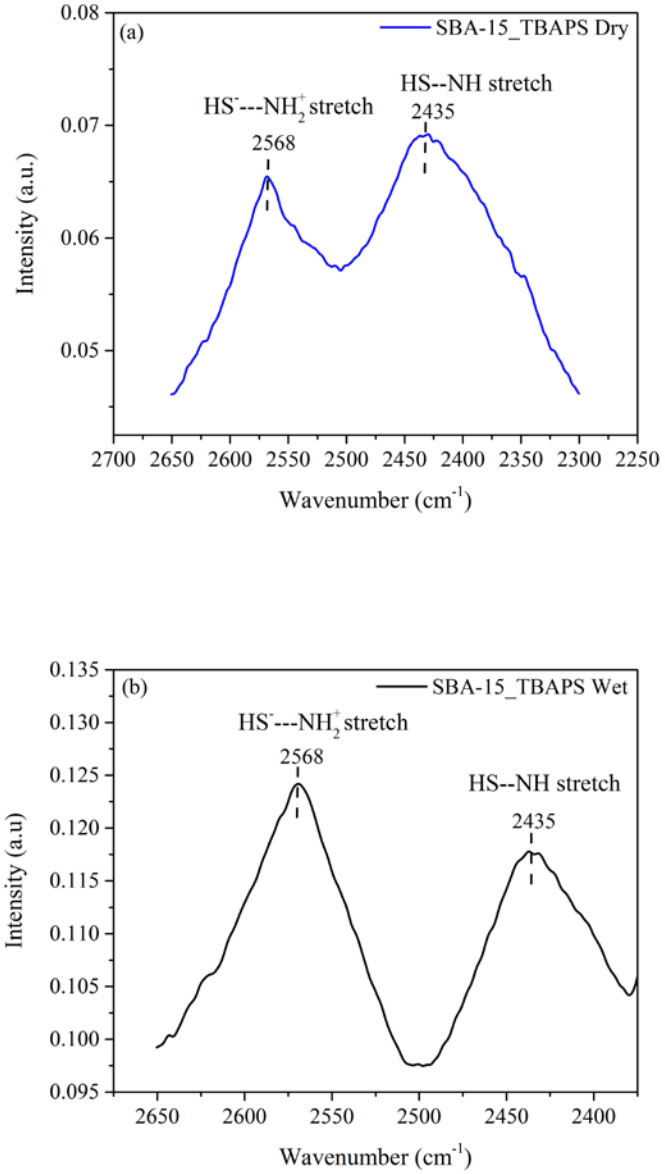

Figure 4.8. The S-H···N and HS^{-}-NH_2^{+} intensity region for (a) SBA-15_TBAPS after dry H_2S sorption and (b) SBA-15_TBAPS after wet H_2S sorption. Sorption conditions: 10% H_2S in N_2 at 30 °C.

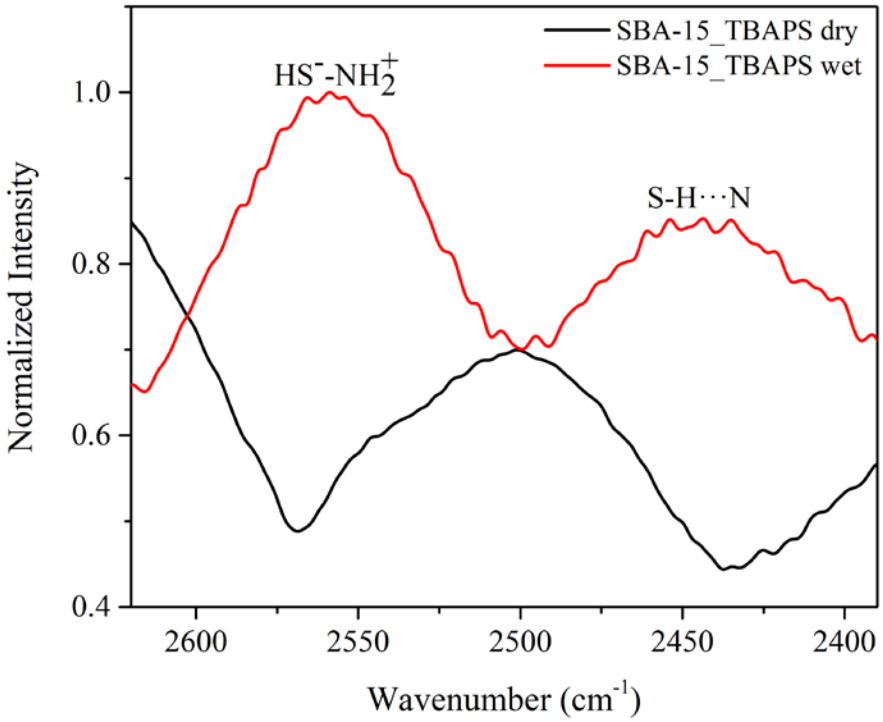

Figure 4.9. The S-H··· N and HS^{-}-NH_2^{+} intensity region during desorption for SBA-15_TBAPS after dry and wet H_2S adsorption. Desorption conditions: UHP He at 120 °C

4.3.5 Sorbent Degradation

Prior studies have investigated the oxidative and thermal stability of the sorbents studied here. It was reported that SBA-15_DMAPS showed good oxidative and thermal stability after exposure to O_2 at 135 °C for 24 h.[59] Furthermore, SBA-15_TBAPS was reported to lose 10% of its nitrogen content after 24 h under similar oxidative and thermal conditions.[42] To evaluate the structural stability of the sterically hindered and unhindered amines used here under humid H_2S conditions, the sorbents were exposed to 1% H_2S in N_2 under humid conditions for six consecutive hours at 30 °C. The sorbents were then characterized using NMR spectroscopy, N_2 physisorption and elemental analysis both before and after humid H_2S exposure.

The quantitative ^{29}Si and ^{13}C DP-MAS NMR spectra acquired for SBA-15 and the functionalized aminosilane samples are reported in **Figure 4.10**; the spectra obtained proved to be adequate in identifying chemical changes in the silica and carbon framework. For the ^{29}Si spectra, distinct resonances were interpreted in terms of Q^n and T^m sites, which correspond to the siloxane and organosiloxane region. The siloxane structural unit, Q^n refers to $[Si(OSi)_n(OH)_{4-n}]$ with n= 2-4. The organosiloxane sites, T^m identifies the Si species bound to an organic moiety and is described by the nomenclature, $[RSi(OSi)_m(OH)_{3-m}]$ with m= 1-3. For SBA-15, three peaks at 111 ppm, 102 ppm and 94 ppm that correspond to Q^4, Q^3, Q^2 groups were observed and are in agreement with previous literature. [60–62] The integrated peak intensities showed that the $[Si(OSi)_4]/Q^4$ group had the highest intensity, which corresponds to the building block of the bulk silica framework (**Table C.1, Figure C.11**). The Q^2 and Q^3 groups represent the presence of one and two –OH groups, respectively, which are present on the surface of silica and the edges of the pores, respectively.[62] The reduction of the Q^2 and Q^3 groups after grafting highlights a successful functionalization of the aminosilanes onto the $[Si(OSi)_3(OH)]$ surface of SBA-15, which led to a change in the silica network.

Changes in the pattern of the Q^n units have previously been reported to indicate disorder in the silica framework, but the silica framework of the sorbents studied here was maintained after humid H_2S sorption. This was observed by the integrated peak areas of the ^{29}Si DP NMR spectra (**Table C.1**), which showed similarities in the Q^n region before and after H_2S sorption.[62] As expected, the T^m signals appear only on the functionalized silica spectra. The fresh sorbents showed efficient condensation of the aminosilanes on the surface of the wall structure, which was confirmed by the higher T^3 to T^2 organosiloxane centers.[63,64] Furthermore, similar T^m and Q^n ratios were calculated for SBA-15_TBAPS before (0.2) and after (0.26) humid H_2S sorption,

which indicated minimal changes in the organosilane groups after prolonged humid H_2S sorption. The T^m:Q^n ratios were calculated for SBA-15_DMAPS and similar results were obtained.

The ^{13}C DP MAS NMR spectra of the functionalized fresh silica sorbents showed four distinct peaks. Intensities at 10.4, 27.6, 45.2 and 50.5 ppm were identified for SBA-15_TBAPS and 62.8, 44.4, 21.5 and 11.8 for SBA-15_DMAPS **(Figure 4.10(b)).** There were no changes observed in the ^{13}C NMR spectra for SBA-15_TBAPS and SBA-15_DMAPS before and after humid H_2S sorption **(Figure C.12)**, which confirms the stability of the carbon atoms after humid H_2S sorption.

Furthermore, N_2 physisorption results confirmed that the surface areas and pore volumes of the sorbents were maintained after humid H_2S sorption (**Figure C.13**). In addition, elemental analysis of CHN and Si showed negligible change before and after humid H_2S sorption. A small amount of sulfur was also detected and represents 3.5% and 1.5% of the total sulfur adsorbed on the surface of SBA-15_TBAPS and SBA-15_DMAPS respectively. Furthermore, the ratio of S/Si was calculated as 0.002 and 0.001 for SBA-15_TBAPS and SBA-15_DMAPS respectively. The presence of sulfur on the surface coupled with the negligible change in the sorbent structure after humid H_2S adsorption further establishes the structural stability of the sorbents studied under the conditions employed.

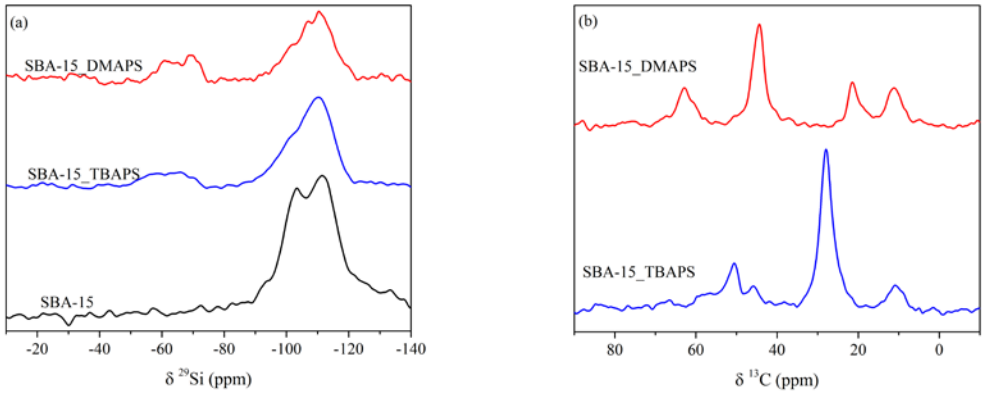

Figure 4.10. (a) ^{29}Si MAS NMR spectra and (b) ^{13}C MAS NMR spectra of the fresh silica sorbents.

4.3.6 Sorbent Regeneration in Humid Conditions

The cyclic stability of the hindered and unhindered sorbents was tested in 1% H_2S in N_2 and the materials were found to be stable under dry conditions (**Figure C.14**). The stable regeneration after each sorption-desorption cycle can be attributed to the weak physisorption of H_2S via a hydrogen bonding interactions.[41]

After humid sorption, the sorbents were desorbed under UHP He flow for 2 h at 120 °C to desorb sorbed H_2S species/water, a dry purge gas was used because it is common in lab scale sorption processes.[66] After three humid H_2S sorption-desorption cycles, the amine efficiency of the sorbents decreased by 50% for SBA-15_TBAPS and 90% for SBA-15_DMAPS from cycle 1 to cycle 2 (**Figure 4.11 (a)**). It is proposed that due to the chemisorption of H_2S to the amine sites, and the stronger H_2S sorption energies under humid conditions, the amine sites are not fully desorbed and some sites are inaccessible after each cycle under dry He desorption conditions. Interestingly, even after the significant decrease in efficiency, the sorbents maintained a H_2S sorption capacity higher than that observed under dry conditions (**Figure**

C.15). Furthermore, it is noted that SBA-15_TBAPS is more stable compared to SBA-15_DMAPS under the conditions studied and this could be a result of the more hydrophobic nature of SBA-15_TBAPS. More hydrophobic materials would have fewer water molecules sorbed and require less energy to desorb bound species, which could lead to increased access to the amine sites after each cycle. This proposition also aligns with the slightly lower H_2S sorption capacities obtained for SBA-15_TBAPS compared to SBA-15_DMAPS under humid conditions.

A few studies using activated carbons and polymeric ionic liquids have reported improved sorbent regeneration after humid H_2S sorption by water regeneration.[30,67] Owing to the incomplete sorbent regeneration obtained using dry inert gas for desorption, and to understand the role of humidity in the regeneration of the silica supported sorbents after humid H_2S sorption, humid UHP He was flowed through the bed during desorption at 80 °C. A 6% and 15% decrease in amine efficiency after 3 cycles was observed for SBA-15_ TBAPS and SBA-15_DMAPS, respectively **(Figure 4.11 (b))**, which suggests a significant improvement in sorbent regeneration under humid swing sorption/desorption conditions. The collected experiments demonstrate that the sorbents are stable and can be regenerated under mild conditions, but the use of water for regeneration could increase the energy required during biogas upgrading.

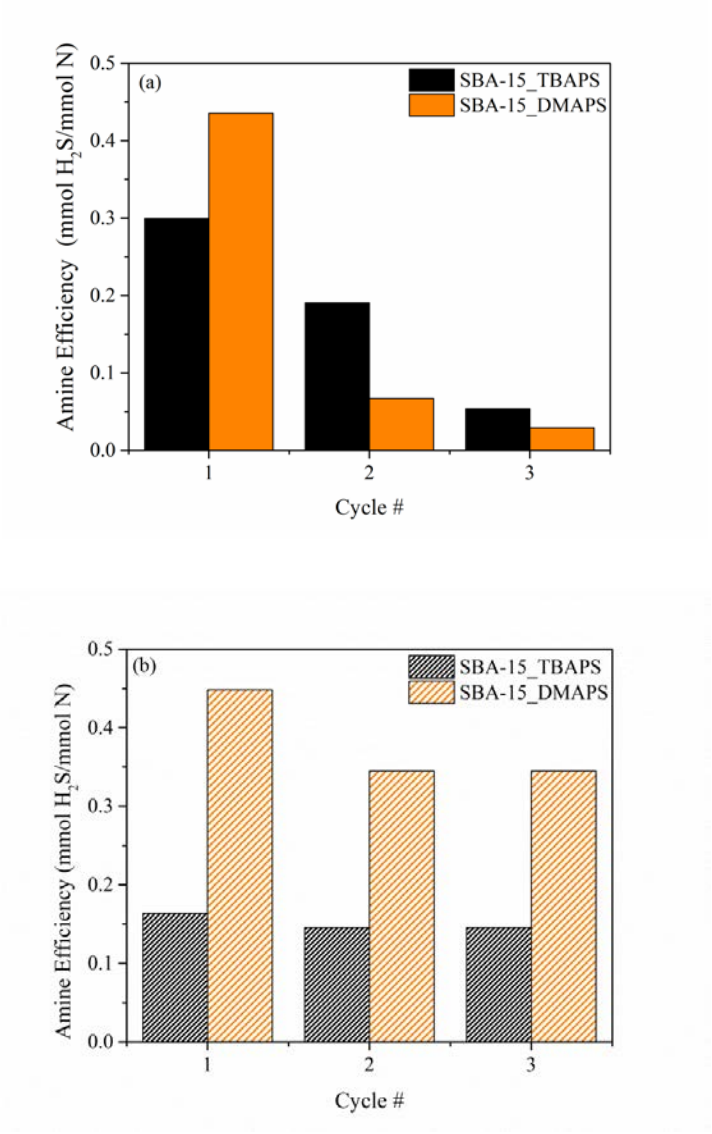

Figure 4.11. Amine efficiencies for SBA-15_TBAPS and SBA-15_DMAPS over 3 cycles of sorption-desorption under humid conditions (49% RH). Sorption conditions: 1% H_2S in N_2 at 30 °C and desorption with (a) dry Helium at 120 °C (b) humid Helium at 80 °C

4.4 Conclusion

This study explored the behavior of solid-supported hindered and unhindered amines under dry and humid H_2S conditions in simulated single and multicomponent biogas streams. In humid conditions, both SBA-15_TBAPS and SBA-15_DMAPS showed an increase in H_2S capacity and good H_2S selectivity in the presence of CO_2. FTIR spectroscopy showed an

increased intensity in the $HS^{-}\cdots NH_2^{+}$ region, which confirmed that chemisorbed species were formed under humid condition for both sorbents. These findings were supported with DFT calculations.

Cyclic stability tests and 6 h humid H_2S sorption exposure tests were performed to evaluate sorbent degradation. The SBA-15_TBAPS sorbent was observed to be more stable than SBA-15_DMAPS after three humid H_2S sorption-desorption cycles, but both sorbents retained their organic loading after H_2S sorption. Although both sorbents sustained great loss in amine efficiency after desorption under dry helium conditions, the NMR spectroscopy results confirmed no obvious detrimental impact of humid H_2S sorption on the stability of the silica framework, organosiloxane centers and carbon atoms. Therefore, the observed loss in amine efficiency was attributed to inaccessible amine sites due to the strongly chemisorbed species on the amine sites, which could be regenerated after humid temperature swing desorption. The H_2S sorption capacities of sterically hindered amines relative to the tertiary unhindered amine are slightly lower under humid conditions, but the structural reversibility upon humid regeneration of sterically hindered amines under cyclic conditions make them more suitable for future H_2S sorption studies.

4.5 References

(1) Rezaei, F.; Jones, C. W. Stability of Supported Amine Adsorbents to SO_2 and NO_x in Postcombustion CO_2 Capture. 2. Multicomponent Adsorption. *Ind. Eng. Chem. Res.* **2014**, *53*, 12103–12110.

(2) Okonkwo, C. N.; Okolie, C.; Sujan, A.; Zhu, G.; Jones, C. W. Role of Amine Structure on Hydrogen Sulfide Capture from Dilute Gas Streams Using Solid Adsorbents. *Energy and Fuels* **2018**.

(3) Didas, S. A.; Choi, S.; Chaikittisilp, W.; Jones, C. W. Amine-Oxide Hybrid Materials for CO_2 Capture from Ambient Air. *Acc. Chem. Res.* **2015**, *48* (10), 2680–2687.

(4) Budzianowski, W. M. Benefits of Biogas Upgrading to Biomethane by High-Pressure Reactive Solvent Scrubbing. *Biofuels, Bioprod. Biorefining* **2012**, *6* (3), 12–20.

(5) Aguilera, P. G.; Gutiérrez Ortiz, F. J. Prediction of Fixed-Bed Breakthrough Curves for H_2S Adsorption from Biogas: Importance of Axial Dispersion for Design. *Chem. Eng. J.* **2016**, *289*, 93–98.

(6) Miller, D. D.; Chuang, S. S. C. The Effect of Electron-Donating Groups and Hydrogen Bonding on H_2S Capture over Polyethylene Glycol/Amine Sites. *J. Phys. Chem. C* **2016**, *120* (2), 1147–1162.

(7) Miller, D. D.; Chuang, S. S. C. Experimental and Theoretical Investigation of SO_2 Adsorption over the 1,3-Phenylenediamine/SiO_2 System. *J. Phys. Chem. C* **2015**, *119* (12), 6713–6727.

(8) Lee, W. Y.; Park, S. Y.; Lee, K. B.; Nam, S. C. Simultaneous Removal of CO_2 and H_2S from Biogas by Blending Amine Absorbents: A Performance Comparison Study. *Energy & Fuels* **2020**, *34*, 1992–2000.

(9) Kapoor, R.; Ghosh, P.; Kumar, M.; Vijay, V. K. *Evaluation of Biogas Upgrading Technologies and Future Perspectives : A Review*; Environmental Science and Pollution Research, 2019.

(10) Sahota, S.; Shah, G.; Ghosh, P.; Kapoor, R.; Sengupta, S.; Singh, P.; Vijay, V.; Sahay, A.; Vijay, V. K.; Thakur, I. S. Review of Trends in Biogas Upgradation Technologies and Future Perspectives. *Bioresour. Technol. Reports* **2018**.

(11) Liu, J.; Wei, Y.; Li, P.; Zhao, Y.; Zou, R. Selective H_2S/CO_2 Separation by Metal-Organic Frameworks Based on Chemical-Physical Adsorption. *J. Phys. Chem. C* **2017**, *121* (24), 13249–13255.

(12) Oliveira, L. H. De; Meneguin, J. G.; Pereira, M. V; Nascimento, J. F. Adsorption of Hydrogen Sulfide , Carbon Dioxide , Methane , and Their Mixtures on Activated Carbon. *Chem. Eng. Commun.* **2019**, *206* (11), 1544–1564.

(13) Belmabkhout, Y.; De Weireld, G.; Sayari, A. Amine-Bearing Mesoporous Silica for CO_2 and H_2S Removal from Natural Gas and Biogas. *Langmuir* **2009**, *25* (23), 13275–13278.

(14) Bandosz, T. J. On the Adsorption/Oxidation of Hydrogen Sulfide on Activated Carbons at Ambient Temperatures. *J. Colloid Interface Sci.* **2002**, *246* (1), 1–20.

(15) Shah, M. S.; Tsapatsis, M.; Siepmann, J. I. Hydrogen Sulfide Capture: From Absorption in Polar Liquids to Oxide, Zeolite, and Metal-Organic Framework Adsorbents and Membranes. *Chem. Rev.* **2017**, *117* (14), 9755–9803.

(16) Xu, X.; Novochinskii, I.; Song, C. Low-Temperature Removal of H_2S by Nanoporous Composite of Polymer - Mesoporous Molecular Sieve MCM-41 as Adsorbent for Fuel Cell Applications. *Energy & Fuels* **2005**, No. 7, 2214–2215.

(17) Quan, W.; Wang, X.; Song, C. Selective Removal of H_2S from Biogas Using Solid Amine-Based "Molecular Basket" Sorbent. *Energy and Fuels* **2017**, *31* (9), 9517–9528.

(18) Didas, S. A.; Kulkarni, A. R.; Sholl, D. S.; Jones, C. W. Role of Amine Structure on Carbon Dioxide Adsorption from Ultradilute Gas Streams Such as Ambient Air. *ChemSusChem* **2012**, *5* (10), 2058–2064.

(19) Ryckebosch, E.; Drouillon, M.; Vervaeren, H. Techniques for Transformation of Biogas to Biomethane. *Biomass and Bioenergy*. 2011.

(20) Huang, H. Y.; Yang, R. T.; Chinn, D.; Munson, C. L. Amine-Grafted MCM-48 and Silica Xerogel as Superior Sorbents for Acidic Gas Removal from Natural Gas. *Energy & Fuels* **2009**, *25* (23), 13275–13278.

(21) Sujan, A. R.; Pang, S. H.; Zhu, G.; Jones, C. W.; Lively, R. P. Direct CO_2 Capture from Air Using Poly(Ethylenimine)-Loaded Polymer/Silica Fiber Sorbents. *ACS Sustain. Chem. Eng.* **2019**, *7* (5), 5264–5273.

(22) Han, C.; Zhang, C.; Tymińska, N.; Schmidt, J. R.; Sholl, D. S. Insights into the Stability of Zeolitic Imidazolate Frameworks in Humid Acidic Environments from First-Principles Calculations. *J. Phys. Chem. C* **2018**, *122* (8), 4339–4348.

(23) Elder, A. C.; Bhattacharyya, S.; Nair, S.; Orlando, T. M. Reactive Adsorption of Humid SO_2 on Metal-Organic Framework Nanosheets. *J. Phys. Chem. C* **2018**, *122* (19), 10413–10422.

(24) Lutz, W.; Suckow, M.; Bülow, M. Adsorption of Hydrogen Sulphide on Molecular Sieves. No Enrichment in the Presence of Carbon Dioxide. *Gas Sep. Purif.* **1990**.

(25) Bülow, M.; Lutz, W.; Suckow, M. The Mutual Transformation of Hydrogen Sulphide and Carbonyl Sulphide and Its Role for Gas Desulphurization Processes with Zeolitic Molecular Sieve Sorbents. *Stud. Surf. Sci. Catal.* **1999**.

(26) Peluso, A.; Gargiulo, N.; Aprea, P.; Pepe, F.; Caputo, D. Nanoporous Materials as H_2S Adsorbents for Biogas Purification: A Review. *Separation and Purification Reviews*. Taylor and Francis Inc. January 2, 2019, pp 78–89.

(27) Shah, M. S.; Tsapatsis, M.; Siepmann, J. I. Hydrogen Sulfide Capture: From Absorption in Polar Liquids to Oxide, Zeolite, and Metal-Organic Framework Adsorbents and Membranes. *Chem. Rev.* **2017**, *117* (14), 9755–9803.

(28) Bagreev, A.; Bandosz, T. J. On the Mechanism of Hydrogen Sulfide Removal from Moist Air on Catalytic Carbonaceous Adsorbents. *Ind. Eng. Chem. Res.* **2005**, *44* (3), 530–538.

(29) Watanabe, T.; Sholl, D. S. Molecular Chemisorption on Open Metal Sites in Cu_3 $(Benzenetricarboxylate)_2$: A Spatially Periodic Density Functional Theory Study. *J. Chem. Phys.* **2010**, *133* (9).

(30) Ge, K.; Wu, Y.; Wang, T.; Wu, J. Humidity Swing Adsorption of H_2S by Fibrous Polymeric Ionic Liquids (PILs). *Sep. Purif. Technol.* **2019**, *217*, 1–7.

(31) Huang, H. Y.; Yang, R. T.; Chinn, D.; Munson, C. L. Amine-Grafted MCM-48 and Silica Xerogel as Superior Sorbents for Acidic Gas Removal from Natural Gas. *Ind. Eng. Chem. Res.* **2003**, *42* (10), 2427–2433.

(32) Tian, S.; Mo, H.; Zhang, R.; Ning, P.; Zhou, T. Enhanced Removal of Hydrogen Sulfide from a Gas Stream by 3-Aminopropyltriethoxysilane-Surface-Functionalized Activated Carbon. *Adsorption* **2009**, *15* (5–6), 477–488.

(33) Wang, X.; Ma, X.; Sun, L.; Song, C. A Nanoporous Polymeric Sorbent for Deep Removal of H_2S from Gas Mixtures for Hydrogen Purification. *Green Chem.* **2007**, *9* (6), 695.

(34) Adib, F.; Bagreev, A.; Bandosz, T. J. Effect of Surface Characteristics of Wood-Based Activated Carbons on Adsorption of Hydrogen Sulfide. *J. Colloid Interface Sci.* **1999**, *214*, 407–415.

(35) Sitthikhankaew, R.; Chadwick, D.; Assabumrungrat, S.; Laosiripojana, N. Effects of Humidity, O_2, and CO_2 on H_2S Adsorption onto Upgraded and KOH Impregnated Activated Carbons. *Fuel Process. Technol.* **2014**, *124*, 249–257.

(36) Petit, C.; Mendoza, B.; Bandosz, T. J. Hydrogen Sulfide Adsorption on MOFs and MOF/Graphite Oxide Composites. *ChemPhysChem* **2010**, *11* (17), 3678–3684.

(37) Belmabkhout, Y.; Bhatt, P. M.; Adil, K.; Pillai, R. S.; Cadiau, A.; Shkurenko, A.; Maurin, G.; Liu, G.; Koros, W. J.; Eddaoudi, M. Natural Gas Upgrading Using a Fluorinated MOF with Tuned H_2S and CO_2 Adsorption Selectivity. *Nat. Energy* **2018**, *3* (12), 1059–1066.

(38) Roller, D.; Bläsing, M.; Dreger, I.; Yazdanbakhsh, F.; Sawada, J. A.; Kuznicki, S. M.; Müller, M. Removal of Hydrogen Sulfide by Metal-Doped Nanotitanate under Gasification-Like Conditions. *Ind. Eng. Chem. Res.* **2016**, *55* (14), 3871–3878.

(39) Quan, W.; Wang, X.; Song, C. Selective Removal of H_2S from Biogas Using Solid Amine-Based "Molecular Basket" Sorbent. *Energy and Fuels* **2017**, *31* (9), 9517–9528.

(40) Okonkwo, C. N.; Lee, J. J.; Vylder, A. De; Chiang, Y.; Thybaut, J. W.; Jones, C. W. Selective Removal of Hydrogen Sulfide from Simulated Biogas Streams Using Sterically Hindered Amine Adsorbents. **2020**, *379* (July 2019).

(41) Sartori, G.; H, W. S.; Thaler, W. A.; Chludzinski, G. R.; Wilbur, J. C. Sterically-Hindered Amines for Acid Gas Absorption.

(42) Lee, J. J.; Yoo, C.; Chen, C.; Hayes, S. E.; Sievers, C.; Jones, C. W. Silica-Supported Sterically Hindered Amines for CO_2 Capture. *Langmuir* **2018**, *34*, 12279–12292.

(43) Bougie, F.; Iliuta, M. C. Sterically Hindered Amine-Based Absorbents for the Removal of CO_2 from Gas Streams. *J. Chem. Eng. Data* **2012**, *57* (3), 635–669.

(44) Lu, J. G.; Zheng, Y. F.; He, D. L. Selective Absorption of H_2S from Gas Mixtures into Aqueous Solutions of Blended Amines of Methyldiethanolamine and 2-Tertiarybutylamino-2-Ethoxyethanol in a Packed Column. *Sep. Purif. Technol.* **2006**, *52* (2), 209–217.

(45) Sartorl, G.; Savage, D. W. Sterically Hindered Amines for CO_2 Removal from Gases. *Ind. Eng. Chem. Fundam.* **1983**, *22* (2), 239–249.

(46) Okonkwo, C. N.; Okolie, C.; Sujan, A.; Zhu, G.; Jones, C. W. Role of Amine Structure on Hydrogen Sulfide Capture from Dilute Gas Streams Using Solid Adsorbents. *Energy and Fuels* **2018**, *32* (6), 6926–6933.

(47) M. J. Frisch, G. W. Trucks, H. B. Schlegel, G. E. Scuseria, M. A. Robb, J. R. Cheeseman, G. Scalmani, V. Barone, G. A. Petersson, H. Nakatsuji, X. Li, M. Caricato, A. V. Marenich, J. Bloino, B. G. Janesko, R. Gomperts, B. Mennucci, H. P. Hratchian, J. V., and D. J. F. Gaussian 16, Revision B.01,. Gaussian, Inc.,: Wallingford Ct 2016.

(48) Allouche, A. Effect of the Damping Function in Dispersion Corrected Density Functional Theory. *J. Comput. Chem.* **2011**, *32* (Sfb 858), 1456–1465.

(49) Grimme, S.; Antony, J.; Ehrlich, S.; Krieg, H. A Consistent and Accurate Ab Initio Parametrization of Density Functional Dispersion Correction (DFT-D) for the 94 Elements H-Pu. *J. Chem. Phys.* **2010**, *132* (15).

(50) Supronowicz, B.; Mavrandonakis, A.; Heine, T. Interaction of Small Gases with the Unsaturated Metal Centers of the HKUST-1 Metal Organic Framework. *J. Phys. Chem. C* **2013**, *117* (28), 14570–14578.

(51) Chiu, C. C.; Vayssilov, G. N.; Genest, A.; Borgna, A.; Rösch, N. Predicting Adsorption Enthalpies on Silicalite and HZSM-5: A Benchmark Study on DFT Strategies Addressing Dispersion Interactions. *J. Comput. Chem.* **2014**, *35* (10), 809–819.

(52) Kortunov, P. V.; Siskin, M.; Paccagnini, M.; Thomann, H. CO_2 Reaction Mechanisms with Hindered Alkanolamines: Control and Promotion of Reaction Pathways. *Energy and Fuels* **2016**, *30* (2), 1223–1236.

(53) Adib, F.; Bagreev, A.; Bandosz, T. J. Adsorption/Oxidation of Hydrogen Sulfide on Nitrogen-Containing Activated Carbons. *Langmuir* **2000**, *16* (4), 1980–1986.

(54) Sumon, K. Z.; Bains, C. H.; Markewich, D. J.; Henni, A.; East, A. L. L. Semicontinuum Solvation Modeling Improves Predictions of Carbamate Stability in the CO_2 + Aqueous Amine Reaction. *J. Phys. Chem. B* **2015**, *119* (37), 12256–12264.

(55) Ma, X.; Wang, X.; Song, C. "Molecular Basket" Sorbents for Separation of CO_2 and H_2S from Various Gas Streams. *J. Am. Chem. Soc.* **2009**, *131* (13), 5777–5783.

(56) Lee, J. J.; Chen, C. H.; Shimon, D.; Hayes, S. E.; Sievers, C.; Jones, C. W. Effect of Humidity on the CO_2 Adsorption of Tertiary Amine Grafted SBA-15. *J. Phys. Chem. C*

2017, *121* (42), 23480–23487.

(57) Socrates, G. *Infrared and Raman Characteristic Group Frequencies. Tables and Charts*; 2001.

(58) Lee, J. J.; Chen, C.; Shimon, D.; Hayes, S. E.; Sievers, C.; Jones, C. W. Effect of Humidity on the CO_2 Adsorption of Tertiary Amine Grafted SBA-15. **2017**, *121*, 23480–23487.

(59) Bollini, P.; Choi, S.; Drese, J. H.; Jones, C. W. Oxidative Degradation of Aminosilica Adsorbents Relevant to Postcombustion CO_2 Capture. *Energy and Fuels* **2011**, *25* (5), 2416–2425.

(60) Melero, J. A.; Stucky, G. D.; van Grieken, R.; Morales, G. Direct Syntheses of Ordered SBA-15 Mesoporous Materials Containing Arenesulfonic Acid Groups. *J. Mater. Chem.* **2002**, *12* (6), 1664–1670.

(61) Zhao, D.; Feng, J.; Huo, Q.; Melosh, N.; Fredrickson, G. H.; Chmelka, B. F.; Stucky, G. D. Triblock Copolymer Syntheses of Mesoporous Silica with Periodic 50 to 300 Angstrom Pores. *Science (80-.).* **1998**, *279* (5350), 548–552.

(62) Cattaneo, A. S.; Ferrara, C.; Villa, D. C.; Angioni, S.; Milanese, C.; Capsoni, D.; Grandi, S.; Mustarelli, P.; Allodi, V.; Mariotto, G.; et al. SBA-15 Mesoporous Silica Highly Functionalized with Propylsulfonic Pendants: A Thorough Physico-Chemical Characterization. *Microporous Mesoporous Mater.* **2016**, *219*, 219–229.

(63) Sadasivan, S.; Khushalani, D.; Mann, S. Synthesis and Shape Modification of Organo-Functionalised Silica Nanoparticles with Ordered Mesostructured Interiors. *J. Mater. Chem.* **2003**, *13* (5), 1023–1029.

(64) Wang, X.; Cheng, S.; Chan, J. C. C. Propylsulfonic Acid-Functionalized Mesoporous Silica Synthesized by in Situ Oxidation of Thiol Groups under Template-Free Condition. *J. Phys. Chem. C* **2007**, *111* (5), 2156–2164.

(65) Sayari, A.; Belmabkhout, Y.; Da'na, E. CO_2 Deactivation of Supported Amines: Does the Nature of Amine Matter? *Langmuir* **2012**, *28* (9), 4241–4247.

(66) Bagreev, A.; Rahman, H.; Bandosz, T. J. Study of H_2S Adsorption and Water Regeneration of Spent Coconut-Based Activated Carbon. *Environ. Sci. Technol.* **2000**, *34* (21), 4587–4592.

CHAPTER 5. A REVIEW OF CO_2 & H_2S ADSORPTION ON SILICA SUPPORTED SORBENTS STUDIED IN THIS DISSERTATION

5.1 Introduction

In this dissertation, we have reported on the performance of unhindered and sterically hindered amines for H_2S capture and in some cases, the effect of a multicomponent gas system containing CO_2, H_2S and CH_4. These class 2 amines, which have been explored for H_2S capture, have also been widely explored for CO_2 capture in dilute gas streams such as simulated air and flue gas. Here, we provide a summary of the findings under CO_2 capture conditions and the interrelationship of the sorbent performance for H_2S capture, specifically pertaining to complex gases such as multicomponent gas conditions where CO_2 and H_2S are present. Below are the amine types that have been assessed thus far.

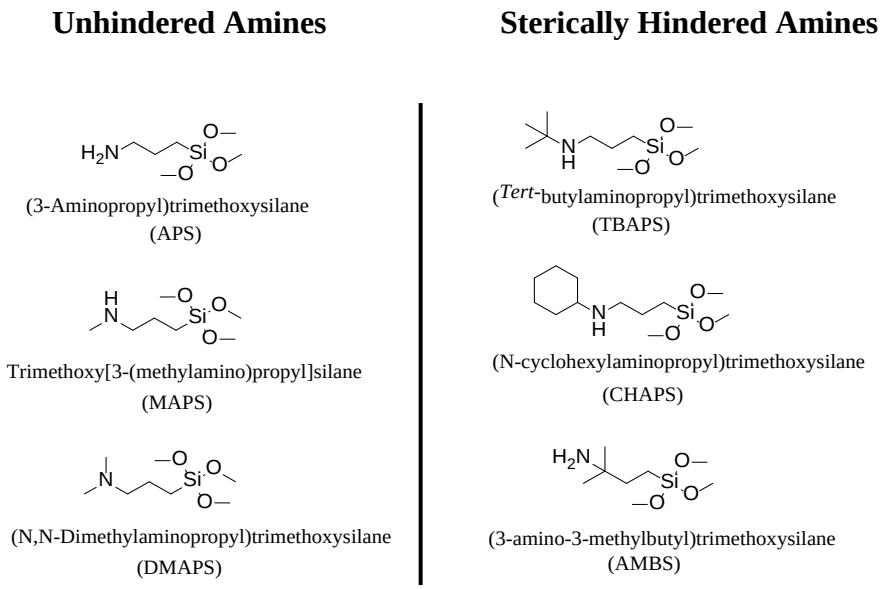

Figure 5.1. Unhindered and sterically hindered amines investigated for CO_2 and H_2S capture.

5.2 Discussion

Several factors are considered for the design of practical adsorbents for H_2S or CO_2 capture. Here, we discuss the factors that have been considered for unhindered and hindered amines evaluated both in this dissertation for H_2S capture and in literature, specifically for CO_2 capture.

5.2.1 Unhindered Amines for CO_2 and H_2S Adsorption

Didas et. al evaluated three unhindered amines functionalized on a mesocellular silica foam support, MCF.[1] To understand the role of amine type on CO_2 adsorption, primary-APS, secondary-MAPS and tertiary-DMAPS were evaluated in ultradilute CO_2 conditions. In pure CO_2 conditions, primary and secondary amines have similar CO_2 amine efficiencies,[2] but in the ultradilute CO_2 conditions studied by Didas et. al, the primary-APS had the highest CO_2 adsorption capacity under dry conditions. On the other hand, secondary-MAPS had moderate CO_2 capacity and tertiary-DMAPS had negligible CO_2 capacity. Furthermore, the calculated heats of adsorption at ultralow CO_2 partial pressures were reported as 130 kJ/mol and 88 kJ/mol for primary-APS and secondary-MAPS respectively, this confirmed the high amine efficiencies obtained for primary-APS.[1] For CO_2-amine interactions, the proposed adsorption mechanism influences the CO_2 adsorption capacity and the theoretical maximum efficiency of the sorbents, specifically the direct reaction of CO_2 with primary and secondary amines via the zwitterion mechanism to form carbamates or carbamic acids and the formation of bicarbonates with tertiary amines in the presence of water, as discussed in chapter 1.

The H_2S capture conditions evaluated in chapter 2 for similar amine types as the work of Didas et. al showed the highest H_2S adsorption capacity for secondary-MAPS in dilute gas

streams with moderate H_2S capacity for primary-APS and the lowest H_2S capacity for tertiary-DMAPS. This result suggests that the amine with the highest basicity had the highest H_2S adsorption capacity of the sorbents studied; therefore, it is important to consider the basicity of the amines used when selecting adsorbents for H_2S capture. Furthermore, the stability of similar amine types under multiple CO_2 adsorption-desorption cycles were evaluated by Sayari et. al.[4] Their results showed urea formation in primary-APS after multiple CO_2 adsorption-desorption cycles, which led to deactivation of the sorbent, whereas, the cyclic stability of the secondary-MAPS was maintained throughout, owing to the lack of urea formation. In H_2S conditions, the best cyclic stability was observed for tertiary-DMAPS due to its steric hindrance, while primary-APS was the most unstable sorbent after 10 H_2S adsorption-desorption cycles with 10% H_2S in N_2. With this knowledge, under multicomponent gas conditions, where selective removal of H_2S is required, the differences in the performance of varying amine types during CO_2 and H_2S adsorption can be leveraged to design a high performing adsorbent with high H_2S/CO_2 adsorption capacity, good stability and selectivity.

5.2.2 Hindered Amines for CO_2 and H_2S Adsorption

In the work of Lee et. al, sterically hindered amine sorbents, i.e. a hindered primary amine and two secondary hindered amines grafted on SBA-15, were evaluated for CO_2 capture under humid and dry conditions.[5] Under humid conditions (49% RH) in 10% CO_2 in He flow, the moderately hindered amine sorbent, SBA-15_AMBS had the highest CO_2 capacity followed by SBA-15_CHAPS. Interestingly, the severely sterically hindered amine sorbent, SBA-15_TBAPS had the lowest CO_2 capacity in dry conditions but in humid conditions, it had the highest CO_2 adsorption capacity, followed by SBA-15_AMBS and SBA-15_CHAPS. Due to the varied adsorption mechanisms between CO_2 and amines, the species formed during CO_2

adsorption were evaluated for sterically hindered amines under humid and dry conditions using *in-situ* IR spectroscopy. Their results showed that under nominally dry conditions, carbamates and carbamic acids were formed during CO_2 adsorption on SBA-15_AMBS and SBA-15_CHAPS, but owing to the severe steric hindrance of SBA-15_TBAPS, only bicarbonates were formed. Under humid conditions, bicarbonates were formed on all sorbents studied but the largest amounts were formed on SBA-15_TBAPS and this was attributed to the increased CO_2 capacity and higher amine efficiency observed compared to SBA-15_CHAPS and SBA-15_AMBS. Furthermore, the isosteric heats of adsorption showed that weakly chemisorbed species were formed for all sorbents compared to the unhindered counterparts and the lower adsorption energy makes the hindered amines easier to regenerate under CO_2 capture conditions.[5]

In chapter 3 and 4, sterically hindered amines were evaluated for H_2S capture under dry and humid conditions respectively. Under dry conditions, SBA-15_TBAPS had the highest H_2S adsorption capacity followed by SBA-15_CHAPS and SBA-15_AMBS. Interestingly, this is the reverse performance of sterically hindered amines for CO_2 capture and as a result, the severely sterically hindered amine, SBA-15_TBAPS is expected to be selective for H_2S in a multicomponent gas stream.

In chapter 3, the results confirmed that SBA-15_TPABS was indeed highly selective for H_2S removal in the presence of CO_2 and CH_4. Furthermore, the effect of humidity (49% RH) on H_2S capture was evaluated for SBA-15_TBAPS in chapter 4. The experimental and computational results confirm a proton transfer mechanism between the sorbent and H_2S. The stronger chemisorbed, HS^--NH^+ species formed required desorption under humid He flow at 80 °C to regenerate the sorbent. When the severely sterically hindered amine was compared to the

unhindered counterpart, SBA-15_DMAPS, it was posited that the hydrophobic nature of SBA-15_TBAPS improved its cyclic stability during desorption. In addition, the selectivity of SBA-15_TBAPS and SBA-15_DMAPS in a multicomponent humid gas stream containing H_2S, CO_2 and CH_4 was evaluated and the results showed negligible change in H_2S adsorption capacity with and without CO_2.

It is proposed that the weaker CO_2 adsorption energies reported for sterically hindered amine coupled with the slow rate of bicarbonate formation during CO_2 capture impedes the adsorption of CO_2 in the multicomponent gas mixture. Contrarily, the proton transfer mechanism for H_2S maintains a consistent H_2S adsorption capacity under the conditions employed.

5.3 Conclusion

This review highlights the key factors used to assess the behavior of hindered and unhindered silica-supported sorbents in the presence of CO_2 and H_2S. It is inferred that there are varying factors to consider in selecting the appropriate sorbent for biogas upgrading and the relationship between these factors should be considered.

First, the role of the amine type and amine structure should be considered. For example, in the case were amines with similar amine basicity but different steric hindrances are considered for H_2S capture, the severely sterically hindered amine is more selective for H_2S compared to the moderately hindered amine in the presence of CO_2, regardless of basicity. On the other hand, for unhindered amines, the higher the basicity, the better the H_2S adsorption capacity and amine efficiency of the sorbent. Therefore, one factor is not completely independent of the other and both should be evaluated upon selecting a practical sorbent for H_2S capture.

Another important factor that was considered is the adsorption mechanism between the gas and the amine. Its importance is especially evident during multicomponent adsorption systems containing CO_2 and H_2S. In the case of sterically hindered amines, the severe steric hindrance coupled with the H_2S adsorption mechanism is posited to improve the H_2S selectivity in the presence of CO_2. Furthermore, the types of species formed during CO_2 or H_2S adsorption influences the adsorption capacity, especially under humid conditions, where an increase in adsorption capacity is observed for all sorbents studied.

Lastly, the end processing of the adsorbed gas is important in determining what amine type should be considered for the H_2S/CO_2 removal process. If selective H_2S is required to obtain elemental sulfur, which can be used to manufacture inorganic chemicals, fertilizers or agrochemicals, the use of TBAPS would be appropriate. In cases such as natural gas upgrading, where simultaneous removal of CO_2 and H_2S is required, this can be achieved with CHAPS or AMBS, but owing to the oxidative stability of AMBS, it would be better to consider AMBS for simultaneous CO_2 and H_2S removal. Understanding the interrelationship of these key performance indicators is essential in designing practical adsorbents for the removal of H_2S, CO_2 or both. Besides, building a knowledge base with this information can be extended to the area of catalysis and computational methods, which can further hasten the development of sustainable sorbents for biogas upgrading.

5.4 References

(1) Didas, S. A.; Kulkarni, A. R.; Sholl, D. S.; Jones, C. W. Role of Amine Structure on Carbon Dioxide Adsorption from Ultradilute Gas Streams Such as Ambient Air. *ChemSusChem* **2012**, *5* (10), 2058–2064.

(2) Ko, Y. G.; Shin, S. S.; Choi, U. S. Primary, Secondary, and Tertiary Amines for CO_2 Capture: Designing for Mesoporous CO_2 Adsorbents. *J. Colloid Interface Sci.* **2011**, *361*

(2), 594–602.

(3) Yoo, C. J.; Lee, L. C.; Jones, C. W. Probing Intramolecular versus Intermolecular CO_2 Adsorption on Amine-Grafted SBA-15. *Langmuir* **2015**, *31* (49), 13350–13360.

(4) Sayari, A.; Belmabkhout, Y.; Da'na, E. CO_2 Deactivation of Supported Amines: Does the Nature of Amine Matter? *Langmuir* **2012**, *28* (9), 4241–4247.

(5) Lee, J. J.; Yoo, C.; Chen, C.; Hayes, S. E.; Sievers, C.; Jones, C. W. Silica-Supported Sterically Hindered Amines for CO_2 Capture. *Langmuir* **2018**, *34*, 12279–12292.

CHAPTER 6. SUMMARY & FUTURE DIRECTIONS

6.1 Summary

A summary of this dissertation along with the conclusions in each chapter is discussed below:

Chapter 1

The upgrading of biogas from renewable natural gas by removing H_2S from the gas stream was discussed. The discussion evaluated the use of adsorbents as an energy efficient method with a focus on different ways to synthesize amines on a support, the CO_2 and H_2S adsorption mechanisms and the effect of humidity on H_2S capture.

Chapter 2

Secondary amines were identified as the high performing amines owing to their high H_2S capacity and amine efficiency compared to primary and tertiary amines. Tertiary amines were identified as the most stable amines compared to primary and secondary amines after 10 H_2S adsorption-desorption cycles under high H_2S concentrations. Overall, to design a promising H_2S adsorbent with high amine efficiency and cyclic stability, amine molecules should have a high ratio of secondary and tertiary amines.

Chapter 3

Single and multicomponent adsorption experiments were performed with sterically hindered amines and $H_2S\backslash CO_2\backslash CH_4$ in the gas stream. Severely sterically hindered secondary

amines were identified to be the most favorable amine type over a moderately hindered secondary and primary amine for H_2S capture. This is as a result of the materials' display of high H_2S selectivity and adsorption capacity. All hindered amines were considered facilely stable after multiple H_2S adsorption–desorption cycles. Furthermore, experimental heats of adsorption results coupled with computational DFT calculations suggests the formation of a strong hydrogen bond between two amines and 1 mol of H_2S under dry conditions.

Chapter 4

Increased H_2S adsorption capacities were observed in humid conditions for a severely sterically hindered secondary amine and an unhindered tertiary amine. The unhindered amines showed the highest H_2S efficiency enhancement when comparing humid to dry conditions. The overall increase in H_2S adsorption capacities and amine efficiencies in humid conditions was posited to result from the formation of a stronger chemisorbed species. The proposed species formed were identified using in-situ FTIR and computational techniques. Furthermore, ^{13}C and ^{29}Si NMR results confirmed the stability of the sorbents after long term exposure to humid H_2S and cyclic studies showed improved regeneration of the sorbents after desorption with water.

Chapter 5

A review of the silica supported amines in this dissertation that have been used for CO_2 capture in previous studies has been assessed. The relationship between the CO_2 and H_2S adsorption mechanisms and their impact on adsorption capacity in humid and dry conditions were discussed.

6.2 Future Directions

This dissertation has reported on the amine-H_2S interaction of class 2 amine adsorbents in both single and multicomponent simulated biogas conditions. To develop a practical adsorbent for biogas upgrading, further investigations are still required. A few suggestions on future steps are proposed below:

6.2.1 Evaluation of Dendrimers for H_2S Capture

Dendrimers are hyper branched macromolecules with a large number of functional groups.[1,2] The synthesis of these organic molecules allows for increased branched units in each generation, which could potentially increase the number of binding sites available for H_2S capture, further leading to an increase in H_2S adsorption capacity.[1,3] In Chapter 2, secondary and tertiary amines have been shown to have the highest adsorption capacity and the best stability respectively. Therefore, with the ability to fine-tune the functional groups of dendrimers and obtain the desired amine combination, the synthesis process can be leveraged to obtain a high capacity and stable adsorbent for H_2S capture. Prior studies have explored dendrimers as a new promising class of polymeric amines for CO_2 [1,4,5] and SO_2 capture, [3] but dendrimers are yet to be studied in detail for H_2S capture.

6.2.2 Expanding the Selection Criteria for H_2S Capture Adsorbents

To understand the fundamental relationship between different adsorbents and H_2S, this dissertation has reported on key performance factors such as: i) the role of amine type (primary, secondary and tertiary amines) ii) the role of amine structure (hindered and unhindered amines) iii) impact of operating conditions (adsorption temperature and H_2S concentration) iv) adsorption

mechanisms v) impact of humidity vi) structural and cyclic stability vii) impact of multicomponent gas streams and viii) heats of adsorption. Although this information provides additional knowledge on amine- H_2S -silica structure-property relationships for the sorbents studied, evaluating other properties such as entropic factors can close the knowledge gap even further.

Alkhabbaz et. al inferred that based on the similar CO_2 isosteric heats of adsorption measured for primary-APS and secondary- MAPS using a calorimeter, the higher amine efficiencies observed for primary-APS are as a result of entropic factors rather than enthalpic factors.[6] Hence, it is important to consider entropic factors in the design of amine adsorbents.

Although there are equipment limitations in directly performing calorimetry measurements for H_2S adsorption, the change in entropy, which stipulates whether an adsorption process is associative or dissociative, can be calculated by a combination of experimental and computational data using the Eyring equation below: [7]

$$\frac{\ln k}{T} = ln\frac{k_B}{h} + \frac{\Delta S}{R} - \frac{\Delta H}{RT}$$

where, k is the adsorption rate constant, k_B is the Boltzman constant, h is the Plank constant, R is the ideal gas constant and T is temperature (K).

$$\Delta G = \Delta H - T\Delta S$$

The slope and intercept of a plot of ln k/T vs. 1/T can be used to determine the values of ΔH and ΔS respectively.[7,8] Aside from spectroscopic evidence, the calculation of the entropy values (which could be either positive or negative) could help to determine when the amine-H_2S

interaction undergoes an associative hydrogen bonding mechanism or a dissociative proton transfer mechanism as discussed in chapters 3 and 4.

6.2.3 Molecular Level Insight into Inter vs. Intra Molecular H_2S Adsorption on Silica-Supported Amine Adsorbents

Apart from the impact of amine types on H_2S capture that have been evaluated in chapter 2, it is also important to consider a variety of amine structures. For CO_2 capture, different amine structures (propylamine, (MONO/primary-APS), propylethylenediamine, (DI), propyldiethylenetriamine, (TRI) and propyltriethylenetetramine, TREN amine containing organosilanes) have been evaluated in order to probe the intramolecular vs. intermolecular interaction of CO_2 with amine modified silica supports.[9] The results in this work suggest that at low amine loadings, aminosilanes with multiple amines on a single chain, specifically TRI and TREN, are capable of intramolecular sorption based on the differences in the measured CO_2 heats of adsorption when the silanol groups of the sorbents are capped. This is an interesting area that is yet to be explored under H_2S capture conditions and should be considered. With a better understanding of how intermolecular or intramolecular interactions influence H_2S adsorption capacity and amine efficiency, better adsorbents for H_2S capture can be synthesized and more details on the adsorption mechanism on different types of amine structures can be elucidated.

6.2.4 Impact of Regeneration Temperature on H_2S Capture

In Chapter 4, it is observed that dry helium thermal desorption is ineffective in desorbing the chemisorbed species on the hindered and unhindered amines studied. In order to regenerate the sorbent, humid helium thermal desorption is required to break the stronger bonds. It was shown that the sorbent regeneration improved drastically at 80 °C, which is similar to the

temperature at which the strong hydrogen bonded species were released for the SHA's under dry desorption conditions, as discussed in chapter 3. As a result of the lower regeneration temperature required to thermally desorb the sorbents both in humid and dry conditions, investigating the impact of varying the regeneration temperature to determine the optimal desorption temperature during H_2S capture should be considered.

6.2.5 NMR Investigation of Chemisorbed Species

The spectroscopic investigation of the chemisorbed species was not elucidated under ^{13}C and ^{1}H NMR detection. To further obtain spectroscopic evidence of the presence of the chemisorbed species, nitrogen labelling should be considered. The ^{15}N spectroscopy of the nitrogen atoms present in the amines before and after H_2S adsorption could show differences in the protonated amine after humid adsorption. This could help provide a better understanding of the H_2S adsorption mechanism and help formulate methods for more extensive regeneration of the sorbent with lower energy requirements.

References

(1) Shah, K. J.; Imae, T.; Shukla, A. Selective Capture of CO_2 by Poly(Amido Amine) Dendrimer-Loaded Organoclays. *RSC Adv.* **2015**, *5* (45), 35985–35992.

(2) Abbasi, E.; Aval, S. F.; Akbarzadeh, A.; Milani, M.; Nasrabadi, H. T.; Joo, S. W.; Hanifehpour, Y.; Nejati-Koshki, K.; Pashaei-Asl, R. Dendrimers: Synthesis, Applications, and Properties. *Nanoscale Res. Lett.* **2014**, *9* (1), 1–10.

(3) Tailor, R.; Abboud, M.; Sayari, A. Supported Polytertiary Amines: Highly Efficient and Selective SO_2 Adsorbents. *Environ. Sci. Technol.* **2014**, *48* (3), 2025–2034.

(4) Thompson, S. J.; Soukri, M.; Lail, M. Phosphorus Dendrimer Derived Solid Sorbents for CO_2 Capture from Post-Combustion Gas Streams. *Energy & Fuels* **2018**, *32*, 8658–8667.

(5) Bhagiyalakshmi, M.; Do, S.; Seog, W.; Tae, H. Applied Surface Science Development of TREN Dendrimers over Mesoporous SBA-15 for CO_2 Adsorption. **2010**, *256*, 6660–6666.

(6) Alkhabbaz, M. A.; Bollini, P.; Foo, G. S.; Sievers, C.; Jones, C. W. Important Roles of Enthalpic and Entropic Contributions to CO_2 Capture from Simulated Flue Gas and Ambient Air Using Mesoporous Silica Grafted Amines. *J. Am. Chem. Soc.* **2014**, *136* (38), 13170–13173.

(7) Saha, P.; Chowdhury, S. Insight Into Adsorption Thermodynamics. *Thermodynamics* Prof. Mizutani Tadashi (Ed.), InTech, **2011**.

(8) Budi, A.; Stipp, S. L. S.; Andersson, M. P. Calculation of Entropy of Adsorption for Small Molecules on Mineral Surfaces. *J. Phys. Chem. C* **2018**, *122* (15), 8236–8243.

(9) Yoo, C. J.; Lee, L. C.; Jones, C. W. Probing Intramolecular versus Intermolecular CO_2 Adsorption on Amine-Grafted SBA-15. *Langmuir* **2015**, *31* (49), 13350–13360.

APPENDIX A. SUPPLEMENT TO CHAPTER 2

A.1 Ex-Situ Characterization of adsorbent after H_2S capture

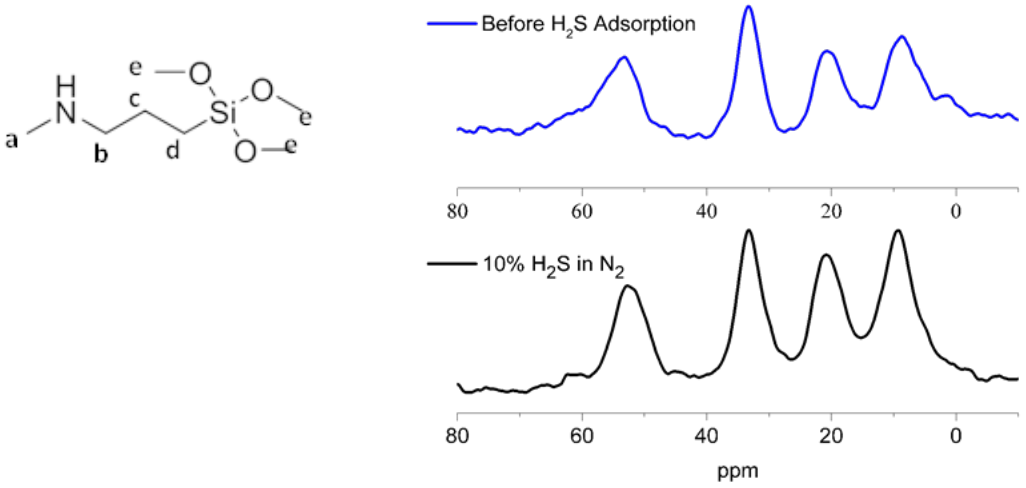

Figure A. 1. ^{13}C CP-MAS Solid State NMR for SBA-15-MAPS before and after adsorption in 10% H_2S in N_2 at 30 °C

Table A. 1. ^{13}C Peak Assignments

	Peak assignment (ppm)				
Amine type	**a**	**b**	**c**	**d**	**e**
SBA-15-MAPS	34.6	54.6	22.9	10.8	50.2

Figure A.1 shows the ^{13}C CP-MAS Solid State NMR spectra for SBA-15-MAPS at an amine loading of 2.0 mmol N/g SBA-15. The materials was exposed to 10% H_2S in N_2 at 30 °C and then analyzed again by ^{13}C CP-MAS NMR. As previously discussed, no significant changes in the carbon species were observed but the absence of the silanol carbon **(e)** at 50.2 for aminosilane compound, MAPS means that the amino-silanol groups have been successfully grafted onto the surface of SBA-15.

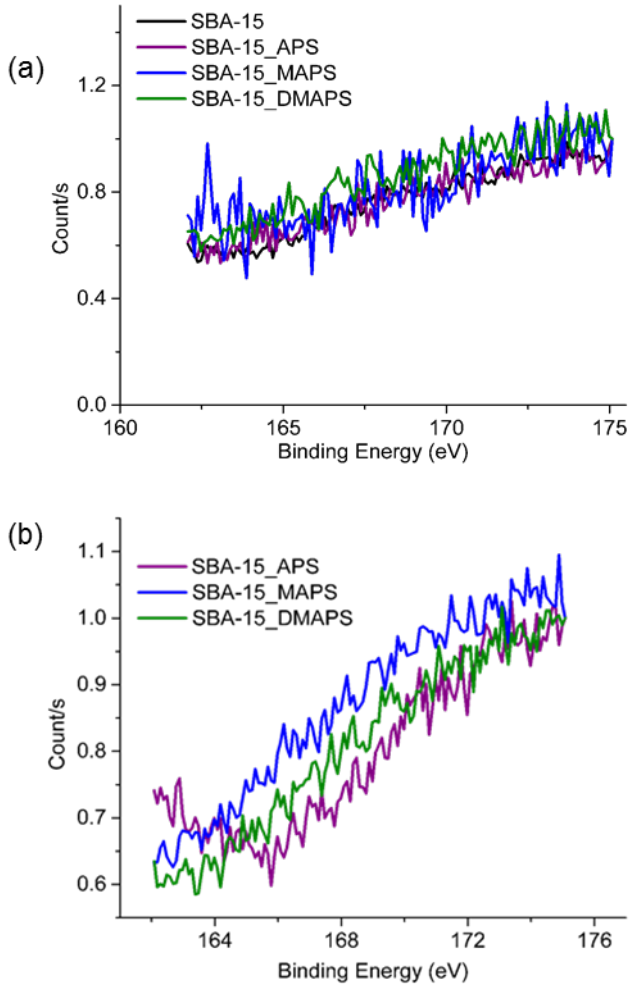

Figure A. 2. XPS, S2p data (a) before and (b) after H_2S adsorption in 10% H_2S in N_2 at 30 °C

Figure A.2 shows the XPS sulfur peaks for the adsorbents studied. The operating conditions were 10% H_2S in N_2 at 30 °C. As discussed, no significant changes in the sulfur peaks were observed for the bare and functionalized materials.

APPENDIX B. SUPPLEMENT TO CHAPTER 3

B.1 Material Characterization

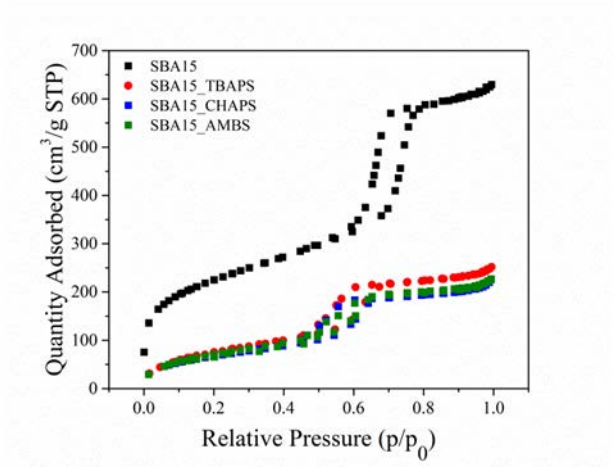

Figure B. 1. Nitrogen adsorption/desorption isotherms at 77 K for bare and functionalized SBA-15 adsorbents

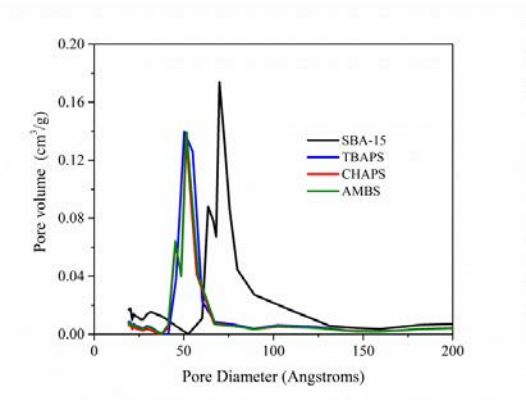

Figure B. 2. Pore size distributions of SBA-15 and all SHA calculated from the N_2 physisorption isotherms using the BdB-FHH method

B.2 Dynamic Adsorption Measurements

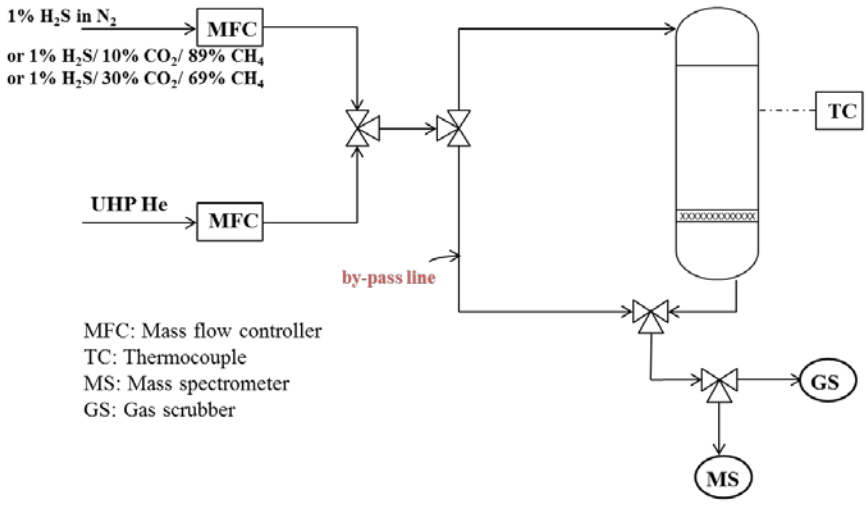

Figure B. 3. Schematic of fixed bed setup for multicomponent adsorption experiments.

B.3 Multicomponent Adsorption Data

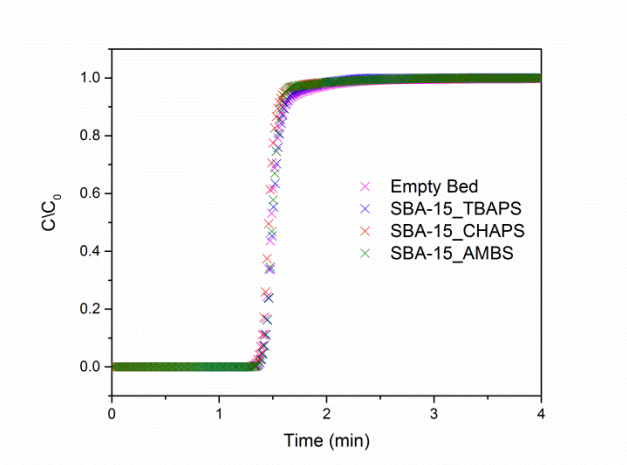

Figure B. 4. Normalized CH_4 breakthrough profile shows that it is non-adsorbing on all hindered amines with a similar breakthrough curve as the empty bed on all sterically hindered amines.

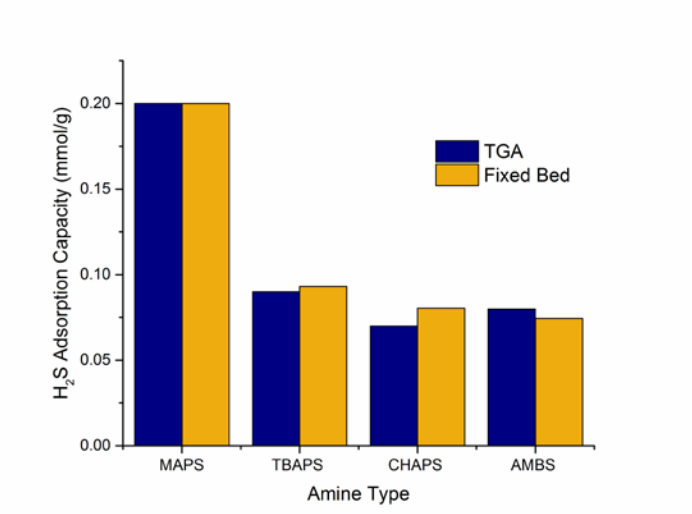

Figure B. 5. TGA vs. Fixed bed H_2S adsorption capacities for 1% H_2S in N_2 at 30 °C

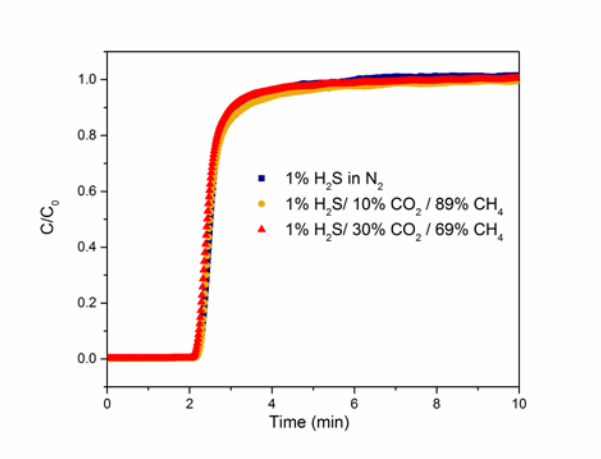

Figure B. 6. The normalized H_2S breakthrough profile of SBA-15_TBAPS shows no significant change before and after the addition of CO_2, which confirms its feasibility for the selective removal of H_2S from biogas streams.

B.4 Single Component Adsorption Data

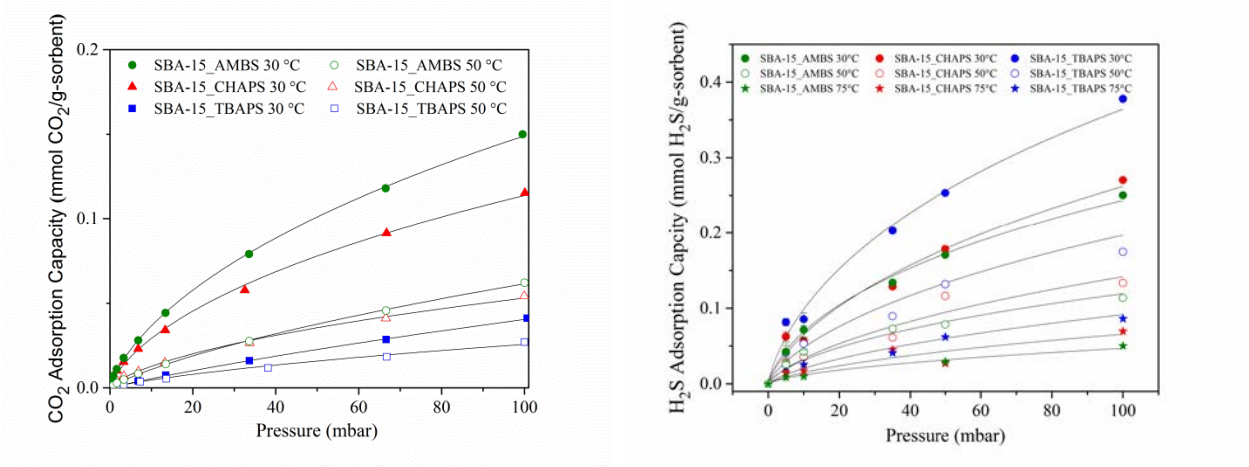

Figure B. 7. Single component adsorption isotherm for (a) CO_2 (b) H_2S at varying temperatures and concentrations.

B.5 Selectivity Comparisons to Literature Data

Table S1 shows the highest H_2S selectivities observed for solid adsorbents reported to date. TRI-PE-MCM-41 was observed to have high selectivities of 70 at low H_2S concentrations of 0.001%, with a drastic decrease in H_2S selectivity to less than 10 as the H_2S concentration increased up to 0.01%. The effect of CH_4 in the gas mixture was not explored.[1]

Belmabkhout et. al[2,3] explored an array of MOF materials, with the highest H_2S/CO_2 selectivity of 7 for Ga-soc-MOF-1a, Y-FUM-fcu-MO and Y-1,4-NDC-fcu-MOF. These MOFs adsorb CH_4 but were found to be highly selective for H_2S.

HKUST-1[4] has a comparable H_2S/CO_2 selectivity to the SBA-15_TBAPS material reported here, but is not regenerable after 1 cycle, with a drastic decrease in H_2S capacity from 1.2 mmol/g to 0.1 mmol/g. Zou et. al [4] found UiO-66, Mg-MOF-74, and MIL-101(Cr), which all

have lower selectivities, to be promising for H_2S/CO_2 separations and the effect of CH_4 was not considered for these solid adsorbents.

SBA-15_TBAPS shows very high selectivities at 1% H_2S concentration in varying CO_2 concentrations in addition to facile regeneration and relative stability at high H_2S concentrations (10%) over 10 cycles. The breakthrough curve of CH_4 was similar to the empty bed, as shown in Figure S4, which illustrates no measurable adsorption of CH_4 on SBA-15_TBAPS. Therefore, SBA-15_TBAPS is the most selective and stable adsorbent for $H_2S/CO_2/CH_4$ separation reported to date.

Table B. 1. H_2S selectivity in solid adsorbents (approximate selectivity values)

Adsorbent	**H_2S in CO_2 Conc. (%)**	**H_2S/CO_2 Selectivity**	**H_2S/CH_4**
SBA-15_TBAPS[this work]	1	40	Non adsorbing
SBA-15_CHAPS[this work]	1	11	Non adsorbing
SBA-15_AMBS[this work]	1	5	Non adsorbing
TRI-PE-MCM-41 [1]	0.01	<10	Not studied
Ga-soc-MOF-1a [2]	5	7	Highly selective
Y-FUM-fcu-MO [3]	5	7	Highly selective
Y-1,4-NDC-fcu-MOF [3]	5	7	Highly selective
HKUST-1 [4]	1	40	Not studied
MIL-101(Cr) [4]	1	3	Not studied
UIO-66 [4]	1	5	Not studied
Mg-MOF-74[4]	1	4	Not studied

B.6 Ideal Adsorption Solution Theory

Table B. 2. Summary of CO_2 and H_2S Toth adsorption isotherm model parameters for IAST selectivity predictions for all adsorbents.

Adsorbate	Adsorbent	Parameters	Toth model parameters		
			30 °C	50 °C	75 °C
H_2S	SBA-15_TBAPS	b	0.0116	0.0227	0.0494
		n	0.395	0.264	0.202
		R^2	0.99	0.98	0.97
	SBA-15_CHAPS	b	0.00762	0.0132	0.0045
		n	0.390	0.325	0.309
		R^2	0.98	0.94	0.96
	SBA-15_AMBS	b	0.0108	0.0909	0.00829
		n	0.298	0.206	0.241
		R^2	0.1	0.99	0.95

CO_2	SBA-15_TBAPS	b	0	0.0008
		n	0.47	0.293
		R^2	1	0.99
	SBA-15_CHAPS	b	0.01	0.0033
		n	0.24	0.219
		R^2	1	0.1
	SBA-15_AMBS	b	0.01	0.0006
		n	0.25	0.291
		R^2	1	0.99

B.7 Computational Data

$$PB = \Delta G°_{H+} + \Delta G°_{Base} - \Delta G°_{HBase^+} \quad \textbf{Equation S1}$$

$$PA = \Delta H°_{H+} + \Delta H°_{Base} - \Delta H°_{HBase^+} \quad \textbf{Equation S2}$$

$$TMBB = \Delta G°_{B(CH_3)_3+} + \Delta G°_{Base} - \Delta G°_{B(CH_3)_3Base} \quad \textbf{Equation S3}$$

$$TMBA = \Delta H°_{B(CH_3)_3} + \Delta H°_{Base} - \Delta H°_{B(CH_3)_3Base} \quad \textbf{Equation S4}$$

Table B. 3. Computational assessment of the TMB basicity and proton affinity of different hindered amines

Adsorbent	TMB Affinity (kJ mol^{-1})	TMB entropy (JK^{-1} mol^{-1})	TMB Basicity (kJ mol^{-1})	Proton affinity (kJ mol^{-1})	TMB Entropy ($JK^{-1}mol^{-1}$)	Proton Basicity (kJ mol^{-1})
TBAPS	48	237	-23	972	106	941
CHAPS	69	234	-1	972	104	942
AMBS	68	219	3	938	104	907
MAPS	86	217	22	945	105	914

B.8 Coordinates of Optimized Structures

$B(CH_3)_3$

5	-0.002172000	-0.000086000	-0.003255000
6	0.701555000	-1.409043000	0.007757000
1	1.775060000	-1.392871000	0.214891000
1	0.216341000	-2.109740000	0.697080000
1	0.569409000	-1.854582000	-0.990317000
6	-1.574234000	0.097390000	-0.005406000
1	-2.100809000	-0.853847000	-0.120180000
1	-1.893730000	0.538106000	0.950914000
1	-1.934512000	0.795280000	-0.770837000
6	0.871324000	1.311253000	-0.003923000
1	0.315575000	2.244375000	-0.128424000
1	1.420218000	1.371754000	0.946973000
1	1.651441000	1.264358000	-0.774393000
1	-2.264610000	-0.883395000	-0.656493000
1	-3.054652000	0.000000000	0.645965000
1	-2.264610000	0.883395000	-0.656494000
7	1.604967000	-0.000001000	0.940660000
1	1.553263000	0.813018000	1.550143000
1	1.553262000	-0.813021000	1.550143000
6	0.582974000	-1.258616000	-0.856703000
1	-0.186640000	-1.298453000	-1.630716000
1	1.562107000	-1.273166000	-1.339800000
1	0.493684000	-2.164527000	-0.247234000
6	0.582975000	1.258616000	-0.856703000
1	1.562109000	1.273166000	-1.339800000
1	-0.186638000	1.298454000	-1.630716000
1	0.493686000	2.164527000	-0.247233000

TBAPS

6	-1.097111000	-0.238621000	0.062025000
1	-1.137171000	-0.829586000	0.993817000
1	-1.074329000	-0.958849000	-0.761703000
6	-2.375876000	0.594896000	-0.049588000
1	-2.395821000	1.329378000	0.765853000
1	-2.332760000	1.169046000	-0.980144000
6	-3.649723000	-0.252517000	-0.001813000
1	-3.719831000	-0.817229000	0.933115000
1	-4.543769000	0.371581000	-0.078784000
1	-3.677368000	-0.972364000	-0.825812000
7	0.081457000	0.621659000	-0.037135000
1	0.038695000	1.318213000	0.701866000
6	1.422528000	-0.003968000	-0.008180000
6	1.606631000	-0.868098000	-1.267208000
6	1.669621000	-0.858739000	1.255045000
1	1.536700000	-0.257724000	2.160539000
1	0.982122000	-1.706672000	1.308351000
1	2.687920000	-1.258950000	1.265336000
1	0.949945000	-1.741650000	-1.261665000
1	2.635276000	-1.232894000	-1.331644000

1	1.387789000	-0.280752000	-2.162062000
6	2.431373000	1.155167000	-0.043402000
1	2.323760000	1.792645000	0.841014000
1	3.458651000	0.782029000	-0.061036000
1	2.265337000	1.773440000	-0.928364000

AMBS

6	0.452157000	0.000000000	0.013926000
6	-0.887836000	0.000001000	0.799943000
1	-0.882468000	-0.876444000	1.460430000
1	-0.882468000	0.876446000	1.460429000
6	-2.185402000	0.000000000	-0.017670000
1	-2.264610000	-0.883395000	-0.656493000
1	-3.054652000	0.000000000	0.645965000
1	-2.264610000	0.883395000	-0.656494000
7	1.604967000	-0.000001000	0.940660000
1	1.553263000	0.813018000	1.550143000
1	1.553262000	-0.813021000	1.550143000
6	0.582974000	-1.258616000	-0.856703000
1	-0.186640000	-1.298453000	-1.630716000
1	1.562107000	-1.273166000	-1.339800000
1	0.493684000	-2.164527000	-0.247234000
6	0.582975000	1.258616000	-0.856703000
1	1.562109000	1.273166000	-1.339800000
1	-0.186638000	1.298454000	-1.630716000
1	0.493686000	2.164527000	-0.247233000

CHAPS

6	-2.004741000	0.141236000	0.252857000
1	-1.893726000	1.202410000	0.007668000
1	-2.036176000	0.078849000	1.357575000
6	-3.328723000	-0.362288000	-0.322576000
1	-3.277627000	-0.295757000	-1.413818000
1	-3.441423000	-1.427440000	-0.082410000
6	-4.542508000	0.408752000	0.202071000
1	-4.477654000	1.470660000	-0.054630000
1	-5.471847000	0.022213000	-0.224064000
1	-4.621985000	0.335896000	1.291178000
7	-0.872833000	-0.591383000	-0.313509000
1	-1.025074000	-1.584198000	-0.157871000
6	0.443913000	-0.235209000	0.226330000
6	2.343612000	1.460729000	0.145976000
6	2.872552000	-1.006756000	0.346781000
6	3.342544000	0.348384000	-0.199364000
6	0.925689000	1.114688000	-0.331555000
6	1.450447000	-1.340574000	-0.123998000
1	0.407407000	-0.149496000	1.330694000
1	2.335509000	1.613751000	1.233070000
1	2.895732000	-0.981155000	1.443800000
1	3.444794000	0.281792000	-1.290121000
1	0.900437000	1.053277000	-1.426183000
1	1.438993000	-1.479207000	-1.212105000
1	2.663437000	2.409556000	-0.296388000
1	3.561624000	-1.800567000	0.041154000
1	4.335147000	0.591544000	0.193588000
1	0.234154000	1.912444000	-0.044721000
1	1.121399000	-2.288668000	0.319011000

TBAPS-H+

6	1.153865000	-0.260012000	0.000001000
1	1.099609000	-0.891856000	-0.885640000
1	1.099611000	-0.891857000	0.885641000
6	2.419217000	0.595072000	0.000000000
1	2.422601000	1.246822000	-0.881432000
1	2.422603000	1.246822000	0.881433000
6	3.681498000	-0.275053000	-0.000001000
1	3.726270000	-0.913869000	-0.885443000
1	4.572045000	0.354444000	-0.000001000
1	3.726271000	-0.913869000	0.885442000
7	-0.084430000	0.612635000	0.000002000
1	-0.036303000	1.231799000	-0.814328000
6	-1.499418000	-0.042833000	0.000000000
6	-1.637344000	-0.882309000	1.270658000
6	-1.637344000	-0.882299000	-1.270664000
1	-1.459064000	-0.290069000	-2.173090000
1	-0.971888000	-1.746908000	-1.275268000
1	-2.659200000	-1.260564000	-1.329334000
1	-0.971890000	-1.746918000	1.275254000
1	-2.659201000	-1.260572000	1.329327000
1	-1.459061000	-0.290086000	2.173088000
6	-2.479424000	1.135501000	0.000004000
1	-2.364933000	1.761735000	-0.889771000
1	-3.501524000	0.754575000	0.000002000
1	-2.364934000	1.761727000	0.889785000
1	-0.036304000	1.231796000	0.814335000

AMBS-H+

6	-0.364520000	0.059638000	0.000001000
6	0.906472000	-0.811969000	-0.000029000
1	0.884444000	-1.465064000	0.881252000
1	0.884444000	-1.465006000	-0.881353000
6	2.223144000	-0.026863000	-0.000002000
1	2.325466000	0.601902000	0.886242000
1	3.059721000	-0.726970000	-0.000022000
1	2.325470000	0.601957000	-0.886207000
7	-1.549428000	-0.957700000	-0.000016000
1	-1.513491000	-1.559732000	-0.827662000
1	-1.513480000	-1.559772000	0.827600000
6	-0.531253000	0.893114000	1.270261000
1	0.250116000	1.651832000	1.311278000
1	-1.490066000	1.419061000	1.286682000
1	-0.445171000	0.282820000	2.173766000
6	-0.531271000	0.893177000	-1.270216000
1	-1.490087000	1.419120000	-1.286599000
1	0.250093000	1.651900000	-1.311204000
1	-0.445197000	0.282928000	-2.173752000
1	-2.451707000	-0.473658000	0.000002000

CHAPS-H+

6	-2.056555000	0.180657000	0.244817000
1	-1.898250000	1.211818000	-0.068612000
1	-2.012126000	0.137605000	1.334411000

6	-3.372641000	-0.374398000	-0.291615000
1	-3.359357000	-0.356498000	-1.387476000
1	-3.480641000	-1.422313000	0.011607000
6	-4.570228000	0.434511000	0.220649000
1	-4.511107000	1.478919000	-0.095286000
1	-5.499319000	0.021029000	-0.173192000
1	-4.631563000	0.409979000	1.311386000
7	-0.874379000	-0.622052000	-0.260820000
1	-1.031495000	-1.606635000	-0.025629000
6	0.517391000	-0.229251000	0.252130000
6	2.369239000	1.473457000	0.140820000
6	2.921241000	-0.988270000	0.364479000
6	3.370309000	0.364046000	-0.202739000
6	0.942717000	1.122491000	-0.323462000
6	1.499717000	-1.349417000	-0.101752000
1	0.402116000	-0.161625000	1.337682000
1	2.362802000	1.644470000	1.223547000
1	2.945022000	-0.957779000	1.459870000
1	3.476203000	0.288697000	-1.291568000
1	0.923272000	1.068083000	-1.420471000
1	1.504029000	-1.497968000	-1.189670000
1	2.666230000	2.418333000	-0.319165000
1	3.606622000	-1.782575000	0.061468000
1	4.357838000	0.620871000	0.187145000
1	0.252484000	1.914247000	-0.021820000
1	1.181581000	-2.293133000	0.356151000
1	-0.860839000	-0.584109000	-1.284589000

TBAPS-B(CH3)3

6	1.319117000	-0.180001000	0.439426000
1	1.432651000	-1.139967000	0.940097000
1	1.363465000	0.585318000	1.211929000
6	2.472160000	-0.010742000	-0.550953000
1	2.423374000	-0.809469000	-1.301085000
1	2.362132000	0.935079000	-1.085506000
6	3.833858000	-0.048210000	0.149144000
1	3.986763000	-0.993551000	0.679112000
1	4.647213000	0.062914000	-0.571646000
1	3.924005000	0.761706000	0.878463000
7	-0.042686000	-0.107367000	-0.204755000
1	0.119488000	-0.053335000	-1.209761000
6	-0.830080000	-1.418167000	-0.023895000
6	-1.015100000	-1.754167000	1.464201000
6	-0.068462000	-2.557605000	-0.732604000
1	0.030345000	-2.357182000	-1.804142000
1	0.929172000	-2.723230000	-0.321730000
1	-0.624579000	-3.491590000	-0.623297000
1	-0.074198000	-1.970118000	1.973079000
1	-1.636188000	-2.649848000	1.542982000
1	-1.515103000	-0.946588000	1.994809000
6	-2.211092000	-1.296285000	-0.679138000
1	-2.140040000	-0.989790000	-1.724619000
1	-2.699671000	-2.273521000	-0.649014000
1	-2.843132000	-0.582959000	-0.155667000
5	-0.799419000	1.540809000	0.019220000
6	-1.469687000	1.611537000	1.490037000
1	-2.372246000	1.001561000	1.614643000
1	-0.785362000	1.359664000	2.311130000
1	-1.782799000	2.647765000	1.670241000
6	0.426936000	2.603350000	-0.147398000
1	1.222518000	2.563983000	0.605720000
1	0.904916000	2.592254000	-1.135989000
1	-0.017981000	3.601086000	-0.050651000
6	-1.837489000	1.767135000	-1.215997000
1	-2.023701000	2.845232000	-1.295922000
1	-1.435518000	1.471113000	-2.196742000
1	-2.820586000	1.299933000	-1.116181000

AMBS-B(CH3)3

6	1.040086000	0.127030000	0.041265000
6	2.160284000	-0.713959000	-0.626436000
1	1.961459000	-1.772086000	-0.413229000
1	2.071201000	-0.596981000	-1.713888000
6	3.600229000	-0.392496000	-0.213295000
1	3.761910000	-0.539868000	0.856830000
1	4.294177000	-1.051501000	-0.740788000
1	3.877171000	0.635020000	-0.459476000
7	-0.266909000	-0.345669000	-0.568937000
1	-0.269329000	-0.042512000	-1.542636000
1	-0.234840000	-1.364361000	-0.613474000
5	-1.916739000	-0.077303000	-0.044083000
6	-2.196220000	-1.110582000	1.178026000
1	-1.715995000	-0.847557000	2.126931000
1	-3.274241000	-1.134489000	1.379262000
1	-1.915315000	-2.150148000	0.950238000
6	-2.717881000	-0.508370000	-1.397434000
1	-2.530441000	-1.544367000	-1.716981000
1	-3.797930000	-0.439228000	-1.224520000
1	-2.508014000	0.140808000	-2.260890000
6	-2.143241000	1.480587000	0.337369000
1	-1.910024000	2.179903000	-0.476492000
1	-3.207461000	1.625830000	0.561624000
1	-1.602013000	1.819928000	1.229623000
6	1.002277000	-0.102091000	1.554624000
1	1.943396000	0.218869000	2.004995000
1	0.194998000	0.466528000	2.013611000
1	0.853148000	-1.157879000	1.795111000
6	1.204780000	1.616573000	-0.283421000
1	0.375518000	2.198683000	0.114311000
1	2.128536000	1.999115000	0.153620000
1	1.254263000	1.782340000	-1.364997000

CHAPS-B(CH3)3

6	1.565781000	-0.684481000	0.589446000
1	1.277353000	-1.326783000	1.422957000
1	2.292029000	0.027319000	0.975177000
6	2.189993000	-1.541695000	-0.510486000
1	1.451811000	-2.270108000	-0.867474000
1	2.450798000	-0.908563000	-1.362021000
6	3.438981000	-2.278774000	-0.017890000
1	3.209023000	-2.937241000	0.825468000
1	3.868339000	-2.894240000	-0.811753000

1	4.208605000	-1.573932000	0.308829000
7	0.356647000	0.099052000	0.135724000
1	0.134573000	-0.214107000	-0.807450000
6	-0.827344000	-0.272685000	1.025546000
6	-1.250257000	-1.739661000	0.818893000
6	-2.087605000	0.612295000	0.901672000
6	-1.821006000	-2.013880000	-0.594078000
6	-3.145917000	0.095349000	-0.104807000
6	-2.530855000	-0.782218000	-1.200042000
1	-0.439386000	-2.437926000	1.038706000
1	-1.799185000	1.630841000	0.672187000
1	-1.027103000	-2.352133000	-1.267860000
1	-3.671015000	0.943142000	-0.552077000
1	-1.826193000	-0.178974000	-1.782313000
1	-2.024300000	-1.940048000	1.566805000
1	-2.523289000	-2.849776000	-0.524012000
1	-3.298628000	-1.105980000	-1.908048000
1	-3.906909000	-0.489266000	0.425000000
1	-2.536063000	0.643084000	1.899631000
1	-0.435275000	-0.143426000	2.035263000
5	0.769600000	1.810151000	-0.133450000
6	2.234418000	1.826367000	-0.857230000
1	3.080914000	1.453755000	-0.268322000
1	2.260891000	1.317100000	-1.830372000
1	2.467829000	2.876288000	-1.071077000
6	-0.302461000	2.423256000	-1.202515000
1	-0.418187000	1.799969000	-2.101943000
1	-1.310679000	2.649621000	-0.842912000
1	0.100710000	3.376858000	-1.564884000
6	0.800713000	2.519017000	1.324778000
1	-0.164946000	2.568872000	1.841862000
1	1.513251000	2.056788000	2.022154000
1	1.133863000	3.557413000	1.205940000

AMBS-H2S

6	0.792131000	0.004988000	0.048461000
6	2.175426000	0.019915000	0.752899000
1	2.218487000	0.916485000	1.387639000
1	2.211409000	-0.838782000	1.438157000
6	3.416869000	-0.011022000	-0.146847000
1	3.457878000	0.853964000	-0.815909000
1	4.327533000	0.003422000	0.460490000
1	3.451199000	-0.914041000	-0.763968000
7	-0.294938000	0.035534000	1.060948000
1	-0.206092000	-0.767658000	1.682856000
1	-0.188149000	0.859419000	1.652194000
6	0.603868000	1.242780000	-0.841802000
1	1.332577000	1.264423000	-1.656537000
1	-0.398178000	1.243380000	-1.279408000
1	0.724001000	2.166009000	-0.261865000
6	0.596755000	-1.277103000	-0.775133000
1	-0.407234000	-1.299700000	-1.207562000
1	1.321544000	-1.342518000	-1.591110000
1	0.718385000	-2.169041000	-0.148592000
1	-2.209037000	-0.017069000	0.388989000
16	-3.508692000	-0.083749000	-0.05526300
1	-3.660970000	1.255591000	-0.053268000

TBAPS-H2S

6	0.897748000	-1.083044000	0.205707000
1	0.703853000	-2.168036000	0.168930000
1	0.964013000	-0.813945000	1.266401000
6	2.242550000	-0.796925000	-0.468463000
1	2.171937000	-1.058139000	-1.534079000
1	2.442077000	0.279778000	-0.427185000
6	3.397452000	-1.573782000	0.169655000
1	3.229661000	-2.655523000	0.118428000
1	4.343472000	-1.360056000	-0.336674000
1	3.519565000	-1.307103000	1.225384000
7	-0.174169000	-0.288798000	-0.411301000
1	-0.118536000	-0.414869000	-1.421667000
6	-1.578776000	-0.566315000	0.000191000
6	-1.745895000	-0.229179000	1.491049000
6	-1.995663000	-2.029918000	-0.261271000
1	-1.861529000	-2.291810000	-1.317391000
1	-1.415554000	-2.736222000	0.339968000
1	-3.051665000	-2.179306000	-0.013370000
1	-1.162328000	-0.899174000	2.129996000
1	-2.795409000	-0.329857000	1.784257000
1	-1.431813000	0.799630000	1.689829000
6	-2.464962000	0.370506000	-0.838201000
1	-2.347184000	0.167260000	-1.909619000
1	-3.521198000	0.227626000	-0.590360000
1	-2.204423000	1.417079000	-0.658981000
1	0.292627000	1.687183000	-0.183438000
16	0.625253000	3.015159000	-0.032052000
1	0.942852000	2.866469000	1.269513000

CHAPS-H2S

6	1.671017000	-1.156763000	-0.084097000
1	1.611574000	-1.000055000	-1.167208000
1	1.481838000	-2.232916000	0.088021000
6	3.078633000	-0.798326000	0.395821000
1	3.252961000	0.268390000	0.214578000
1	3.137317000	-0.944663000	1.484094000
6	4.164456000	-1.632792000	-0.289288000
1	4.153919000	-1.481279000	-1.374267000
1	5.159768000	-1.358838000	0.073091000
1	4.025175000	-2.703508000	-0.102148000
7	0.653865000	-0.318557000	0.565251000
1	0.815399000	-0.352804000	1.571394000
6	-0.742096000	-0.725096000	0.318291000
6	-2.646207000	-0.772055000	-1.365108000
6	-3.143221000	-0.361024000	1.083946000
6	-3.570304000	-0.068184000	-0.361436000
6	-1.171187000	-0.412505000	-1.124937000
6	-1.665953000	-0.008358000	1.315092000
1	-0.853219000	-1.816775000	0.473730000
1	-2.775384000	-1.860104000	-1.275022000
1	-3.299856000	-1.427401000	1.299616000
1	-3.534524000	1.015989000	-0.536139000

1 -1.015026000 0.658594000 -1.308168000
1 -1.520152000 1.074504000 1.205815000
1 -2.928469000 -0.511358000 -2.391586000
1 -3.772380000 0.193786000 1.789526000
1 -4.610465000 -0.376855000 -0.519379000
1 -0.538961000 -0.952925000 -1.838152000
1 -1.373380000 -0.266439000 2.342456000
16 1.235250000 2.934987000 -0.274799000
1 1.408068000 3.327951000 1.002976000
1 0.983911000 1.627427000 0.077087000

2AMBS-H2S
6 3.062734000 -0.231421000 -0.058485000
6 3.961426000 -1.348795000 -0.654473000
1 3.326771000 -2.228315000 -0.834597000
1 4.301320000 -1.012271000 -1.644203000
6 5.181781000 -1.777631000 0.169172000
1 4.895463000 -2.172485000 1.148903000
1 5.735098000 -2.566476000 -0.350779000
1 5.875270000 -0.947118000 0.332961000
7 1.935404000 0.065285000 -0.977095000
1 2.300489000 0.367198000 -1.879916000
1 1.410644000 -0.789495000 -1.159406000
6 2.442756000 -0.667403000 1.278136000
1 3.210087000 -0.850888000 2.035298000
1 1.770666000 0.110509000 1.650223000
1 1.863318000 -1.591163000 1.158629000
6 3.846700000 1.077505000 0.124269000
1 3.182438000 1.868728000 0.482085000
1 4.658720000 0.959069000 0.846953000
1 4.289034000 1.406264000 -0.824115000
1 0.707093000 1.767203000 -0.392963000
16 -0.016531000 2.863144000 -0.026520000
1 -1.070073000 2.119405000 0.423382000
6 -3.112363000 -0.171011000 0.083421000
6 -4.360742000 -0.929201000 0.611422000
1 -4.122126000 -1.309772000 1.614792000
1 -5.164577000 -0.192440000 0.750359000
6 -4.891534000 -2.085041000 -0.245314000
1 -4.146086000 -2.876395000 -0.372630000
1 -5.769258000 -2.538315000 0.226817000
1 -5.195106000 -1.748043000 -1.241249000
7 -2.735135000 0.915622000 1.019309000
1 -3.517979000 1.559017000 1.129821000
1 -2.556123000 0.527120000 1.944542000
6 -1.897932000 -1.107361000 -0.021823000
1 -2.070406000 -1.905639000 -0.749269000
1 -1.013079000 -0.542886000 -0.328417000
1 -1.681308000 -1.577882000 0.945103000
6 -3.393305000 0.490222000 -1.275076000
1 -2.532360000 1.086307000 -1.589380000
1 -3.600840000 -0.254457000 -2.048530000
1 -4.261585000 1.157387000 -1.213094000

2TBAPS-H2S
6 -2.691219000 1.476955000 -0.523368000
1 -3.047763000 1.891060000 0.426489000
1 -3.492656000 1.648453000 -1.262789000
6 -1.440608000 2.244587000 -0.959879000
1 -0.657022000 2.097993000 -0.208052000
1 -1.061542000 1.812312000 -1.897444000
6 -1.705479000 3.739340000 -1.160275000
1 -2.048788000 4.208168000 -0.231529000
1 -0.798111000 4.262146000 -1.478005000
1 -2.472952000 3.912665000 -1.923189000
7 -2.385088000 0.054896000 -0.324827000
1 -1.939394000 -0.294935000 -1.172254000
6 -3.508117000 -0.864228000 0.004163000
6 -4.122708000 -0.458774000 1.354428000
6 -2.889753000 -2.266994000 0.128640000
1 -3.354827000 -0.414388000 2.132005000
1 -2.120006000 -2.280961000 0.905092000
1 -4.618722000 0.515201000 1.302924000
1 -2.428519000 -2.577468000 -0.817013000
6 3.211556000 0.689819000 -0.253366000
1 2.408508000 1.064998000 -0.898435000
1 4.110447000 0.603390000 -0.888087000
6 3.481601000 1.715288000 0.851250000
1 2.579970000 1.823029000 1.464014000
1 4.266396000 1.327831000 1.516860000
6 3.912117000 3.076670000 0.298258000
1 3.133298000 3.509853000 -0.339396000
1 4.109200000 3.786839000 1.106984000
1 4.824965000 2.995106000 -0.302890000
7 2.785780000 -0.591522000 0.321641000
1 3.475416000 -0.873608000 1.017215000
6 2.573519000 -1.740024000 -0.597895000
6 1.401188000 -1.422697000 -1.542451000
6 2.201614000 -2.938271000 0.291874000
1 0.512832000 -1.140026000 -0.969843000
1 1.314319000 -2.715815000 0.890831000
1 1.642390000 -0.606115000 -2.230059000
1 3.020579000 -3.184991000 0.978520000
16 -0.042453000 0.030044000 2.326054000
1 1.047755000 -0.234877000 1.544853000
1 -0.912665000 0.017651000 1.273346000
6 -4.600574000 -0.882273000 -1.087586000
1 -4.176658000 -1.160619000 -2.059740000
1 -5.380507000 -1.611516000 -0.843944000
1 -5.086431000 0.092130000 -1.196535000
6 3.832449000 -2.088763000 -1.422452000
1 4.683106000 -2.299954000 -0.763937000
1 3.658984000 -2.978447000 -2.037162000
1 4.118873000 -1.275710000 -2.096245000
1 -3.654756000 -3.007714000 0.381717000
1 -4.875417000 -1.192805000 1.658619000
1 1.158333000 -2.300750000 -2.149414000
1 2.002249000 -3.826246000 -0.316136000

2CHAPS-H2S
6 -1.897239000 2.524411000 -1.008084000

1	-2.312007000	3.082470000	-0.160858000
1	-2.594413000	2.675228000	-1.854476000
6	-0.526475000	3.103607000	-1.362622000
1	0.144413000	2.966224000	-0.506956000
1	-0.096144000	2.526691000	-2.194209000
6	-0.592615000	4.583226000	-1.750754000
1	-0.984401000	5.190911000	-0.927679000
1	0.398967000	4.970350000	-2.004404000
1	-1.243203000	4.740792000	-2.618491000
7	-1.794870000	1.109838000	-0.632060000
1	-1.275540000	0.627617000	-1.364664000
6	-3.079604000	0.412347000	-0.454857000
6	-5.098246000	0.079590000	1.055809000
6	-4.128487000	-1.895812000	-0.197120000
6	-4.852323000	-1.435550000	1.076671000
6	-3.794523000	0.861855000	0.831516000
6	-2.832224000	-1.103781000	-0.421251000
1	-3.755612000	0.628171000	-1.307080000
1	-5.810428000	0.319871000	0.253361000
1	-4.793450000	-1.758254000	-1.061530000
1	-4.238521000	-1.688761000	1.952101000
1	-3.113866000	0.702939000	1.677878000
1	-2.120083000	-1.318255000	0.386717000
1	-5.567286000	0.402876000	1.992233000
1	-3.905448000	-2.967875000	-0.144875000
1	-5.800186000	-1.974824000	1.191045000
1	-4.009938000	1.935543000	0.794412000
1	-2.355369000	-1.421245000	-1.359121000
6	3.923847000	0.562642000	0.057992000
1	3.369926000	1.020791000	-0.769944000
1	4.832501000	0.112302000	-0.386069000
6	4.325261000	1.653921000	1.051968000
1	3.416717000	2.096464000	1.475923000
1	4.868076000	1.195008000	1.890751000
6	5.196818000	2.740603000	0.416690000
1	4.668962000	3.245627000	-0.400081000
1	5.474895000	3.502550000	1.151004000
1	6.122126000	2.322481000	0.004264000
7	3.068733000	-0.446425000	0.691841000
1	3.530057000	-0.760685000	1.544606000
6	2.777849000	-1.631279000	-0.130292000
6	1.428700000	-2.544277000	-2.085145000
6	1.816585000	-3.989293000	-0.042601000
6	0.853457000	-3.650562000	-1.189859000
6	1.801189000	-1.295079000	-1.271209000
6	2.193104000	-2.736979000	0.762313000
1	3.708179000	-2.020724000	-0.591664000
1	2.323574000	-2.923610000	-2.598728000
1	2.727384000	-4.443535000	-0.457774000
1	-0.104261000	-3.313129000	-0.769413000
1	0.899020000	-0.851831000	-0.828713000
1	1.306065000	-2.337498000	1.271243000
1	0.712573000	-2.277536000	-2.871576000
1	1.371300000	-4.738705000	0.621928000
1	0.637376000	-4.547510000	-1.782448000
1	2.235044000	-0.537827000	-1.934180000
1	2.916204000	-2.997744000	1.547174000
16	0.228102000	0.946120000	2.247722000
1	1.305354000	0.411313000	1.600693000
1	-0.545670000	0.983960000	1.122580000

B.9 References

(1) Y. Belmabkhout, N. Heymans, G. De Weireld, A. Sayari, Simultaneous Adsorption of H_2S and CO_2 on Triamine-Grafted Pore-Expanded Mesoporous MCM-41 Silica, Energy & Fuels. 25 (2011) 1310–1315. doi:10.1021/ef1015704.

(2) Y. Belmabkhout, R.S. Pillai, D. Alezi, O. Shekhah, M. Pang, M. Suetin, A.J. Cairns, V. Solovyeva, Metal – organic frameworks to satisfy gas upgrading demands : fine-tuning the soc-MOF platform for the operative removal of H_2S, J. Mater. Chem. (2017) 3293–3303. doi:10.1039/c6ta09406f.

(3) P.M. Bhatt, Y. Belmabkhout, A.H. Assen, Ł.J. Weseliński, H. Jiang, A. Cadiau, D. X. Xue, M. Eddaoudi, Isoreticular rare earth fcu-MOFs for the selective removal of H_2S from CO_2 containing gases, Chem. Eng. J. 324 (2017) 392–396. doi:10.1016/J.CEJ.2017.05.008.

(4) J. Liu, Y. Wei, P. Li, Y. Zhao, R. Zou, Selective H_2S/CO_2 Separation by Metal-Organic Frameworks Based on Chemical-Physical Adsorption, J. Phys. Chem. C. 121 (2017) 13249–13255. doi:10.1021/acs.jpcc.7b04465.

APPENDIX C. SUPPLEMENT TO CHAPTER 4

C.1 Dynamic Adsorption Measurements

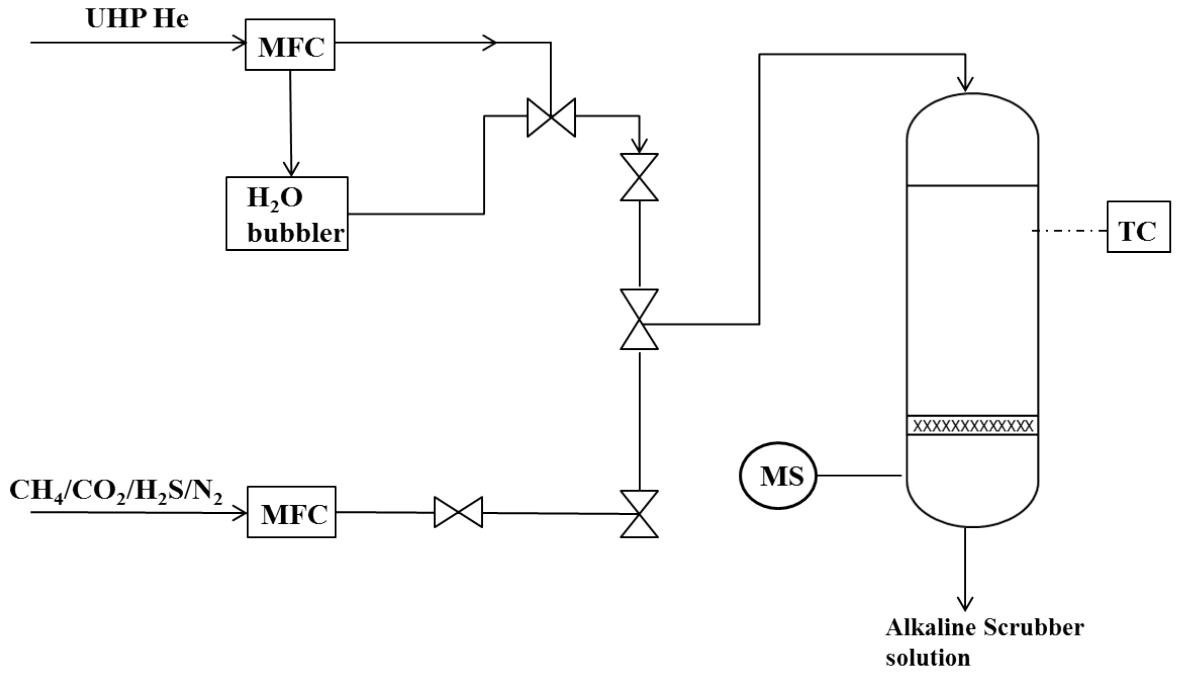

Figure C. 1. Fixed bed adsorption system schematic

C.2 Material Characterization

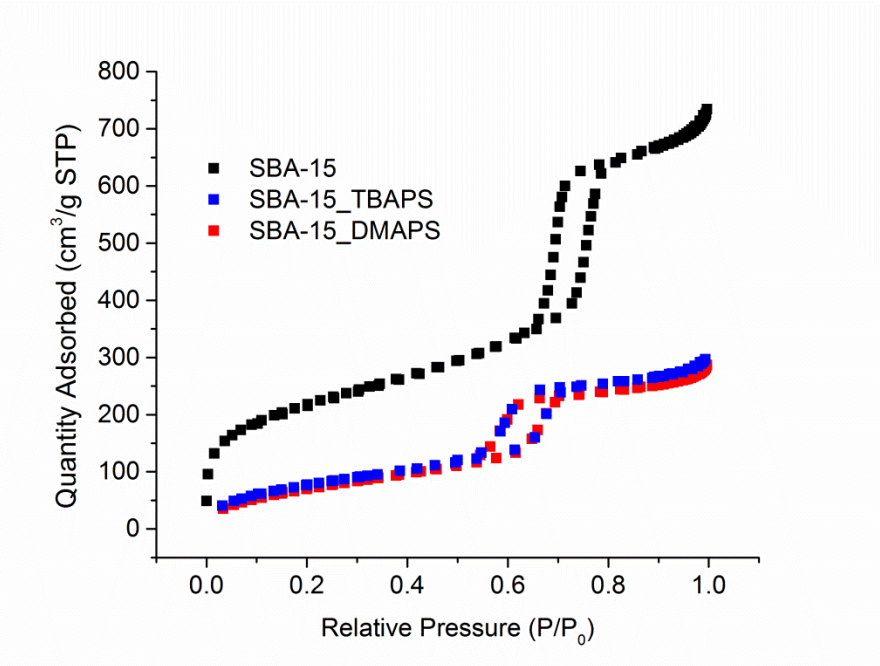

Figure C. 2. Nitrogen physisorption isotherms for SBA-15, SBA-15_TBAPS and SBA-15_DMAPS.

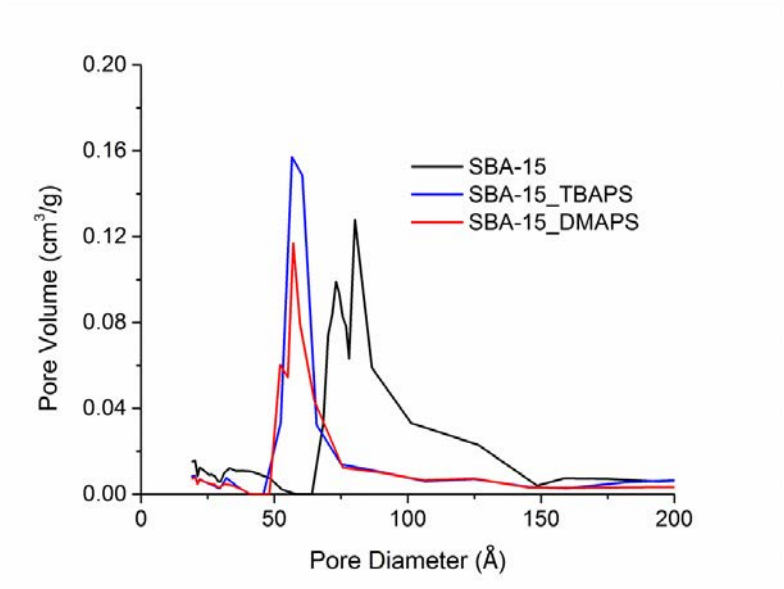

Figure C. 3. Pore size distribution of bare and amine functionalized SBA-15 calculated from N_2 physisorption isotherms using the BdB-FHH analysis method.

C.3 Fixed Bed Measurements

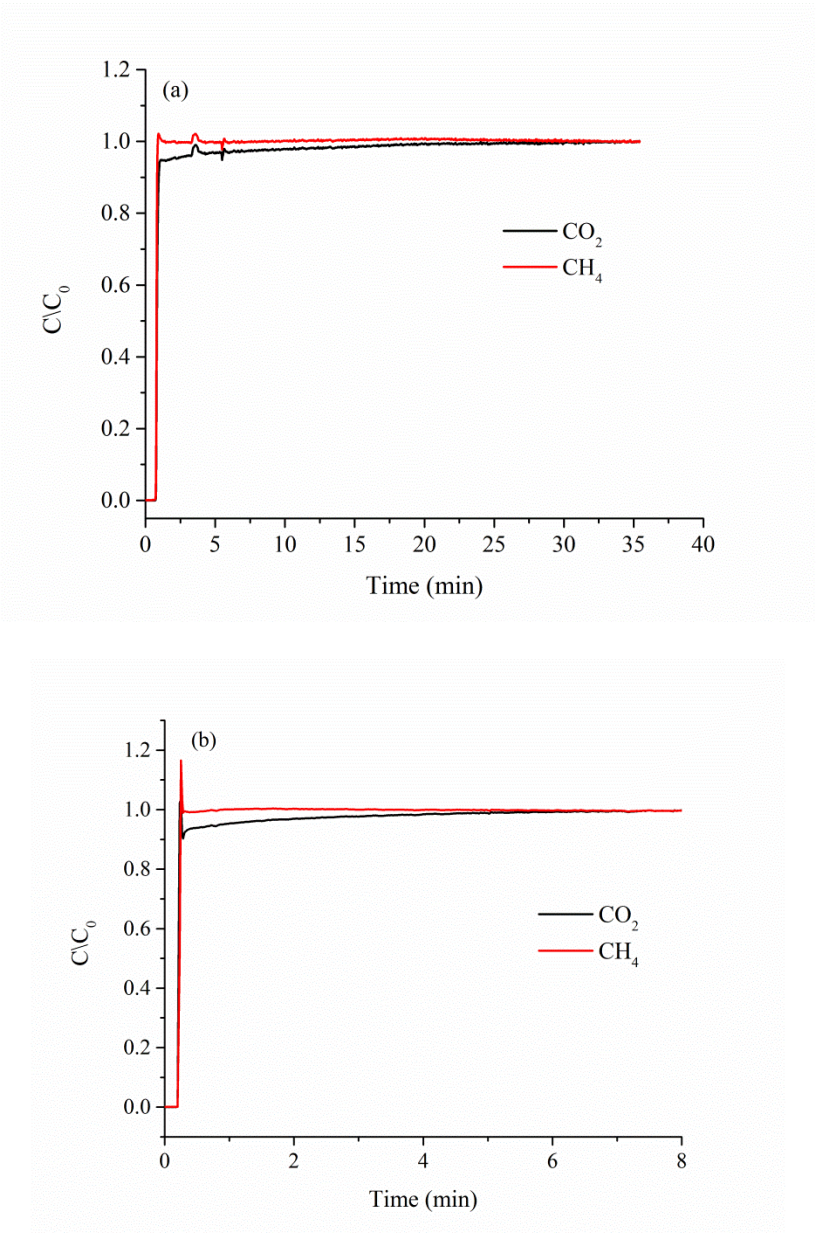

Figure C. 4. The normalized CO_2 and CH_4 breakthrough profiles for (a) SBA-15_TBAPS and (b) SBA-15_DMAPS shows CO_2 is non-adsorbing using 1% H_2S/30% CO_2/ 69% CH_4 with 49% RH.

C.4 Sorption Measurements

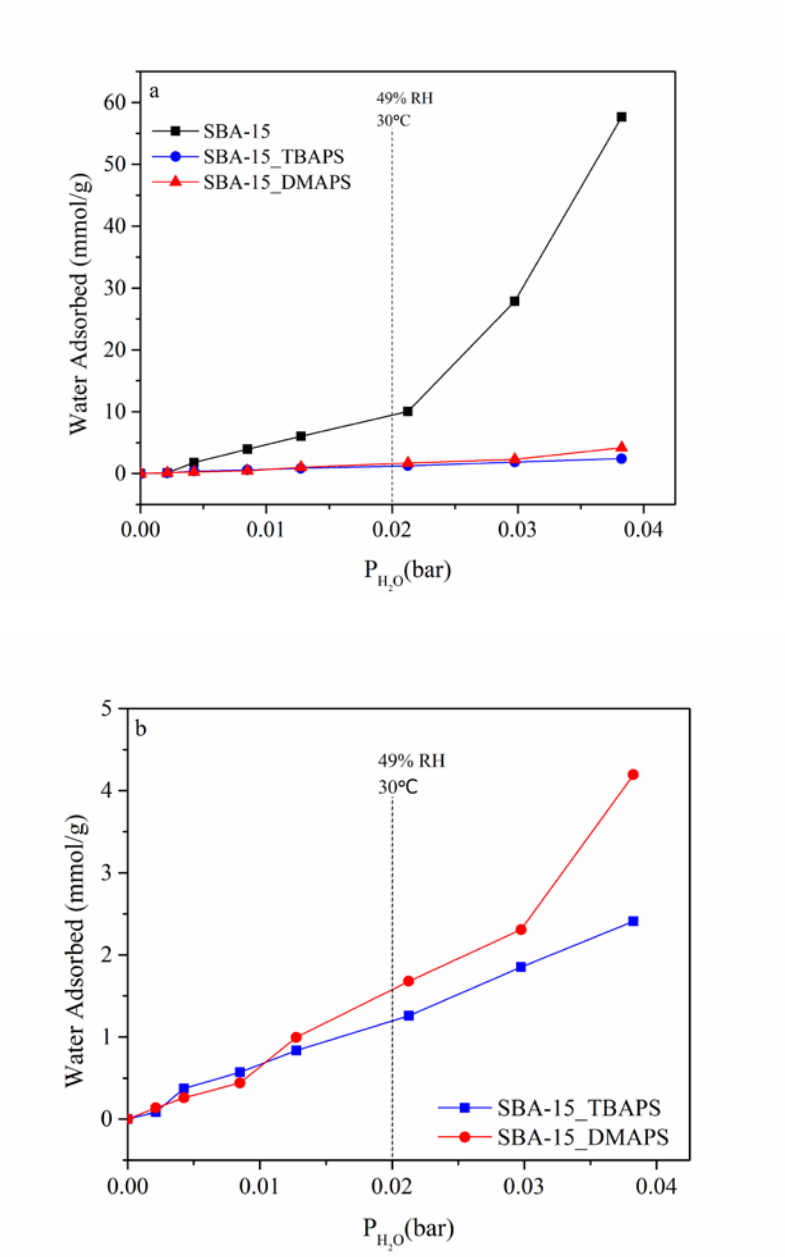

Figure C. 5. Water sorption isotherms of the sorbents studied.

C.5 Computational Analysis

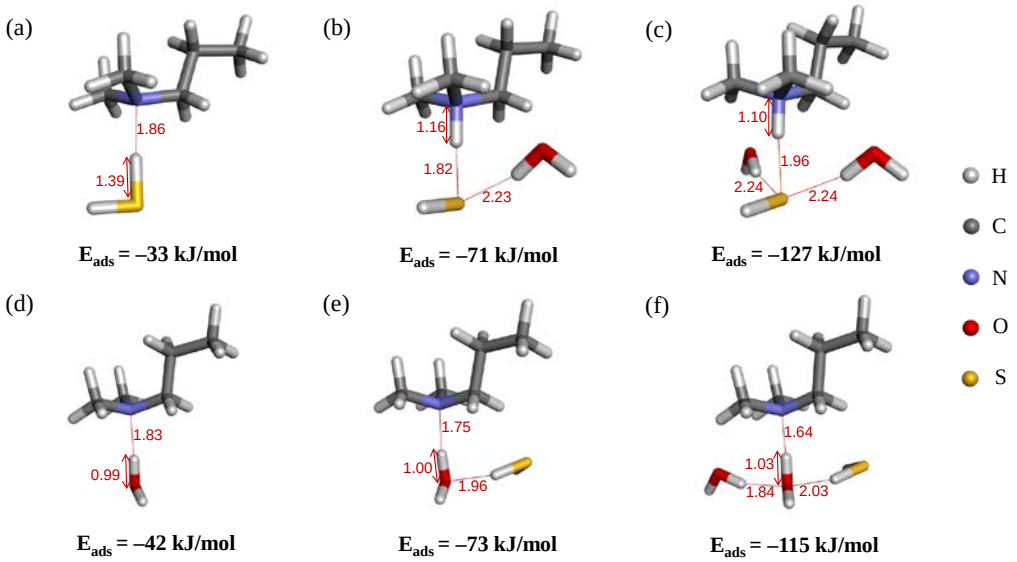

Figure C. 6. Computationally optimized structures for sorption complexes of H_2S and H_2O on one amine site of the SBA15-DMAPS sorbent through (a–c) H_2S-amine interactions and (d–f) H_2O-amine interactions. Sorption energies of the molecules (in kJ/mol) and main atomic distances (in Å) are shown.

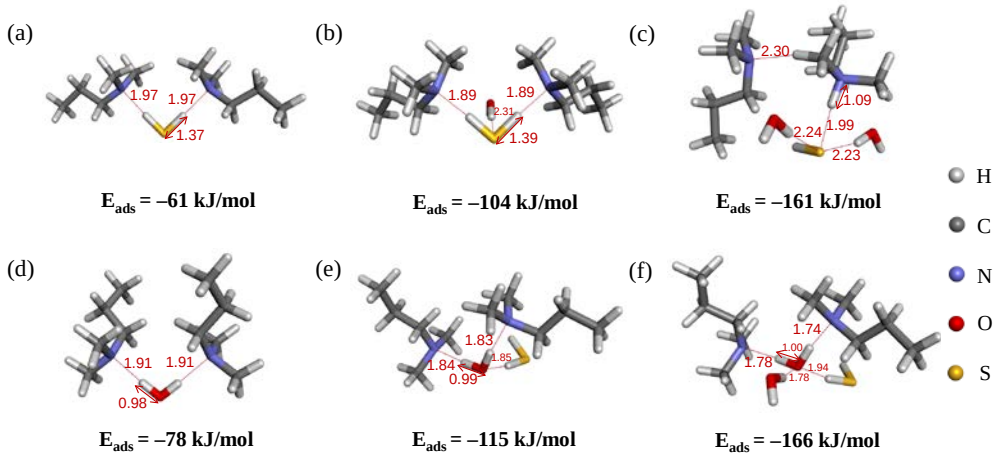

Figure C. 7. Computationally optimized structures for sorption complexes of H_2S and H_2O on two amine sites of the SBA15-DMAPS sorbent through (a–c) H_2S-amine interactions and (d–f) H_2O-amine interactions. Sorption energies of the molecules (in kJ/mol) and main atomic distances (in Å) are shown.

C.6 In-situ FTIR Spectroscopy

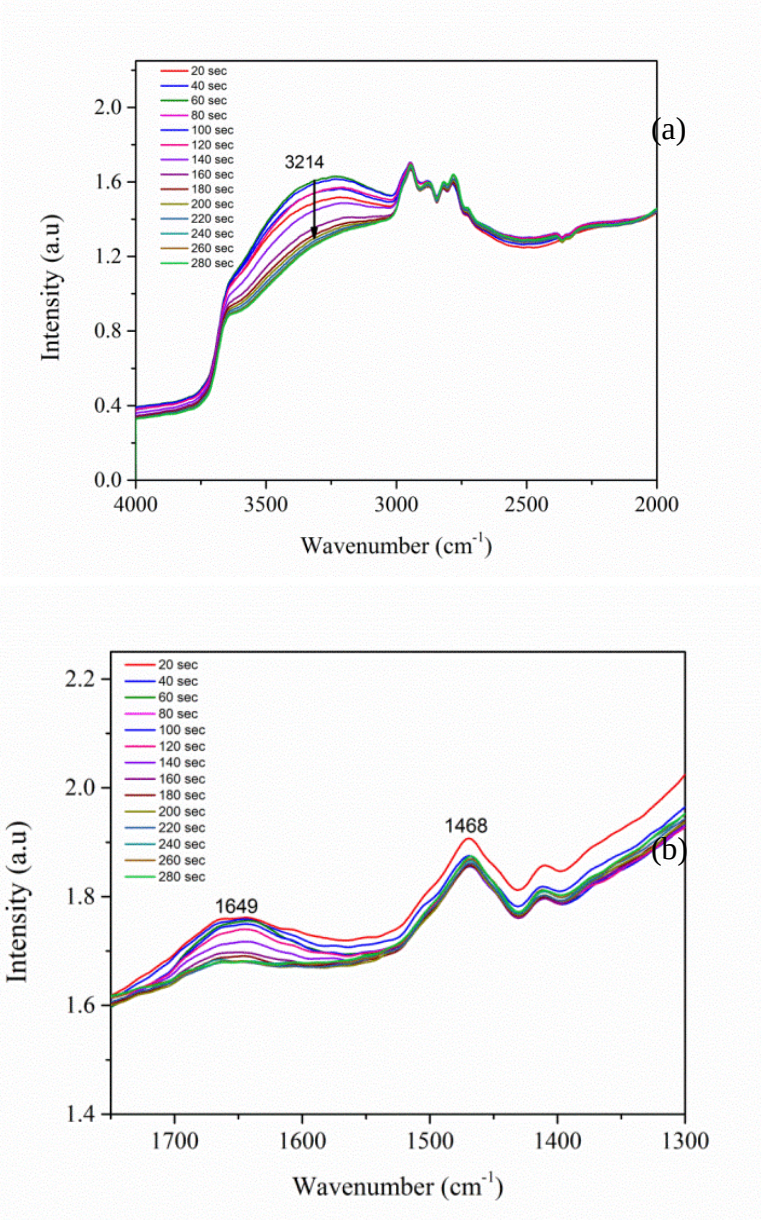

Figure C. 8. FTIR spectra for SBA-15_DMAPS, (a) 4000−2000 wavenumbers and (b) 1800−1300 wavenumbers using 10% H_2S in N_2 under wet conditions.

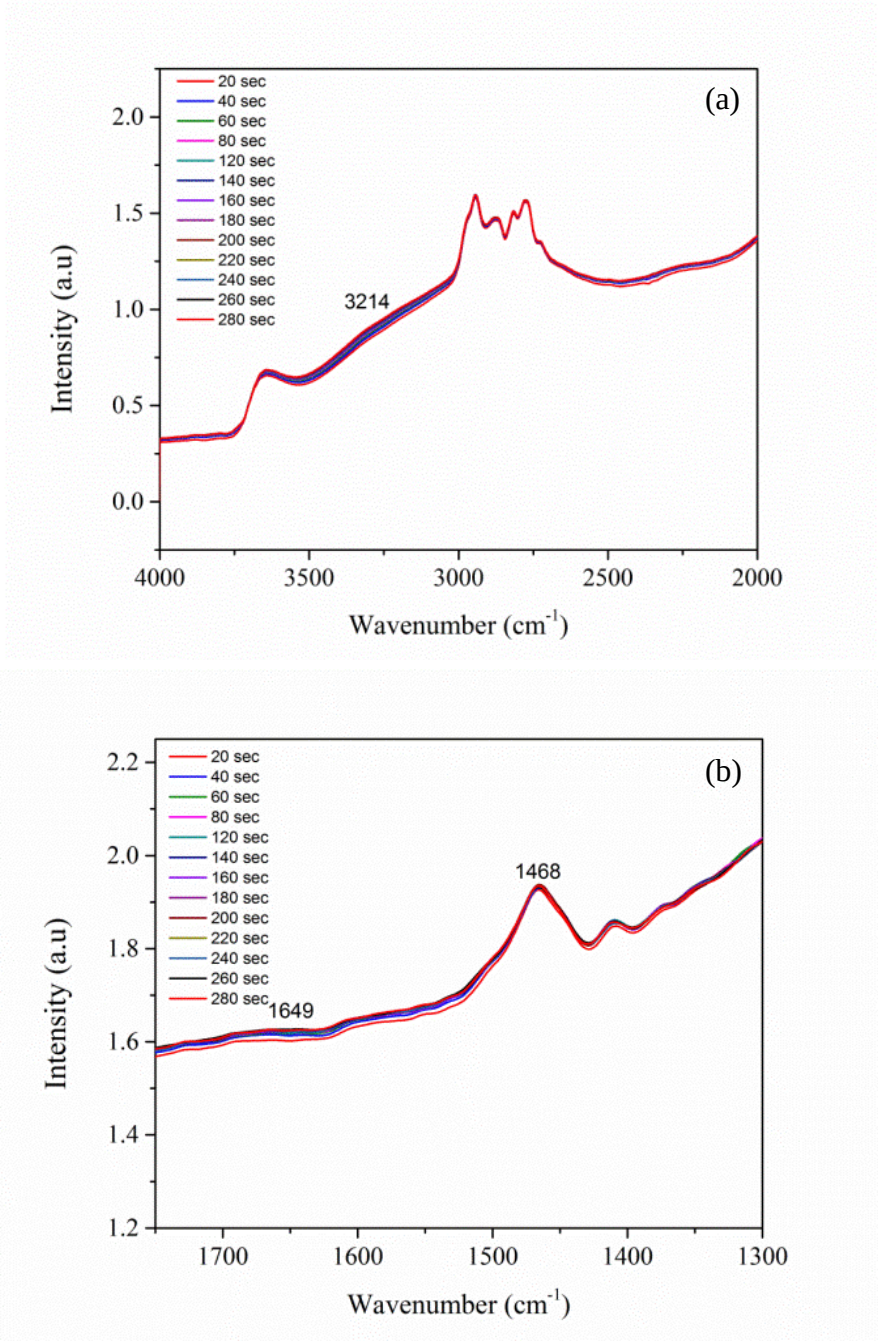

Figure C. 9. FTIR spectra for SBA-15_DMAPS, (a) 4000−2000 wavenumbers and (b) 1800−1300 wavenumbers in 10% H_2S in N_2 under dry conditions.

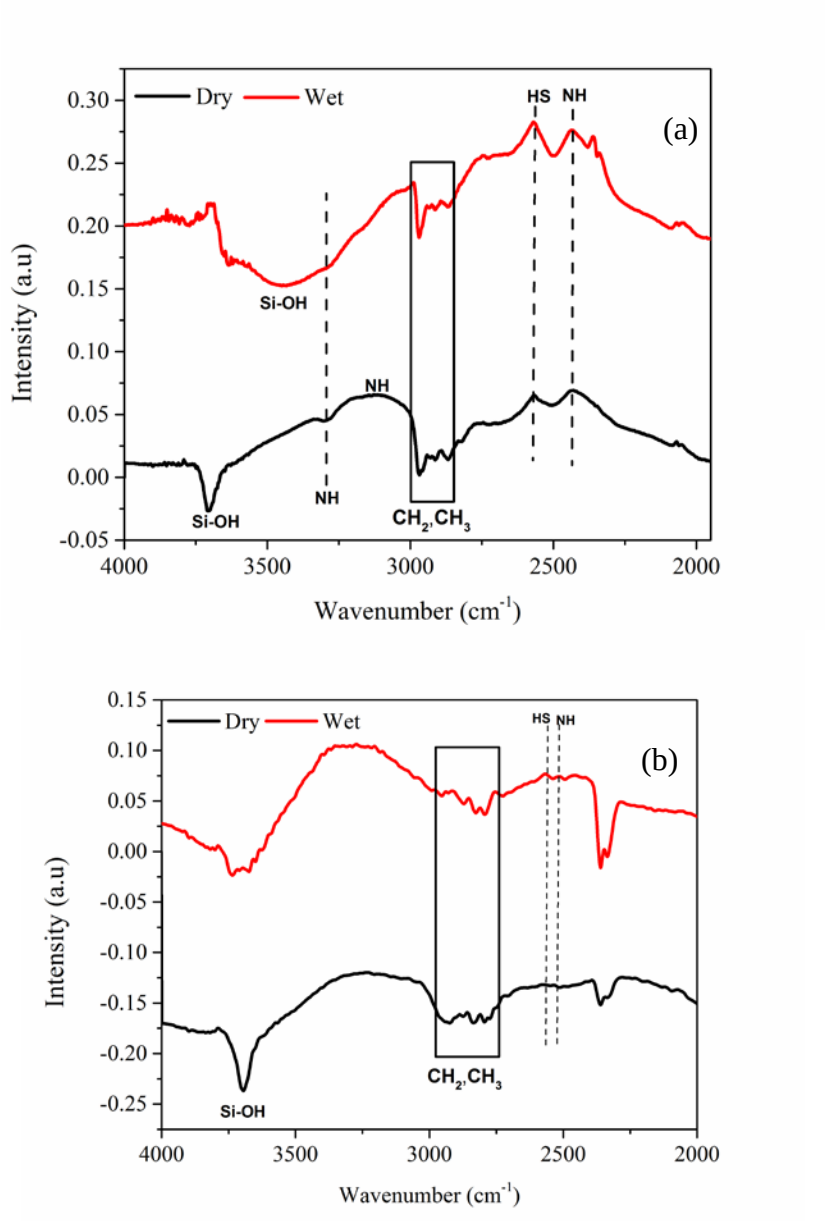

Figure C. 10. FTIR spectra for 10% H_2S in N_2 sorption under dry and wet conditions on (a) SBA-15_TBAPS (b) SBA-15_DMAPS.

C.7 NMR Spectroscopy

Table C. 1. ^{29}Si DP MAS NMR data for bare and functionalized SBA-15 before and after humid H_2S experiments. Values in square brackets indicate the relative integrated peak intensities as area percentages.

Sample	**Q^4**	**Q^3**	**Q^2**	**T^3**	**T^2**	**T^m: Q^n**
SBA-15	-111 [59.6]	-102 [36.2]	-94 [4.1]	-	-	-
SBA-15_TBAPS	-110 [56.6]	-102 [26.3]	-90 [1.3]	-66 [7.6]	-58 [8.2]	0.2
SBA-15_TBAPS (after 6 h adsorption)	-111 [57.2]	-102 [20.3]	-93 [1.9]	-65 [10.9]	-54 [9.8]	0.26
SBA-15_DMAPS	-110 [60.2]	-103 [13.5]	-96 [2.3]	-66 [10.6]	-59 [13.4]	0.36
SBA-15_DMAPS (after 6 h adsorption)	-11 [56]	-102 [14.2]	-95 [5.5]	-65 [15]	-58 [9.5]	0.32

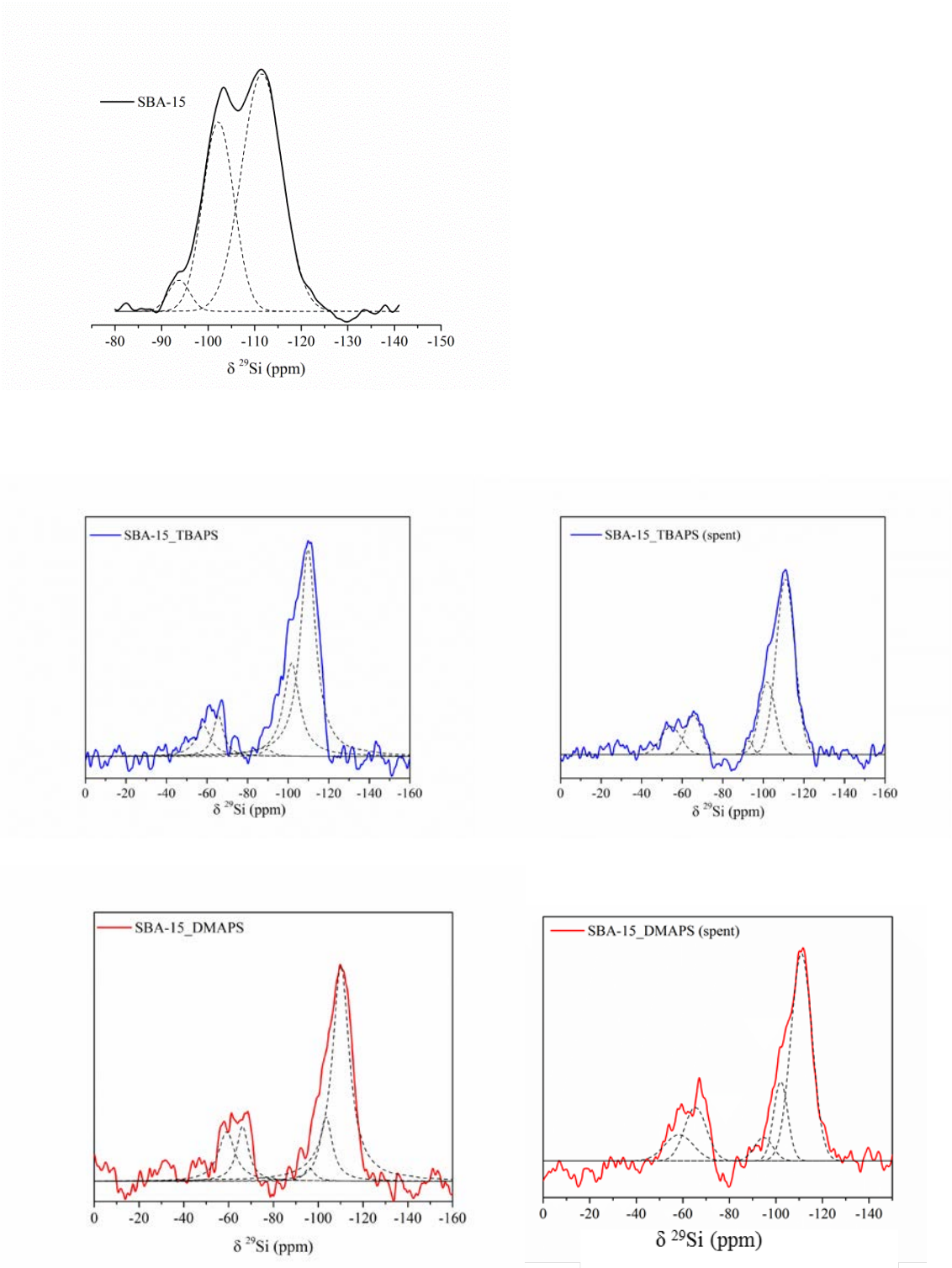

Figure C. 11. ^{29}Si DP-MAS NMR spectra (solid line) of SBA-15. The dashed black lines indicate the deconvolution of the spectral line shapes summarized in Table S1.

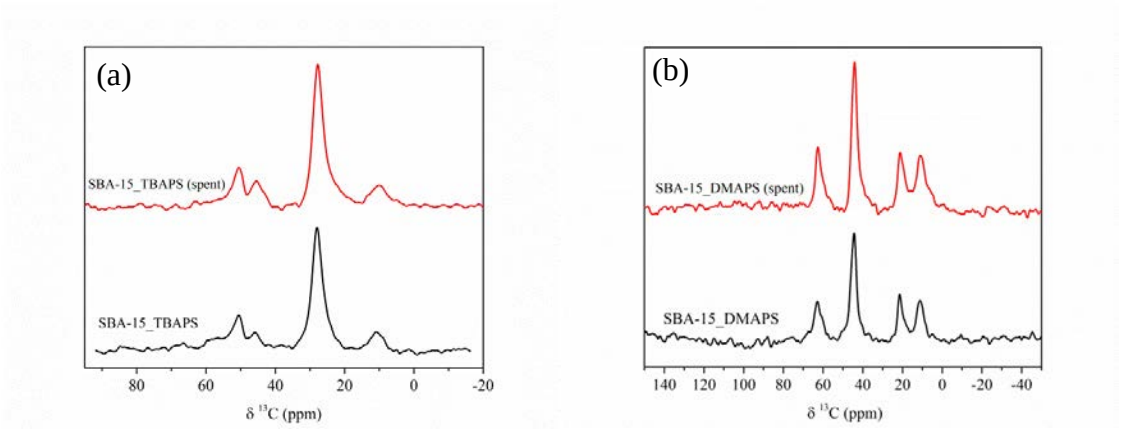

Figure C. 12. ^{13}C DP-MAS NMR spectra of (a) SBA-15_TBAPS and (b) SBA-15_DMAPS

C.8 N_2 Physisorption Post H_2S Adsorption

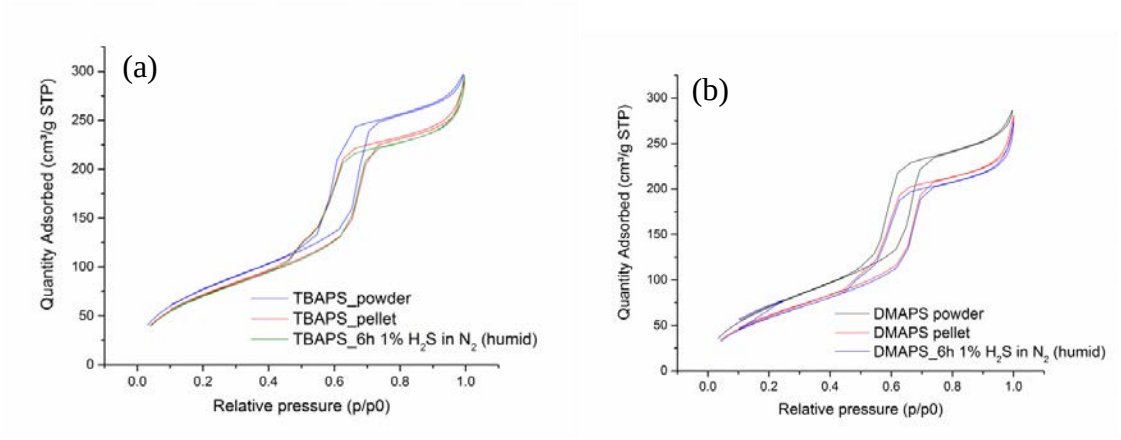

Figure C. 13. Nitrogen physisorption isotherms for (a) SBA-15_TBAPS and (b) SBA-15_DMAPS before and after humid H_2S sorption.

C.9 Cyclic Stability

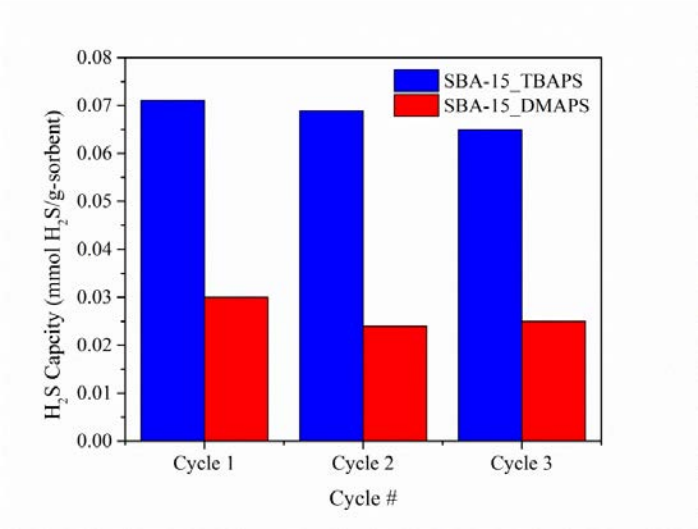

Figure C. 14. Sorption capacities for SBA-15_TBAPS and SBA-15_DMAPS over 3 cycles of sorption and desorption under dry conditions with 1% H_2S in N_2 at 30 °C.

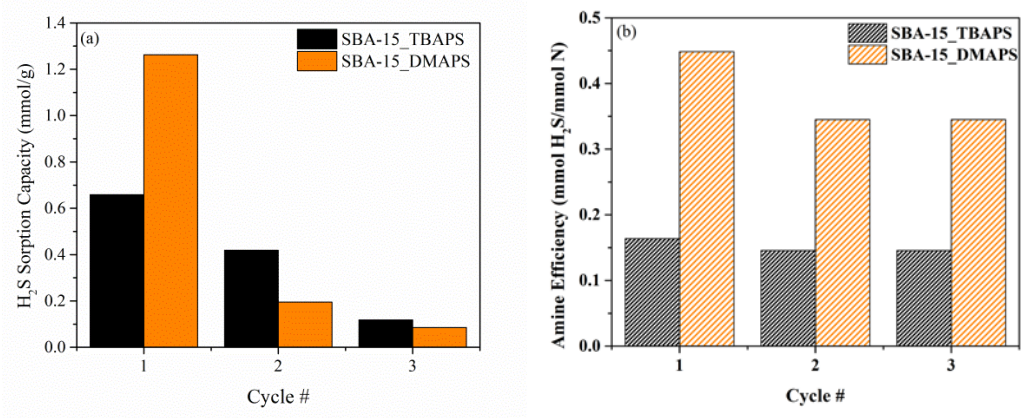

Figure C. 15. Sorption capacities for SBA-15_TBAPS and SBA-15_DMAPS over 3 cycles of sorption and desorption under humid conditions with sorption conditions: 1% H_2S in N_2 at 30 °C and desorption with (a) dry helium at 120 °C and (b) moist helium at 80 °C